UiT
THE ARCTIC
UNIVERSITY
OF NORWAY

Faculty of Science and Technology

Department of Geosciences

Stress distribution calculations through a snow slab of varying hardness; comparison with stability evaluation in the field

—

Laura Josephine Swinkels

Master's thesis in Geology
May 2017

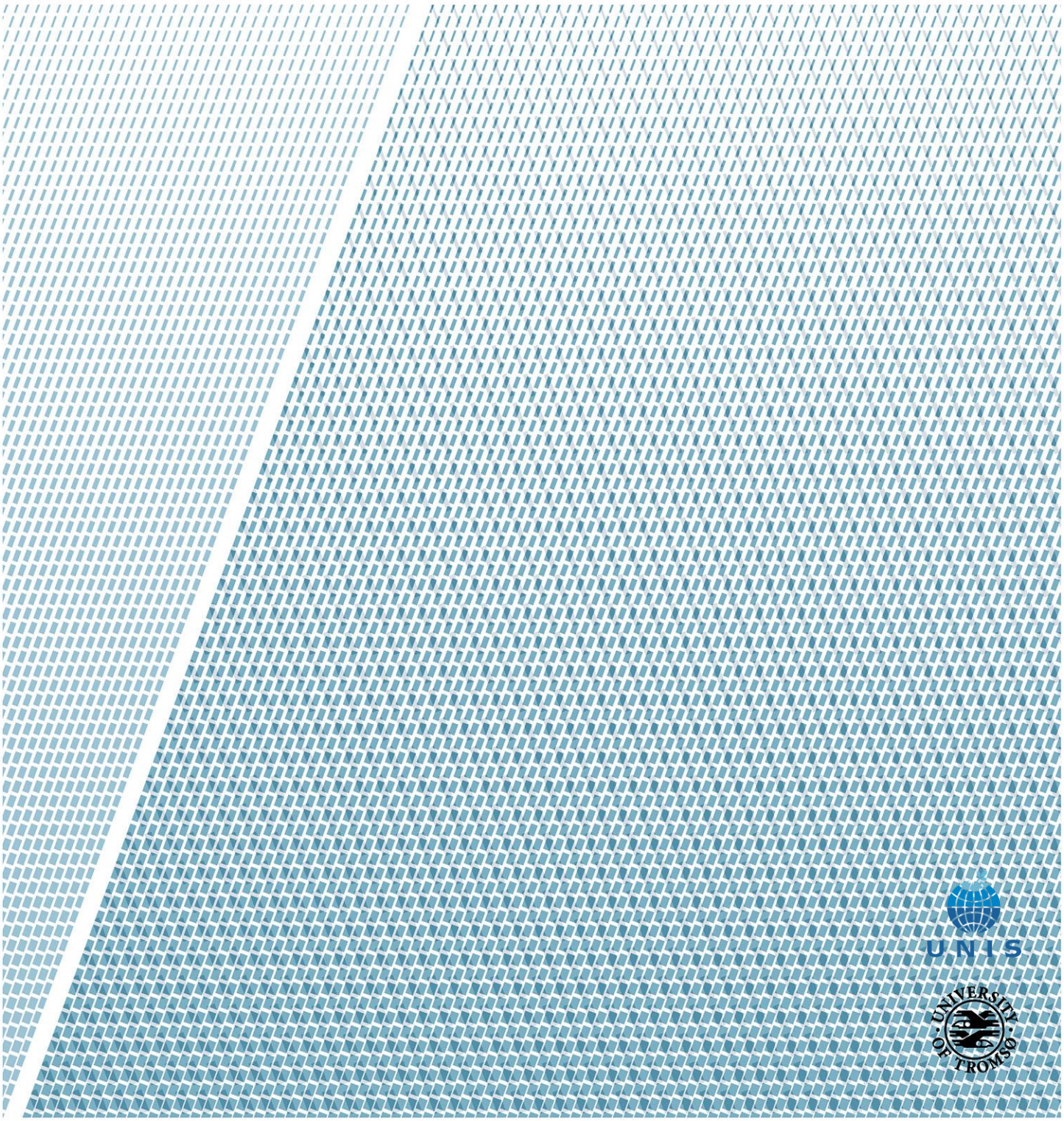

Abstract

Field observations are the main tools for assessing the snow stability concerning dry snow slab avalanche release. Often, theoretical studies cannot directly be translated into useful information for avalanche recreationists and forecasters in the field, and vice versa; field observations are not always objective and quantifiable for theoretical studies. Moreover, numerical models often oversimplify the snowpack and generally use an isotropic single layer slab which is not representative of the real-life situation.
The aim of this study is to investigate the stress distribution in a snowpack with an elastic modulus that continuously varies with depth. The focus lies on the difference between a slab with a gradient in hardness and a slab with isotropic hardness, and the effect on the calculated maximum stress and the stability evaluation in the field.
Approximately 20 different snow pits were evaluated in the mountains around Tromsø, Norway and Longyearbyen, Svalbard. In addition to the standard snowpack observations, the hardness was measured using a thin-blade gauge. Extended column tests were executed for stability evaluation. Measurements from the field served as input for stress calculations for each snow pit using a line load solution for a sloping half space with a non-homogeneous elastic modulus. The hardness measurements were used to calculate the elastic modulus and a power law relation was fit through the modulus in the slab. The calculated shear stress was applied in a stability index, and compared to the estimated stability and character of the specific snowpack
The results show that the approach used for this study improves the calculation of stress at a given depth, although many assumptions and simplifications were still needed. Comparison with the snow profiles indicate that the stability index correlates well with the observed snowpack properties and stability. The blade hardness is proven to be a useful and easy to measure property and it is suggested to replace the snow density with blade hardness as a standard snow pit observation.

Keywords

Snow avalanches; Snow Hardness; Thin-blade hardness gauge; Snow Stability; Snow Mechanics; Elastic Modulus.

Acknowledgements

With this thesis, I broadened my horizon in many ways and I had the opportunity to combine hobby and study. Special thanks to my supervisors Chris Borstad and Holger Stünitz for standing me by with their knowledge and experience, and UNIS and UiT for making this possible. I would like to thank my Svalbard field partners, Franz Czech and Markus Richter, and everybody helping me with the fieldwork around Tromsø: Mats, Helen, Tilman, Hanna, and Willem. Thanks to Evelyn Swinkels and Amando Lasabuda for reviewing my text. I would not be at this stage without my parents, Harry and Dorothé. Thank you for introducing me to the world and for stimulating me to never stop learning. This thesis was presented at the EGU general assembly 2017 in Vienna. I am grateful for the useful feedback from the snow science community.

Table of contents

1. INTRODUCTION

Dry snow slab avalanches are a major concern in mountainous areas. It is the type of avalanche that causes the most damage to infrastructure and the most deaths among back country recreationists. An avalanche can either occur naturally or be triggered by an external force, like a skier (McClung & Schaerer, 2006). Although much research has been done on avalanche initiation mechanisms, slope stability, and snow in general, predicting when and where an avalanche will happen is far from possible.

For a dry slab avalanche to occur, a propagating fracture below a cohesive slab is required. Tensile stresses in the slab increase when the fracture spreads across the slope, until the slab detaches and starts sliding down. Factors leading to avalanche formation can be divided into two groups: (1) external conditions such as terrain and meteorological conditions and their interaction with the snowpack, and (2) the physical properties and mechanical processes within the snowpack (Schweizer et al., 2003). The first group of factors is mainly used in the process of avalanche forecasting. However, a good understanding of the snowpack itself is needed to explain and predict the interplay between the two types of factors leading to fracturing and avalanche initiation. It is therefore beneficial to use a fracture mechanics approach to study slab avalanches.

Modelling is a powerful tool to create a better understanding of the internal behaviour of the snowpack. However, it is difficult to construct a representative model of the snowpack because of the complexity of the material and the number of variables involved. The snow physical properties change rapidly through time, and throughout the snowpack, perpendicular and parallel to the layering. In the past decades, the snowpack has been modelled many times with many different approaches (Schweizer, 1999). In avalanche models, slope failure is reduced to snow failure at a certain depth within the snowpack at a given location and time. Often, models focus on fracture initiation in the weak layer. The most commonly used models are variations of the stability index where weak layer shear strength is related to the shear stress, both from gravity and external loads (Föhn 1987; Schweizer et al. 2003). However, properties of the slab above and the snowpack below are often not considered. Little research has been done to the distribution of the stress through the snowpack, from where it is induced until it reaches a weak layer or interface. Another limitation is that most models only use slab depth and the average density as input variables. The density is normally used to calculate the hardness and/or elastic modulus. However, several studies show that density is not a good parameter in snow behaviour calculations and that the hardness correlates much better with properties like snow strength and elastic modulus (Mellor, 1975; Shapiro et al., 1997; McClung & Schaerer, 2006; Borstad & McClung, 2011). The density is mainly used because it is simple to measure in the field and because of the lack of a good alternative in the past.

The widely-known hand hardness test is most frequently used to determine the snow hardness (Quervain, de, 1950). Although it is easy to execute, this test has many downsides such as inconsistency between observers and a lack of quantitative data. Besides, determining the hand hardness of thin weak layers is difficult because the test involves the penetration of several objects into the snow, which are generally thicker than the weak layer itself. Therefore, the hand hardness test only gives a rough estimation of the hardness difference between layers. To overcome the complications of the hand hardness test and other hardness test, like the rammsonde (Haefeli, 1939), Borstad and

McClung (2011) developed a thin-blade gauge. The thin-blade hardness gauge performs better in many aspects compared to the rammsonde. The gauge is better at distinguishing the snow layers, and finding thin weak layers in particular. Furthermore, the flat and thin blade reduces the compaction at the tip significantly compared to the rammsonde tip, which is cone-shaped (DeVito et al., 2013; Borstad & McClung, 2011). The thin-blade hardness gauge is already accepted by various researchers and avalanche forecasters but a gap exists between the obtained data and the translation into desired knowledge such as snow stability. Mellor (1975) underlined the importance of a good connection between theory and field observations to increase the applicability and usefulness of the information available.

The aim of this study is to improve snow stability evaluations by combining field observations and measurements with mechanical models of snow behaviour. A mathematical line load solution for a sloping elastic half-space with an elastic modulus changing with depth is applied to calculate the portion of the stress induced by an external force reaching the weak layer. In this case, the additional load is a skier standing on an inclined single-layer slab with the hardness varying with depth. Field measurements are used as input for the models, with the blade hardness as most important parameter. The hardness is used to estimate the weak layer strength and a simple stability index is applied. The results of the models are compared with the physical properties and the evaluated stability of the specific snowpack configurations. Stable and unstable blade hardness profiles will be quantified. This paper shows the advantages of thin-blade hardness over density and the doors this relatively simple field measurement opens. The goal is to eventually replace density with blade hardness as an index property for various mechanical properties.

2. BACKGROUND

2.1 Dry snow slab avalanche formation

In the event of a dry snow slab avalanche, a large portion of snow gets detached and starts sliding down under the influence of gravity. The avalanche can either occur naturally or be triggered by an external force. For a slab avalanche to form, four different fractures are needed. Initially, failure will occur in the weak layer or weak interface. The initial failure happens in a relatively small area. In order to form an avalanche, the fracture has to spread across the slope. If the fracture is able to propagate and exceeds the critical size for self-propagation, sufficient tensile stress can develop, leading to the formation of a crown fracture (Schweizer et al., 2003; McClung & Schaerer, 2006) (Figure 1 and 2). After the crown fracture, two fractures on the flanks of the slab are formed and the slab releases. The bottom of the slab is marked by the stauchwall (McClung & Schaerer, 2006; Quervain, de, 1966).

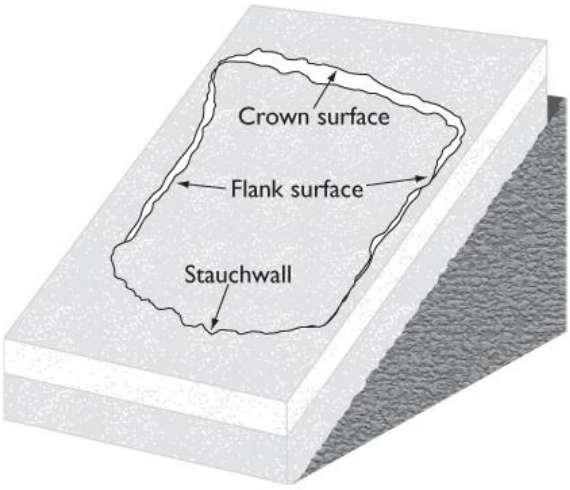

Figure 1. Overview of the different fractures forming in the event of a dry slab avalanche (McClung & Schaerer, 2006).

Figure 2. Crown fracture cutting the west face of Ytterdalsgrubben, Svalbard, 2015.

Snowpack characteristics

A number of external factors and factors within the snowpack promote dry snow slab avalanche release due to a skier triggering. The aspects are described below.

Slab

Statistical research done by Schweizer and Jamieson (2001) highlights several characteristics of the slab that seems to provoke avalanche release. First, soft slabs are most commonly found in skier-triggered avalanches. Hard slabs have a bridging effect and dissipate the stress parallel to the layer resulting in less deformation at depth (Camponovo & Schweizer, 1996; McClung & Schaerer, 2006). Secondly, in the case of a skier as a trigger, a shallow slab is needed, because the load of the skier needs to reach the bottom of the slab in order to provoke fracture initiation. Finally, the importance of a significant hardness difference between the slab and the weak layer is underlined (Schweizer & Jamieson, 2001). The combination of the factors above is often found in

wind-deposited snow. Wind slabs are often soft, well consolidated, and transmit the impact of the skier deeper into the snowpack (McClung & Schaerer, 2006).

Weak layer

The snowpack must contain a weakness in the form of a weak layer or weak interface. A large contrast in hardness between the structural weakness, the overlying slab, and the substratum facilitates failure (Schweizer et al., 2003). Weak layers with very low hardness are prone to failure. The weak layer does not necessarily have to have a lower density compared to the adjacent layers (McClung & Schaerer, 2006). The properties of the weak layer are controlled by the type of snow crystal, which will be described in the next section. The snowpack most frequently fails on a weak layer of anisotropic persistent crystals: crystals that are weak in shear and strong in compression. Such crystals are usually persevered in the snowpack for a longer period of time, or even the entire winter season (Schweizer & Jamieson, 2001; Schweizer & Jamieson, 2000). Moreover, failure tends to occur in weak layers with sufficiently large crystals (van Herwijnen & Jamieson, 2007).

A large number of authors assume in their slab failure models that initial failure of the weak layer takes place in a super weak spot within the weak layer, the so called deficit zone (Bader & Salm, 1990; Heierli et al., 2008), but this is still debated. Field studies of spatial variability do indicate that some parts of a slope are more prone to triggering than others, but this is not necessarily due to a deficit zone (Campbell & Jamieson, 2007; Schweizer et al., 2003).

Similarly, the way the weak layer fails is disputed. It can be divided into two major groups: mixed mode anticrack and shear failure. Initial failure in shear by a mode II crack is the most accepted theory and will be used for this study. An anticrack is the opposite of a mode I opening crack. In the anticrack theory, it is assumed that the weak layer decreases volume during initial failure, moving the two crack faces closer together. It involves a slope parallel and slope normal movement of the slab (Heierli et al., 2008)

Reiweger and Schweizer (2010) performed loading experiments on samples with a weak layer of surface hoar. Two major results of the experiments are: First, increasing loading rates resulted in fracturing with less stress. Secondly, at increasing slope angle, the shear component of the load will increase and the stress at fracture will be smaller compared to more gentle slopes. This means that the surface hoar layer is stronger in compression than in shear, because the shear component controls the failure in this case. Therefore, the results of Reiweger and Schweizer (2010) support the idea of initial failure in shear rather than the anticrack model when considering a weak layer of surface hoar. Reiweger et al. (2015) shows a similar decrease in strength with increasing slope angle, for slopes steeper than 22 degrees. On slopes of less than 22 degrees, slope normal compression was more important.

Substratum

Less research has been done on the characteristics of the substratum. However, it is important to consider the properties of the bed surface, especially in the case of failure on weak interfaces. Weak interface failure often involves a very hard layer, like a crust (Schweizer & Wiesinger, 2001). Habermann et al. (2008) found a significant increase in shear stress in the weak layer if the substratum is very stiff.

Terrain characteristics

The snowpack itself is not the only crucial aspect in avalanche formation, the underlying terrain is also a decisive factor in whether or not an avalanche will be released. As a rule of thumb, a slope angle of 30° is used as a minimum requirement, based on avalanche statistics (Schweizer et al., 2003). Avalanches occur more frequently on steeper slopes, but avalanches on slopes above 55° are very rare as loose snow is often removed in small sluffs (McClung & Schaerer, 2006). Furthermore, the shape of the slope is of importance. Convex slope features are easier to trigger, whereas wide even, smooth terrain and ridge tops are usually safer (Schweizer et al., 2003; McClung & Schaerer, 2006).

If the ground surface below the snowpack is smooth it can act as a glide surface, whereas a rough surface with big boulder or tree trunks can anchor the snow. On the other hand, the snowpack is usually thinner near and above these features and thus more of the stress induced by a skier can reach a potential weak layer.

The slope aspect is important because of both the prevailing wind direction and the incoming solar radiation. On the lee side of the mountain snow can be collected and a wind slab can form. However, thinner snow covers on the windward side are possibly easier to trigger. Slopes directed away from the sun are generally colder enabling a larger temperature gradient and facilitating the growth of weak faceted crystals (McClung & Schaerer, 2006).

2.2 Snow as a material

Snow is a sintered granular material where the individual grains are ice crystals. The ice crystals are connected in chains and form a highly porous open-cell type cellular solid with connected pore spaces (Fierz et al., 2009; Petrovic, 2003). In general, the pore space is filled with air and water vapour, but after periods with higher temperatures the pore spaces can also be filled with liquid water. The snow temperature is always near its melting point on an absolute scale, therefore, snow is considered to be a warm material (Fierz et al., 2009).

Changes on the ground

The initial snow crystals that form in the air will be altered in many ways once they reach the surface. Wind plays a significant role and can modify and redeposit large amounts of snow. The dendrites of fresh precipitation particles break and the grains become smaller and more rounded. Wind deposited snow will be more densely packed than the initial fresh snow layer (McClung & Schaerer, 2006).

Within the snowpack, the snow and its properties are constantly changing through time. As soon as snow gets deposited, sintering and metamorphism starts. The snow settles, becomes denser, and bonds form between the individual snow grains under the influence of the overburden pressure. The fresh snow on the ground is thermodynamically unstable because the crystals are no longer in the supersaturated atmosphere. The grains cannot continue to grow and should change their shape to a more stable form with less surface area: rounded forms. The transition from precipitation particles to rounded forms leads to an initial decrease of the diameter, but the rounded grains start to grow again due to sublimation of water vapour onto their surface (McClung & Schaerer, 2006).

The main control of metamorphisms is the temperature gradient within the snowpack (Pomeroy & Brun, 1990). The temperature at the base of the snowpack is relatively constant and often close to zero due to stored heat from warming by the sun in combination with the insulating capacity of snow. The temperature of upper layers of the snowpack is highly influenced by warming during the day and cooling during the night, the so called diurnal fluctuations. The temperature gradient is the vertical change in temperature per meter. Therefore, thicker snowpacks generally have a smaller temperature gradient than thin snowpacks. The temperature gradient tends to be the largest just below the surface of the snowpack, caused by the temperature fluctuations of the atmosphere (McClung & Schaerer, 2006).

The description of the temperature gradient is not entirely valid for regions in the high north or south, like Svalbard. In these areas, the temperatures at the base of the snowpack are generally lower due to permafrost. Furthermore, diurnal fluctuations are absent during the first winter months due to the lack of sun during the day, and in late spring due to the constant presence of the sun.

The shape of snow crystals affects bonding between the grains. The bond characteristics of the different grain types determine the mechanical properties of the snow relevant for stress distribution and ultimately for avalanche release. Metamorphism plays a major role in the change in mechanical properties of the snow as it can alter the shape of the snow crystals rigorously over time. Snow metamorphism has two main endmembers: rounded grains and faceted crystals. When a snow layer is subjected to a temperature gradient of 10°C/m or more, rounded grains will turn into facets. With a lower gradient, rounded grains are more stable and will grow at the expense of the facets. Rapid changes in weather conditions and thus changes in the temperature gradient can lead to the formation of transitional forms of rounded facets or faceted rounds (Colbeck, 1982). The temperature gradient enables water vapour diffusion and the movement of heat through the snowpack. Air filling the pores can hold more water vapour where the snow is warmer, typically lower in the snowpack (McClung & Schaerer, 2006). Here, the crystals sublimate, preferably at the sharpest convex edges, were the water vapour pressure is the highest (Pomeroy & Brun, 1990). The gradient in water vapour pressure forces the moist air to move up through the pore spaces. As it reaches the grain above, it cannot move further up and the water is deposited onto the crystal (McClung & Schaerer, 2006). This leads to a local re-crystallisation at the expense of the rounded grains. The new crystals grow stepwise and facets are formed. The larger the temperature gradient, the larger the growth rate of the facets (Colbeck, 1982). Early in the season, when the snowpack is thin and the temperature gradient is high, the faceted crystals can develop to large cup-shaped crystals at the bottom of the snowpack. These crystal cups are called depth hoar (figure 3), and once formed they can survive the entire season (McClung & Schaerer, 2006). Crusts in the snowpack, formed by melt-freeze cycles, are an obstruction for the water vapour moving through the pores. Therefore, faceted crystals often form just above or below a crust. The grains are often not well bonded to the crust and form a potential hazard (McClung & Schaerer, 2006).

Persistent crystals

Persistent forms are crystals, such as surface hoar, facets, and depth hoar, that form at a high growth rate and that can survive over a longer period of time within the snowpack.

Figure 3. Cup-shaped depth hoar crystals (0.5-1 cm), near Longyearbyen, Svalbard, 2015.

Layers with persistent forms experience less settlement and compaction due to their anisotropic structure: the crystals are stronger in compression than in shear. The anisotropic nature is the reason that these crystals are of major concern with respect to avalanche formation (McClung & Schaerer, 2006). Schweizer and Jamieson (2001) showed that failure of the snowpack leading to avalanche formation most frequently occurs in weak layers consisting of persistent crystals forms. 82% of the investigated avalanches failed on a layer containing surface hoar, facets, or depth hoar (Schweizer & Jamieson, 2001).

The only persistent form that does not form within the snowpack is surface hoar. Surface hoar crystals form on the snow surface during cold, clear sky conditions. Water vapour precipitates directly onto the surface creating feather- or needle-like ice crystals (figure 4). For this, a high temperature gradient is needed just above the snow surface. The clear sky enables heat radiation away from the snow surface, resulting in the required gradient. Furthermore, high humidity is required in combination with a little breeze to ensure the

Figure 4. Slope surface covered with feather-shaped surface hoar crystals (1-2 cm), Fløya, Tromsø.

supply of water vapour. Surface hoar crystals are very fragile and can easily be destroyed by changing weather conditions. Wind speeds that are too high destroy the crystals and the near-surface temperature gradient. Therefore, much of the formed surface hoar will never become buried and never form a weak layer within the snowpack (McClung & Schaerer, 2006).

2.3 Physical and mechanical properties

Snow is a complex and highly variable material. Universal constants that describe the physical snow properties do not exist. The properties vary from case to case and layer to layer. An individual homogeneous snow layer can be considered as sintered ice grains, which subsequently, can be approached with the mechanical properties of ice, such as temperature-sensitive nonlinear viscoelasticity. In contrast to ice, snow has a highly irreversible compressibility and high porosity. This high porosity is one of the properties that makes snow a unique material and different form other natural and engineering materials (Mellor, 1975).

Density

Snow has a relatively low density due to its large pore spaces. Typical densities of snow are 30 to 600 kg/m^3, whereas ice for example has a density of 917 kg/m^3 (McClung & Schaerer, 2006). The density, like most other snow properties, changes through time under the influence of external factors, such as temperature and the weight of the overlying snow layers (McClung & Schaerer, 2006).

Density is the most commonly used property in relation to the elastic modulus (E). However, it is shown that the density does not correlate well with the elastic properties of snow (Shapiro et al., 1997). The major reason for this misfit is the variation in microstructure of snow with the same density (Kirchner et al., 2001) The bonds between the individual crystals depend on the microstructure. They grow over time after the deposition in a process called sintering. Thus, sintering will increase the strength of the snow with time, but the density does not increase with the same rate. Most elastic experiments were done in snow that is well bonded. Less cohesive snow with a similar density will give significantly lower values of E (Mellor, 1975). Even though density is proven to be less useful, it is still used as major index for the mechanical properties of snow, mainly because it is objective and easy to measure in the field.

Strength

Snow strength is usually defined as the maximum stress that can be reached before failure takes place. Therefore, the strength can be obtained from the failure stress reached in experiments (Mellor, 1975). Strength is highly dependent on the rate of deformation. It decreases with the loading rate above the brittle-ductile transition (the transition from elastic to viscous behaviour) and increases below the transition (Narita, 1980; Reiweger, & Schweizer 2010). The strength is also dependent on the temperature. The warmer the snowpack, the weaker the snowpack (Schweizer et al., 2003). Snow strength varies though time. Changes already start shortly after the snow is deposited, when the process of sintering begins. The snow increases its strength by the formation of bonds, as mentioned before. Sintering is also temperature dependent and is faster at warmer temperatures and low temperature gradients (McClung & Schaerer 2006). Snow can also ‘heal’ and regain strength after small scale failure and rearrangement of grains. New

bonds form directly after deformation and crack formation (Salm, 1982). Grain type and size strongly influence the strength of the snow. Layers consisting of rounded grains are closer packed than for example facets. Such layers therefor have more bonds per unit volume, and a higher strength. In general, the strength increases with increasing density. Density usually increases with depth, but for strength this is often not the case (McClung & Schaerer, 2006).

Hardness

Hardness is resistance to penetration, measured in force (N). Like for snow strength, the bonding between snow grains determines the hardness. Consequently, the hardness depends on the shape of the snow crystals and their orientations as this influences the bonds between them. The overall hardness generally increases with depth due to compaction by the weight of the overlying layers. Just as most of the properties of snow, hardness is constantly changing under the influence of processes like creep and settlement. These processes lead to densification of the snow and an increase in hardness (McClung & Schaerer, 2006).

Hardness, and thus bonding between the snow grains, is the most important controlling parameter for the stress transmission below an applied load and the behaviour of the snowpack in response (Shapiro et al., 1997; Schweizer et al., 1995; Schweizer & Jamieson, 2001; Thumlert & Jamieson, 2014; Monti et al., 2016). Shapiro et al. (1997) proposed the use of hardness as an index property for snow microstructure, among other properties like electrical properties, elastic wave velocity, and dynamic elastic moduli. Density does not qualify as an index property according to the requirements given by Shapiro et al. (1997). However, density is still most frequently used.

The problem with hardness is that it is most commonly estimated in the field with the hand hardness test developed by De Quervain (1950). This involves penetration of the snow layers with different objects for estimation of the relative hardness, but it does not give an objective value to the hardness. Many methods are proposed quantify the hardness of snow but none of them have been widely accepted. The most known and used of these methods is the rammsonde, developed by Haefeli (1939). The rammsonde involves a rod that is vertically pushed into the snow. It measures the force needed for penetration to a certain depth. The complication of the penetrating instruments is that the results depend on the shape of the tip and the rate at which it is pushed into the snow. A relatively large amount of compaction at the tip results in an overestimation of the hardness and does not represent the properties of the snow's microstructure (Shapiro et al., 1997; Borstad & McClung, 2011). A blade penetration device developed by (Fukue, 1977) minimizes the compaction at the tip. Fukue's results showed that penetration force is linearly related to compressional strength, Borstad and McClung (2011) improved Fukue's blade by using a thinner and longer blade, closer to the scale of the snow's microstructure. Laboratory tests done by Borstad and McClung (2011) showed that the tensile strength correlates significantly better with blade hardness than with the snow density. Furthermore, they also showed the possibility to estimate the snow density from the blade hardness index.

To make hardness manageable and comparable, Schweizer and Wiesinger (2001) classified 10 typical hardness profiles (figure 5). It was suggested that profiles with hard over weak layers and overall soft snowpacks, like profile 1, 5, 7, and 9, are more likely to

be unstable. Snow profiles which are relatively hard or gradually increase in hardness (profile 6 and 10) are marked as generally stable (Schweizer & Wiesinger, 2001). This seems to disagree with the principle of bridging for some of the profiles (Camponovo & Schweizer, 1996; McClung & Schaerer, 2006). Thumlert and Jamieson (2014) measured stress below a skier directly in the field. A bridging index (BI) was used to quantified the stress distribution through the upper snow layers with respect to their hardness. The bridging index is the hand hardness of a specific layer multiplied by the thickness of that layer. Thumlert and Jamieson (2014) found a strong relation between the shear stress and the bridging index where the shear stress decreases significantly with increasing bridging index, confirming the effect of bridging by hard layers in the upper part of the snowpack.

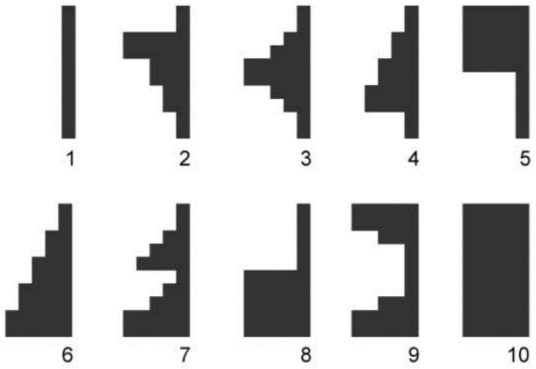

Figure 5. Hardness profiles as defined by (Schweizer & Wiesinger, 2001).

Finite element models of Schweizer (1993) show that soft over hard snow layers lead to better transfer of stress to depth, in contrast to the case of hard over soft layers where the shear stress at depth is significantly lower. This in agreement with the field study of Schweizer et al. (1995). The field experiments show that a hard layer on top will lead to bridging and a more horizontal spreading and dissipation of the stress.

2.4 Deformation of snow

The deformation of snow occurs primarily in the bonds between the grains: bond bending and rupture (Camponovo & Schweizer, 2001). The snow structure with its connected grains can be regarded as a foam of ice (cellular solid), therefore the properties of ice can be used when deformation is evaluated. Field observations, experimental testing, and theoretical models show that snow is a quasi-brittle viscoelastic material. Snow can deform both in a viscous and elastic manner depending on the strain rate (Narita, 1980; Schweizer, 1998; Kirchner, et al. 2001). At low strain rates, small scale cracks (5-6 mm) cause unrecoverable plastic deformation (creep). Grain contacts break and the crystals rearrange leading to a decrease in pore space and an increase in density. Creep is initiated by gravity and starts immediately after the deposition of snow on a slope. Layers consisting of specific types of crystals with an anisotropic nature, like depth hoar, surface hoar, or faceted crystals, are less prone to the changes in density (McClung & Schaerer, 2006). Snow is a strain softening material (Kirchner et al. 2001). Deformation weakens the snow and the stress drops after the yield stress is reached. The snowpack can sustain very large strains at a low rate because sintering will counteract the strain softening by healing microcracks (Camponovo & Schweizer, 2001).

For linear elastic behaviour, very high strain rates are needed. The elastic response to a rapid loading leads to brittle fracturing (Salm, 1982). Linear elasticity is the type of behaviour expected for fast loading of the snow pack by a skier. Young's modulus (E), or elastic modulus of a material describes the relation between the stress applied and strain experienced by the material in the case of linear elasticity ($E= \sigma/\varepsilon$) (figure 6). At high strain rates, the elastic modulus is equal to the initial tangent modulus, or stiffness

(Mellor, 1975; Schweizer, 1998). A small elastic modulus means a low stiffness: the material is easy to deform. Several studies showed a good correlation between Young's modulus and hardness data obtained from penetration resistance instruments (Borstad & McClung, 2011; Sigrist, 2006). Young's modulus is linearly related to the hardness and can be obtained using the equation:

$$E = C * B \qquad (1)$$

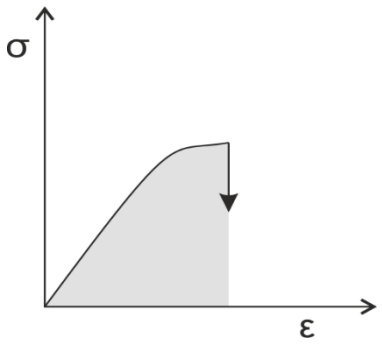

Figure 6. Elastic behaviour leading to brittle failure with a small inelastic component. The grey area under the curve e is related to the fracture toughness of the material.

where B is the blade hardness and C a constant depending on the blade-tip area (Borstad, unpublished). Variations in Young's modulus can therefore be obtained directly from variations in blade hardness in the field.

The fracture toughness of snow expresses the resistance to fracture. The fracture toughness determines, together with the applied load and the geometry of the system, the fracture propagation propensity. The propagation propensity is the work needed for failure and can be obtained integrating stress over strain (Schweizer, 1998) (figure 6). For brittle failure, snow and ice have the same slope of the stress-strain curve (elastic modulus), but stress concentration in the bonds between snow grains leads to a lower amount of stress required for brittle failure (Kirchner et al., 2001). Thus, snow has a lower fracture toughness than ice.

Another important parameter to describe the deformation of snow is Poisson's ratio. Snow is compressible and experiences volume loss when exposed to stress either from gravity or by an external load. The compressibility is expressed in the value of Poisson's ratio (between 0 and 0.5).

Effect of porosity

Compaction plays an important role in the deformation of the soft upper layers of the snowpack. Compaction refers to the decrease in volume under the influence of stress due to the removal of air or fluids in the pores of the material. This is widely studied for soils, normally involving water: consolidation (Biot, 1941; Biot, 1955; Biot, 1956). However, in the case of dry snow, liquid water is not present and the pores are solely filled with air in the initial state. At long time scales, compaction is caused by gravity and only involves the solid ice structure of the snow. Therefore, the pore pressure is of minor interest and is not included in studies on the long term behaviour of snow (Mellor, 1975; Shapiro et al., 1997; Wu et al., 2005).

When considering rapid loading (for example by a skier), the stress is also mainly accommodated by the crystal structure. For very porous fresh snow, the solid ice structure consists only of a few bonds that carry all the weight of the load. This causes internal failure of the soft snow layer. The energy dissipates and a significant portion of the stress will not be distributed deeper into the snowpack. In a denser snowpack with less pore space the ice structure is stronger due to a larger number of bonds. The snow will not compact and the applied stress is accommodated and distributed by the ice

structure in an elastic manner. The stress is transmitted deep into the snowpack by the bending of bonds (reversible deformation) before it reaches a weaker layer that fails in a brittle way. Therefore, harder snow layers can be approximated as a solid without pores, that behaves elastically, enabling the use of the general solutions (Wu et al., 2005). Moreover Schweizer et al. (1995) argued that compaction does not have a significant effect on the stress distribution, except for very soft snow.

2.5 Failure models

Years of snow and avalanche research resulted in a broad understanding of the physical behaviour of snow related to avalanches. Numerical modelling is an important tool in the investigation of snow avalanches. Field measurements and laboratory experiments are destructive methods, and therefore not reproducible. Experiments are hard to execute, mainly because of the fragile nature of snow. Models increase the general understanding of the response of the snowpack to several processes, leading to avalanche release. Numerical modelling using data from the field provides a link between micro-scale processes and the macro-scale effects (Schweizer et al., 2003).

Stability index

Various fracture initiation models are based on a simple stability index (Jamieson & Johnston 1998; Monti et al. 2016), developed by Föhn (1987). It is based on the principal that the stresses induced by the overlying slab, and possibly an additional load, exceed the strength of the weak layer. Consequently, the weak layer fails in shear. A stability index S is simply defined as:

$$S = \frac{\tau_s}{\sigma_{xz}} \qquad (2)$$

where τ_s is the shear strength, and σ_{xz} is the shear stress (Föhn, 1987). This stability index is only valid for isotropic snowpacks. The shear strength can be related to the normal stress using the Mohr-Coulomb law for fracture. The shear stress σ_{xz} is a combination of gravitational stress due to the weight of the slab and the external load, such as a skier, in addition.

Stress distribution

Already in 1878, the French mathematician Boussinesq developed a fundamental solution for the stress evolution through a homogeneous elastic half space, induced by a point load acting normal to the surface of the half space. The Boussinesq solution has been used in several models for snow instability. Föhn (1987) used Boussinesq's solution to expanded the stability index for the additional load of a skier or other human trigger by adding a shear stress component to the denominator. A skier is represented as a line load, and the additional shear stress may be given by:

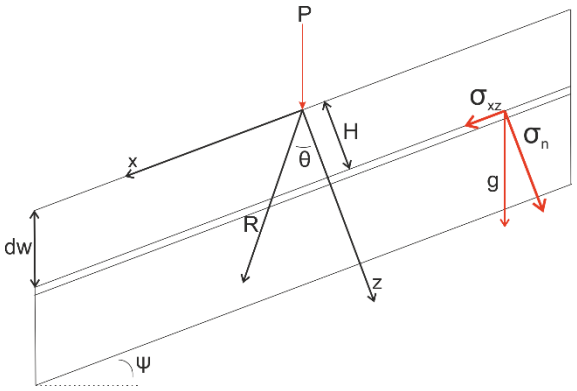

Figure 7. Overview of the snow slab and substratum with a line load P (skier), weak layer depth dw, slab thickness H, slope angle ψ, and θ the angle between the z-axis and the point of maximum stress from the line load. R and θ are spherical coordinates. The different stress components are shown in red at the right side.

$$\Delta\sigma_{xz} = \frac{P}{\pi R}\sin(\alpha + \psi)\sin 2\alpha \qquad (3)$$

where P is the line load, R the radius to a specific point in the snowpack, α the angle between the snow surface and R (α = 90- θ), and ψ the slope angle (figure 7). By differentiating this equation with respect to α, the point in the snowpack with the maximum shear stress can be found. This point is typically located downslope of the load (α < 90- ψ). The point of maximum shear stress at the weak layer can be found by substituting $R = dw * \sin(90 - \psi)/\sin\alpha$ in equation (3), resulting in:

$$\Delta\tau_{xz} = \frac{2P\cos\alpha}{\pi dw\cos\psi}\sin(\alpha + \psi)\sin^2\alpha \quad (4)$$

where dw is the weak layer depth, vertically down (figure 7).

The stability index above focusses on the relation between weak layer strength and state of stress, but does not consider snowpack properties for the stress distribution from the load through the snow. However, the amount of stress (from the external load) reaching the weak layer is strongly dependent on the mechanical properties.

Jamieson and Johnston (1998) adjusted the stability index by focussing on the microstructure of the weak layer. They measured the shear strength of the weak layer using a shear frame and included this in the numerator of the stability index. Furthermore, they included the effect of ski penetration on the shear stress. It is shown that their method was better at predicting the snow stability. In particular, it significantly reduces false stable predictions with respect to Föhn's stability index (Jamieson & Johnston, 1998).

Homogeneous elasticity, as used by Föhn (1987) and Jamieson and Johnston (1998), is a simple but poor way to approach the snow behaviour. It is widely known from field observations that the elastic properties of snow strongly vary with depth and that snow layering plays an important role.

Monti et al. (2016) expanded the stability index by introducing layering and investigated both failure initiation and propagation. They developed a model for the stress caused by a skier using a multi-layered elastic theory. A general theory of elasticity in a layered system was first discussed by Burmister (1945). Monti and others (2016) simplified the layered snowpack in two steps: First, the multi-layered slab is reduced to a single layer with height h_{tot} and representative Young's modulus. The equivalent Young's modulus is found by calculating the average of the moduli:

$$E_e = \left[\frac{\sum_{i=1}^{n} h_i \sqrt[3]{E_i}}{\sum_{i=1}^{n} h_i}\right]^3 \text{ and } h_{tot} = \sum_{i=1}^{n} h_i \qquad (5) + (6)$$

Secondly, the two-layered system (slab and weak layer) is reduced to one single layer by calculating the equivalent depth:

$$h_e = h_{tot}\sqrt[3]{\frac{E_e}{E_{wl}}} \qquad (7)$$

with Young's modulus of the weak layer E_{wl}. The skier-induced stress can be calculated by substitution of the depth in equation (4) from Föhn (1987) with the equivalent depth. The stress obtained from the model is incorporated in the stability index of Föhn (1987).

Monti et al. (2016) showed that largest stresses at the weak layer can be found for a snowpack with a soft slab and hard substratum and vice versa. According to Monti's findings, Boussinesq's method (equation 3) overestimates the additional stress when the slab is harder than the weak layer due to bridging properties. The additional skier stress also strongly decreases with slab depth and becomes less important with respect to the stress caused by the load of the slab. The skier induced stress even becomes negligible when the slab is thicker than approximately 1 meter, depending on the slab density (Monti et al., 2016). Monti's model improves the stability evaluation with respect to standard stability indexes, but a major downside of the method is its inability to discriminate between the layer order which is of major importance for the bridging of the stress.

Booker et al. (1985) developed a solution for the stress below a line load in an elastic half-space where Young's modulus varies with depth according to the simple power law:

$$E = E_0 z^k \text{ for } 0 \leq k < 1 \qquad (8)$$

where E_0 is a constant, and k describing the shape and direction of the curve. Giannakopoulos and Suresh (1997) expanded Boussinesq's solution allowing the elastic properties to vary with depth according to both a power law and exponential description. They found that a decreasing elastic modulus leads to larger stresses close to the surface rapidly declining with depth, whereas an increasing elastic modulus promotes stress transmission to deeper layers. Borstad (unpublished) modified the line load solution of Booker et al. (1985) for a snowpack at an incline. The maximum shear stress at the weak layer (defined by depth H) is given by:

$$\sigma_{xzmax} = \frac{cos^{k+2}\theta_{max} PF}{H}\left[cos\psi cos\beta\theta_{\max} + \frac{k+1}{\beta} sin\psi sin\beta\theta_{max}\right] sin\theta_{max} \quad (9)$$

Where β and F are variables dependent on k and Poisson's modulus ν, P is the line load applied at the surface, ψ is the slope angle, and θ the angle from the z-axis to R (figure 7).

The approach of Borstad described above, provides an opportunity to improve the knowledge of stress transmission from a skier to deeper layers. A model that accounts for continuous variation in elastic modulus can improve stress calculations with respect to a multi-layered approach. These stress calculations combined with the detailed hardness data from the thin-blade hardness gauge contributes to a more accurate prediction of the shear stress reaching a structural weakness in the snowpack. Therefore, it can help improve the stability index and the interpretation of snow pit observations.

3. METHODS

3.1 Field methods

In the winter of 2015-2016, fieldwork was executed in areas around Tromsø and Longyearbyen, Norway. The snow pit locations within these study areas were selected based on the accessibility and safety. The goal is to investigate several different kinds of snowpacks. Often, small slopes were chosen which were representable for large slopes. In other words, small features with the same aspect, elevation, and inclination as the slope of interest, but at a much smaller scale and thus with less consequences if an avalanche would release during the observations. This was not always the case. Sometimes, random slopes were chosen in search for specific features, as the purpose of this study is to look at the differences in stress distribution and not to forecast avalanches.

At each location, a snow pit was dug and a full snow profiles were made. The set-up of the snow pit is shown in figure 8. The stability of the snowpack was assessed by executing one or two extended column tests. A detailed description of the methods used for the snow pit and the stability test is given in the section below. At several locations, a second snow pit was dug after a couple of days. The aim was to monitor the effect of changes over time, like sintering. However, the field methods are destructive; therefore, the exact experiment or measurement cannot be done twice and one specific configuration cannot be monitored exactly.

Besides the observations at the chosen locations, more general observations of a wider area were noted down. For example: characteristics of the snow surface, any recent avalanche observed, wind erosion and deposition, and indications for instability, such as whoomph sounds.

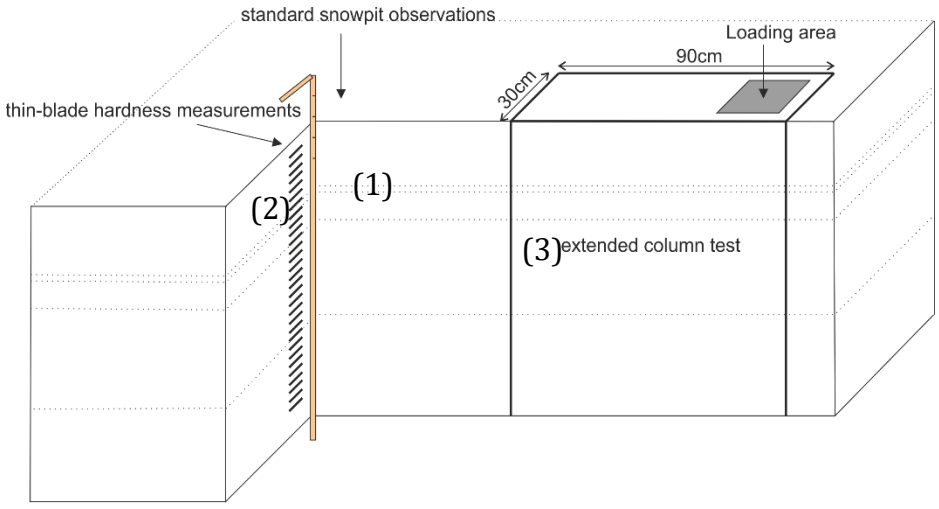

Figure 8. Snow pit set-up with: (1) Standard snow pit observations were done in the corner of the snow pit. (2) thin-blade hardness measurements in the pit wall, near the corner of the snow pit and the standard observations. Measurements were taken every 2 or 5 cm, parallel to the layering. (3) Extended column tests were done in the upslope wall of the snow pit. Here one or two blocks of 90x30x snow pit depth were isolated.

Snow pit procedures

The observations and measurements of the snowpack and its surroundings were made according to the Observation Guidelines and Recording Standards for Weather, Snowpack and Avalanches (OGRS), established by the Canadian Avalanche Association (2014). For every snow pit, the location, slope characteristics, and the weather conditions were described and recorded.

The snowpack observations were done in the side of the snow pit in the shadow to avoid alteration by incoming solar radiation (figure 8). The snow depth, depth of the pit and the height of all individual layers was measured. In cases where the snow pit is dug the full height of the snowpack, 0 cm was taken as the ground level. When the pit is not dug all the way to ground level, the snow surface was taken as 0. The grain type and size of the snow crystals per layer was determined using a hand lens and crystal card. The layer hardness was evaluated using the standard hand hardness test (Quervain, de, 1950) (table 1). For the density, a 250cc RIP cutter and a digital scale are used. The density was only measured occasionally due to the focus on hardness rather than density, and the limited access to a density measurement tool. The temperature was measured starting at the surface, 10 cm below the surface, and then every 10th cm. When coming across a wet snow layer with a temperature near 0°C, the liquid water content was recorded.

Table 1. Hand hardness classification as used for standard snowpack observations (Quervain, de, 1950)

	Hand hardness index	**Object**	**Code**
Very soft	1	Fist	F
Soft	2	4 fingers	4F
Medium	3	1 finger	1F
Hard	4	Pencil	P
Very hard	5	Knife blade	K
Ice	6	-	I

Thin-blade Hardness Gauge

In addition to the standard hand-hardness test, the hardness of the snowpack was measured with a thin-blade hardness gauge (figure 9). The thin-blade hardness gauge is developed by Borstad and McClung (2011). The device consists of a paint scraper attached to a simple push-pull gauge measuring peak resisting force in Newton, the blade hardness index. The thin-blade hardness gauge is objective and gives an actual value to the hardness of the snowpack which can be used to do various calculations, in contrast to the hand hardness test that only gives an approximation of the hardness. Two

Figure 9. Blade hardness gauge, similar to the gauges used in this study. Modified from Borstad and McClung (2011).

different gauges were used. On Svalbard, a 250 N gauge was used with a 0.5 x 10 mm blade. For the fieldwork around Tromsø, a 50N gauge with a 0.6 x 10 mm blade was used.

The hardness was measured in the side wall of the snow pit (figure 8) with a depth interval of 2 cm and in some cases every 5 cm, depending on the snowpack and weather conditions. The snow surface is always taken as 0 depth. To obtain the hardness, the blade is simply pushed 3-5 cm into the snow, parallel to the layering at a constant speed. It is important that the blade is pushed into the snow with a relatively high speed to prevent any effects of rate-dependent deformation. The peak resisting force can be read from the display. This value was later divided by the cross-sectional area of the blade tip.

Extended Column Test

Extended Column Tests (ECT) were performed to evaluate the stability of the snowpack in the field. Since it has been developed by Simenhois and Birkeland (2006), it has been widely used by avalanche forecasters and recreationists. The ECT is easy to execute and is slope representative. It provides information about both the fracture initiation and propagation propensity, in contrast to the compression and stuff block test, which only identify the layers that are prone to fracturing (Simenhois & Birkeland, 2006; Simenhois & Birkeland, 2007).

The ECT has some downsides, however. The tests often overestimate the snowpack instability, especially in the situation of a weak layer below a thick slab. Furthermore, complications occur when the upper layers of the snowpack are too soft. The shovel that is used to apply the load will distort the upper layers.

For an ECT, a column of 90 cm length across the slope and 30 cm in width was isolated using a snow saw and rutschblock cord (figure 8). A sequence of loading steps was applied to one end of the column, starting with 10 taps from the wrist, followed by 10 taps from the elbow, and, finally, 10 taps from the shoulder. These are the same steps as used in the compression test (Greene et al., 2010). The number of taps needed to initiate the fracture and the additional taps needed for the fracture to propagate through the entire column were recorded. The test scores were noted down following the codes described in table 2 with the number of taps and the depth of the fracture in addition (Simenhois & Birkeland, 2007). As an example: the test score of a column that fractured on the 8th tap and propagated on the 12th at a depth of 22 centimetres will be noted as ECTP 8+4 @22cm.

Table 2. Extended column test score recording guidelines (Canadian Avalanche Association, 2014).

Code	Description
ECTPV	Fracture propagates across the entire column during isolation.
ECTP #	Fracture initiates at # and propagates across the entire column on the +# tap.
ECTN #	Fracture initiates on the # tap, but does not propagate across the entire column.
ECTX	No fracture occurs during the test.

3.2 Field areas

Fieldwork was conducted in the area around Tromsø, Norway, and Longyearbyen, Svalbard, Norway (figure 10). These locations were mainly chosen because of logistical convenience. Even though both areas are located far north in arctic Norway, their climates differ and several kinds of snowpack configurations can be studied.

Figure 10. Location of the field areas marked with the squares.

Longyearbyen

Part of the fieldwork was done around the town Longyearbyen on the Norwegian archipelago of Svalbard in the high Arctic. Longyearbyen is located at 78° north at the coast of Adventfjorden in the centre of the Island Spitsbergen.

The snow climate of Svalbard deviates from the three generally defined snow climates: maritime, continental and transitional (McClung & Schaerer, 2006). The snow climate of central Svalbard is described by Eckerstorfer and Christiansen (2011) and is called "High Arctic Maritime Snow Climate". Their study of Svalbard's snow climate was done in the area around Longyearbyen, the same area where most of the fieldwork for this project was done. According to Eckerstorfer and Christiansen (2011), the general snow pack of central Svalbard is relatively thin and cold, with several ice layers and a persistent weakness in the form of depth hoar at the bottom of the snowpack. Svalbard is dominated by direct action avalanches that occur during, or shortly after snowstorms, either involving only newly fallen snow, or failing on structural weaknesses within the 'old' snowpack (Eckerstorfer & Christiansen, 2011).

Despite the influence of the warm sea current, the precipitation is generally low and the snowpack is thin on average. Due to the wind, the snow distribution is extremely uneven. Wind has a major influence on snow distribution on Svalbard, mainly due to a lack of trees. In some areas, the morphology of the mountains plays a significant role. Around Longyearbyen, several mountaintops are flat plateaus where the wind can reach high speeds as it does not experience any resistance of topography or structures over large distances. The prevalent wind direction promotes the formation of cornices on the lee side of ridges. Exposed areas are often completely bare, as the wind swept all the snow away before it had the chance to settle, whereas depressions in the landscape allows the snow to accumulate several meters deep.

The warm seawater causes large fluctuations in temperature throughout the season. The average winter temperature is -16.2°C (Norsk Meteorologisk Institutt, 2016), but periods with positive degrees are common. Reoccurring periods with warmer temperatures lead to the formation of ice crusts in the snowpack when the snow surface melts and subsequently refreezes when the temperatures drop. Large temperature gradients within

the snowpack can occur during periods with very low air temperatures. It is not unusual for the temperatures to drop below to -20°C regularly during winter. However, the temperature at the base of the snowpack is controlled by permafrost and thus typically colder than the 0°C which is the normal case in most mountainous regions at lower latitudes.

Tromsø

Tromsø is a city located in northern Norway (figure 10), approximately 300 kilometres north of the Arctic Circle. The fieldwork is conducted in both the coastal and the inland areas around the city of Tromsø. One of the major locations is the Island of Kvaløya, west of Tromsø.

The specific snow climate of the Tromsø region has not been described yet. Like Longyearbyen, Tromsø is located near the coast. Therefore, the climate is largely influenced by the northern branch of the Gulf Stream: the warm Norwegian Current. This leads to large fluctuations in the winter temperature: during the season, temperatures above 0°C are frequently reached, but also colder periods when the temperatures drop below -10°C are common. Wind from the west brings in warm moist air, whereas wind from the east leads to stable cold weather. The moist wind from the sea can lead to rapid snow accumulation. Not far inland the climate changes, and the coastal influence becomes less. This leads to a colder climate with less precipitation. The most representative predefined snow climate for Tromsø would be Maritime. The average winter temperatures in Tromsø are relatively mild and the snowpack is generally thick (Norsk Meteorologisk Institutt, 2016). These two characteristics lead to a relatively low temperature gradient, typical for maritime snowpacks (McClung & Schaerer, 2006).

3.3 Stress calculations

To improve the understanding of the stress distribution through the snowpack with respect to its physical properties, numerical models were constructed. The data gathered in the field was used as input for the models, with foremost the detailed blade hardness data. Figure 11 shows the concept of the stress distribution below a skier represented by a line load.

The variation of blade hardness with depth was approximated using different analytical functions by least square regression (figure 12). These relations simplify the hardness or elastic modulus as a parameter and enables the use of the elastic modulus in general solutions like Booker et al. (1985) and Giannakopoulos & Suresh (1997). A simple power law and exponential law were fitted to plots of the hardness profiles and their goodness (R^2) was determined. As the blade hardness and elastic modulus are linearly related it is not of concern which is used for the fitting of the functions.

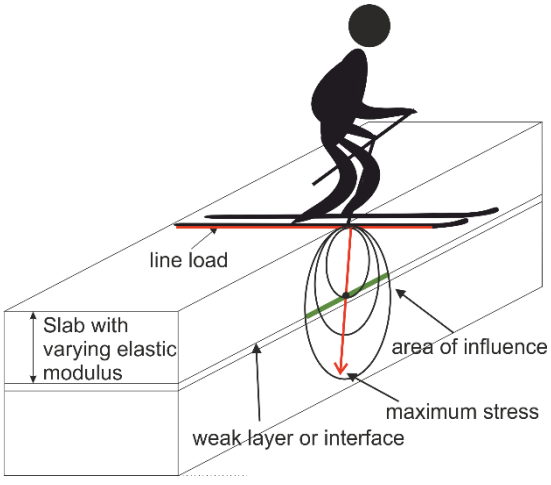

Figure 11. Conceptual model of the stress distribution below a skier as a line load in a non-homogeneous snowpack. The red vector shows the direction of the maximum stress, with the point of maximum stress at the weak layer. The green line represents the area of influence on the weak layer.

Equation 1 was applied to calculate the elastic modulus from the measured blade hardness:

$$E = 0.475 * B \qquad (10)$$

However, C = 0.475 is not valid for both blades used.

The line load solution for a sloping, non-homogeneous half space from Borstad (unpublished) was used to calculate the radial stress and shear stress induced by a skier at any point in the snowpack (equation 9). The maximum shear stress that can reach the weak layer is of major interest and was calculated for several slope angles and hardness variations. The value of Poisons' ratio was estimated to be 0.25, which is often used as a representative value for snow (Habermann et al., 2008; Monti et al., 2016).

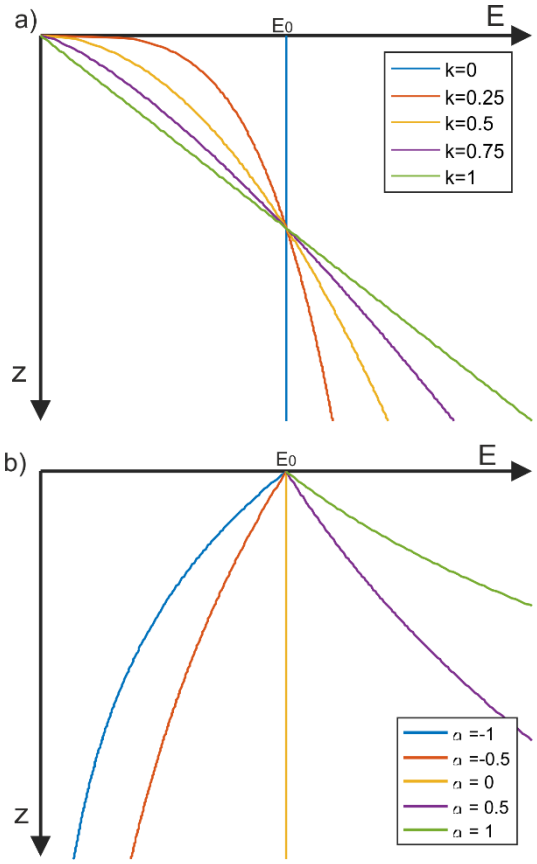

Figure 12. Models that are fit to the hardness data from the field. a) power law curves $E = E_0 z^k$ with 0 < k < 1, and b) exponential curves, $E = E_0 e^{z\alpha}$. Homogeneous slabs are represented by k=0 or α=0.

For the models, the response of the snow to stress was assumed to be elastic instead of viscoelastic behaviour, which would be a more accurate rheological description of snow. Deformation in snow is largely strain rate dependent: the response of the snow is more elastic with high rates, whereas low strain rates lead to plastic behaviour. The simplification to elastic behaviour was made because in the case of a skier triggering an avalanche, the loading is generally rapid. Loading by a skier lasts approximately 0.05 to 0.20s (Wu et al., 2005) which was assumed to fall entirely in the elastic regime. Also, the loading steps of the stability tests were assumed to be in the elastic regime, and between the different steps the load is removed. Furthermore, pure elastic behaviour makes the calculations much simpler. The high temperature sensitivity is expressed in the mechanical properties of the investigated snowpack such as the hardness and the density. The stress distribution is therefore indirectly dependent on changes in temperature, but temperature itself is not part of the equation.

The calculations solely analyse the stress added by an external load. The stress caused by gravity was later added to the results and is simply expressed as:

$$\sigma_{xzsw} = \rho g H sin\psi cos\psi \qquad (11)$$

with average slab density ρ. The density has only been measured occasionally in the field and therefor the density is estimated for the different snow layers, using the density measurements of Geldsetzer and Jamieson (2000).

The shear strength of the weak layer, needed for the stability index, was not measured in the field, but was calculate according to the method of Höller and Fromm (2010):

$$\tau_S = \frac{1}{b} \ln(\frac{B_{wl}}{a}) \qquad (12)$$

where B_{wl} is the weak layer hardness, and a and b are constants, 9041 and $4.86*10^{-4}$ respectively. By inserting equation 9, 11, and 12, in equation 2 the stability index becomes:

$$S = \frac{\tau_s}{\sigma_{xzmax} + \sigma_{xzsw}} \qquad (13)$$

For each snow pit, the results of the numerical stress model and the stability index were compared with the ECT test results of that pit. If the model predicts a significant shear stress at the weak layer, an unstable test score might be expected depending on the nature of the weak layer. Snowpacks which were classified as stable in the field are expected to have physical properties that avert stress penetration to the weak layer, according to the calculations. Furthermore, the calculated shear stresses reaching the weak layer was compared to a homogeneous model using the k-value of Habermann et al. (2008). The k-value expresses the ratio between the additional shear stress calculated with the particular method of interest and the maximum shear stress calculated with equation 3 (Föhn, 1987) for the homogeneous case. To avoid confusion, Habermann's k-value will be referred to as kh due to the use of k in equations described later in this paper. kh<1 represents a reduced stress with respect to the homogeneous slab, whereas kh>1 indicates higher stress values.

To compare the relation between hardness in the slab and shear stress at the weak layer, a modified version of the bridging index (BI) from Thumlert & Jamieson (2014) was used. Instead of multiplying hardness with the layer thickness, the sum of the blade hardness values of the slab was taken, multiplied by the interval of the measurements:

$$BBI = \sum_{i=1}^{n} B_i * interval \qquad (14)$$

Where n is the total amount of hardness measurements in the slab. The interval was either 2 or 5 cm.

4. RESULTS

4.1 Field measurements

In the winter season of 2016, 23 snow pits were dug of which 21 were useful for evaluation. Appendix 1 gives an overview of all measured parameters for each pit. The data for each pit is displayed in a standard snow profile (figure 13 and appendix 2). Five times, no fracture occurred during the extended column test (ECTX), six tests resulted in fracturing without propagation (ECTN) and in nine of the snowpacks propagation occurred (ECTP). However, a snowpack with a propagating fracture is not necessarily regarded as an unstable snowpack. In many cases, the high number of taps between initiation and propagation of the fracture and the shear quality indicated stability. Based on the snow profiles and the stability test results, the stability of 6 of the 23 snowpacks are classified as 'fair' and 16 out of 23 are classified as 'good'. Only one of the snowpacks observed has a 'poor' stability. Two of the ECTN results were dubious due to collapsing of the very soft slab during the execution of the test. The fracture might have had propagated if it was not for the deformation around the shovel. One snowpack contained moist snow all throughout the whole snowpack. These three results are discarded in further evaluations of the data.

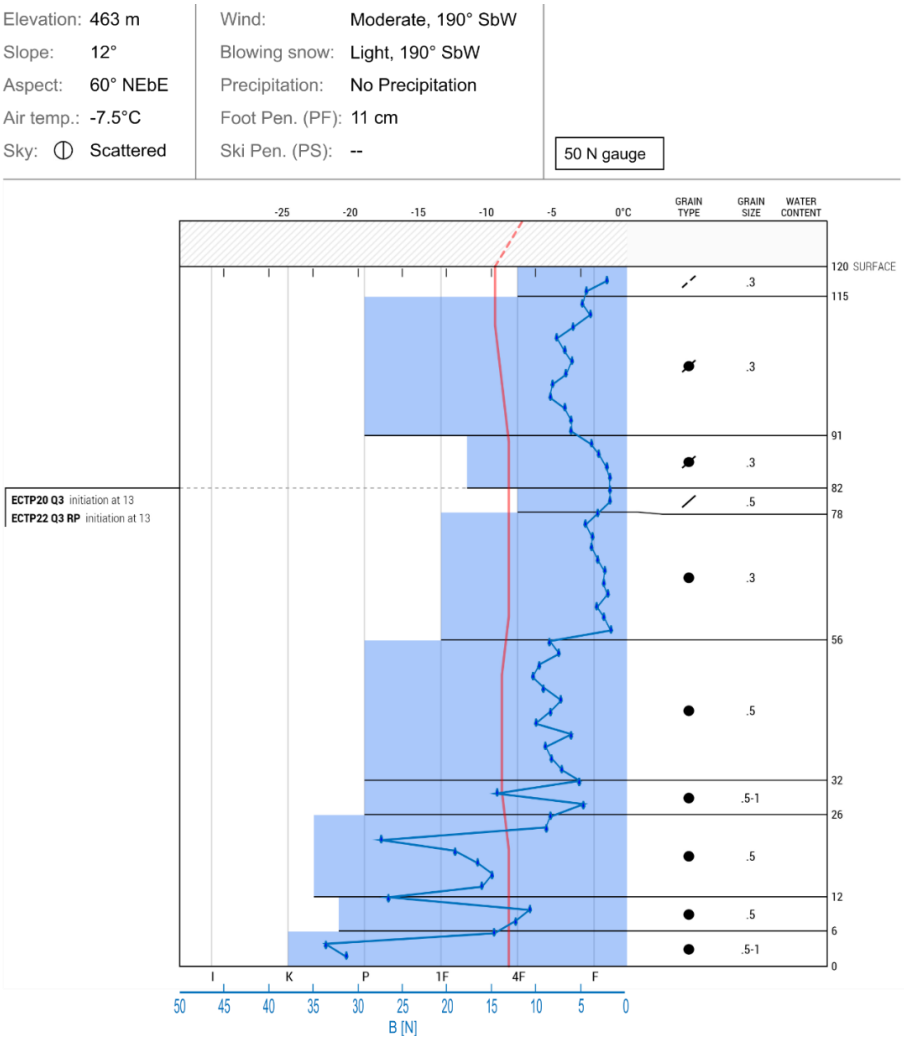

Figure 13. Example of a full standard snow profile with additional thin-blade hardness data. The full profile can be found in appendix 2, 20160303

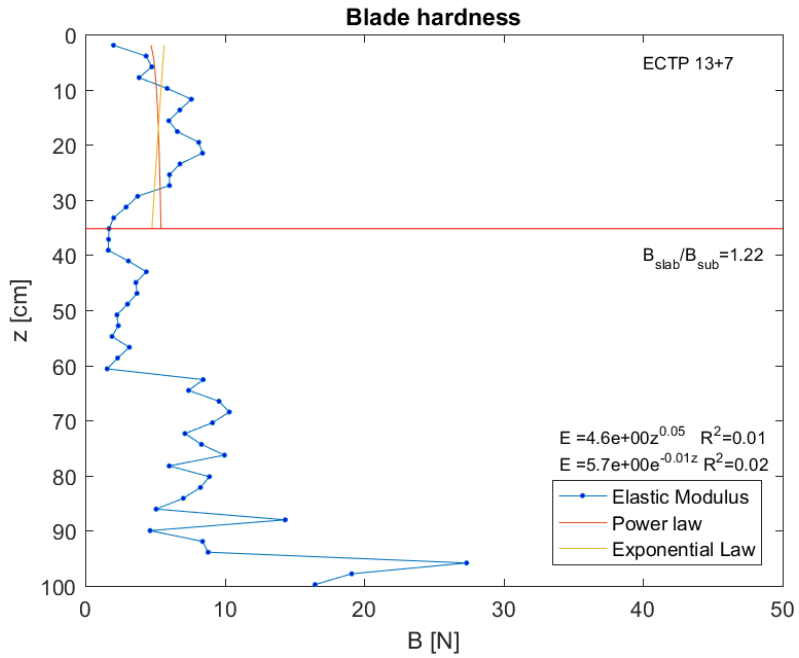

Figure 14. Thin-blade hardness profile with fitted exponential and power law regressions. Equations and goodness of fit are given above the legend. B_{slab}/B_{sub} represents the ratio between the blade hardness of the slab, measured directly above the weak layer, and the hardness of the substrate, measured directly below the weak layer. The ECT score of the specific snow profile is given in the upper right corner.

Hardness

The thin-blade hardness measurements are plotted on top of the hand hardness in the snow profiles (figure 13, appendix 2). The blade hardness is more detailed and shows many variations where the hand hardness is uniform. However, some layers that were smaller than the measurement interval are missed by the blade hardness. The blade hardness measurements in the slab are of main interest and are approximated for each case by a power law equation and an exponential equation (figure 12, appendix 2). Figure 14 shows an example of a snow pit where the power law gives a slightly better fit than the exponential law and a homogeneous solution. The power of the power law (k-value) is

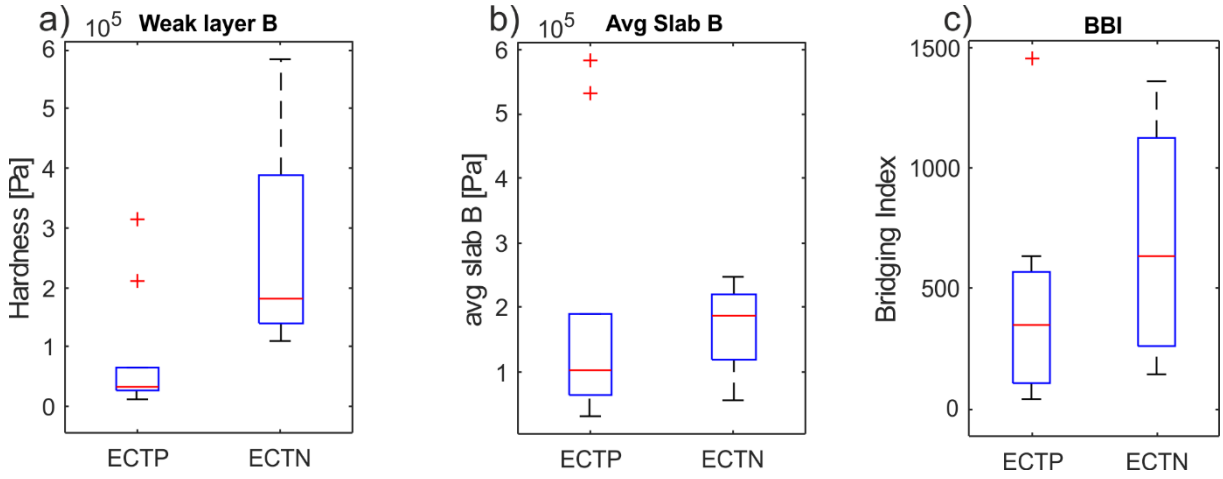

Figure 15. Summary of the blade hardness values (B) obtained in the field, sorted by ECT score. a) the weak layer blade hardness, b) the average hardness of the slab. C) represents the bridging index, calculated using the blade hardness.

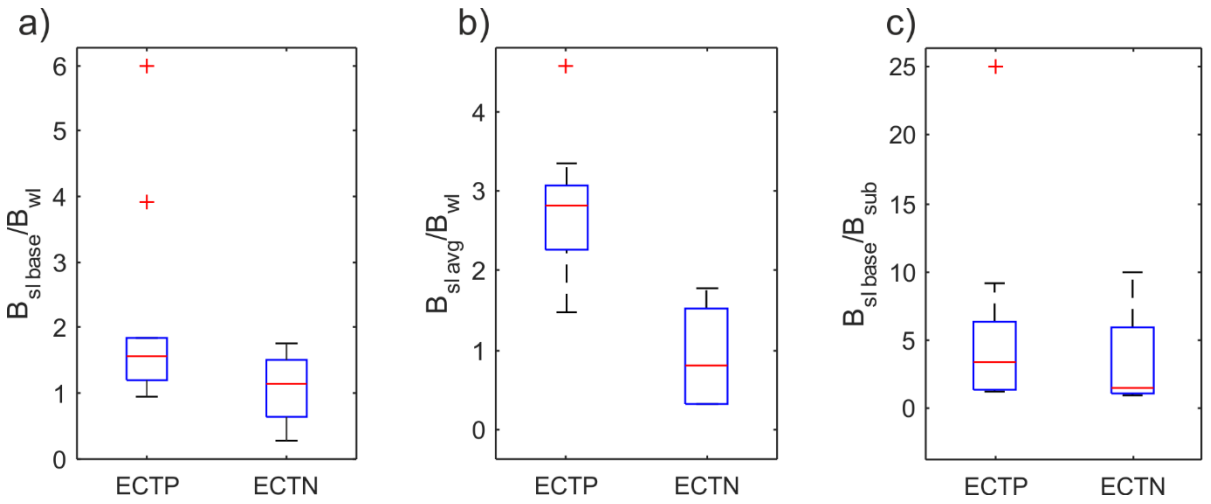

Figure 16. Blade hardness ratios between a) the base of the slab and the weak layer, b) the slab average and the weak layer, and c) the slab base and the substrate. The hardness measurement directly below the weak layer is used for the substrate hardness.

used for further calculations. For 10 out of 21 snow profiles, the power law is a reasonable fit. For the 11 remaining profiles, the exponential equation provides a better fit.

Figure 15a shows measured blade hardness of the weak layer and figure 15b illustrates the average blade hardness for the slabs investigated and their correlation with the ECT scores. In general, the harder the slab the higher the ECT score. However, propagation occurred below slabs with a wide range of hardness values and the highest value measured was in a slab with an ECTP result. Fracture propagation happened most often in soft weak layers, but also here, a wide range of values were measured. The same trend with ECT score is shown by the bridging index (figure 15c). The boxplot of the bridging index shows again a wide range for the 2 test scores, but it becomes clear that propagation has an overall lower BBI than just fracture initiation. There is a significant difference in the median BBI. No data is available for ECTX stability tests, because the weak layers were not identified or did not exist.

Ratios of the blade hardness between the slab, weak layer, and substratum were calculated (figure 16). All three figures indicate a trend that it is more likely to propagate a fracture when the hardness ratio is high, but the figure also expresses the large uncertainty in the data. The slab average to weak layer hardness ratio displays most pronounced difference between ECTP and ECTN.

Depth of the structural weakness

Furthermore, the depth weak layer (or weak interface) depth was recorded and compared (figure 17). Most often, propagating fractures were found below thin slabs, and propagation was predominantly absent when the weak layer was deeper than 30 cm.

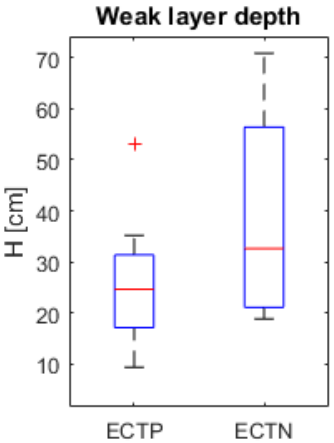

Figure 17. Weak layer depth of all snow pits sorted for the ECT results.

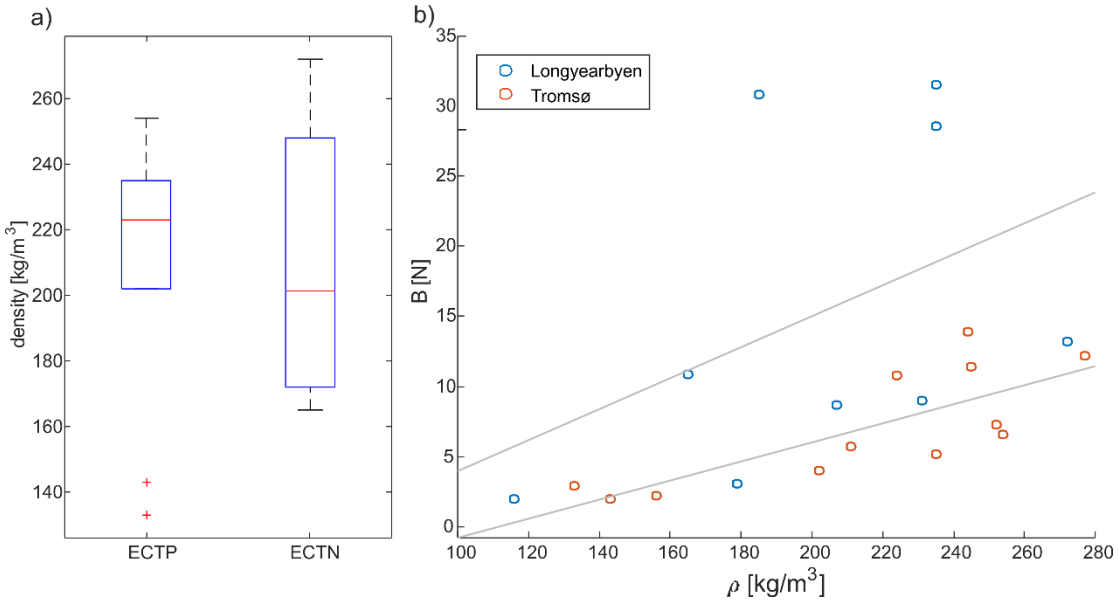

Figure 18. a) estimated densities for each snow pit ordered per ECT score, b) the relation between the density and blade hardness with trendline for the two datasets from Longyearbyen and Tromsø.

Density

The density of the slab of each snow pit was estimated according to the method of Geldsetzer and Jamieson (2000) using the hand hardness and the grain type from field observations. The density demonstrates a poor correlation to the ECT scores (figure 18a). Snow profiles with ECTX have on average the highest densities and the lowest densities were measured in slabs with a ECTP score. The estimated densities were plotted against the blade hardness and are shown in figure 18b. The trendlines indicate a weak relationship between both properties, where the correlation is better for the Tromsø data than for the data from Longyearbyen. In general, the snowpack around Longyearbyen had a greater hardness than the snow in the Tromsø area whereas both had a similar average density.

4.2 Calculations

Theoretical solution

The stress below a skier or line load can be represented as a two-dimensional bulb below the load (figure 19). The shape and orientation of this bulb changes with changing slab properties and slope angle. The shear stress through a homogeneous slab (k=0) and a slab with a linearly increasing hardness (k=1) are considerably different. The bulb of the k=1 slab penetrates significantly deeper into the snowpack, but has a lesser horizontal extent.

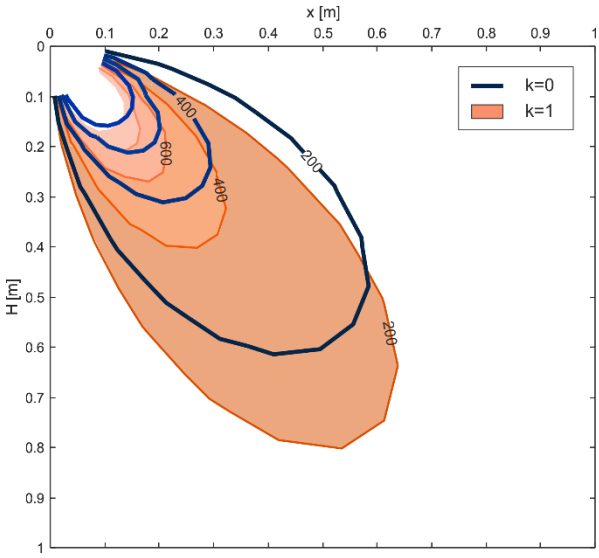

Figure 19. Shear stress bulb through a snow slab, induced by a surface load of 500N, at a slope of 35°. k=0 represents a homogeneous snowpack whereas for k=1 the hardness increases linearly with depth. Stresses are in Pascal [Pa]. H is the depth perpendicular to the snow layering, and x is the axis along the snow surface (figure 7).

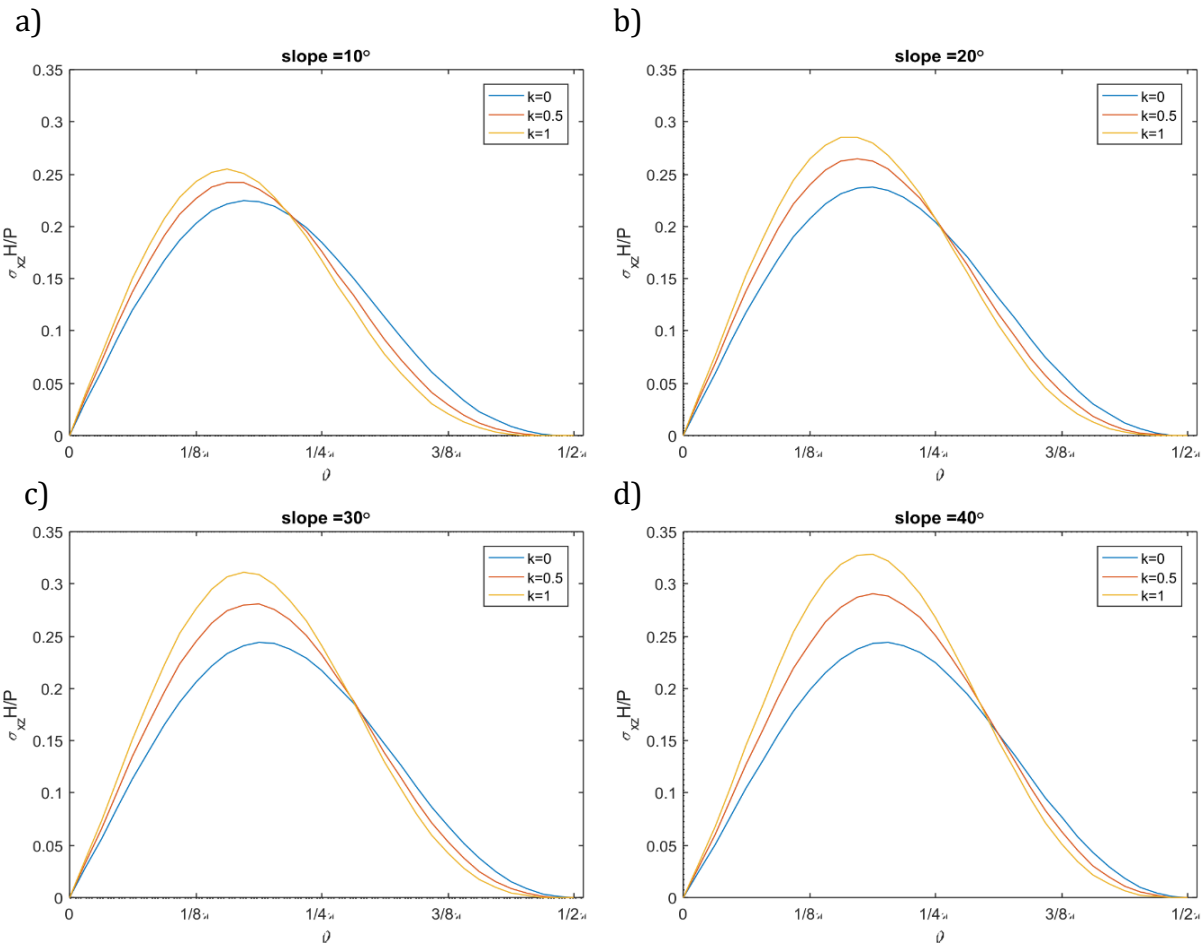

Figure 20. Shear stress for a given weak layer depth H and line load P for various values of k and slope angles: a) 10°, b) 20°, c) 30°, and d) 40°. k=0 represents a homogeneous slab.

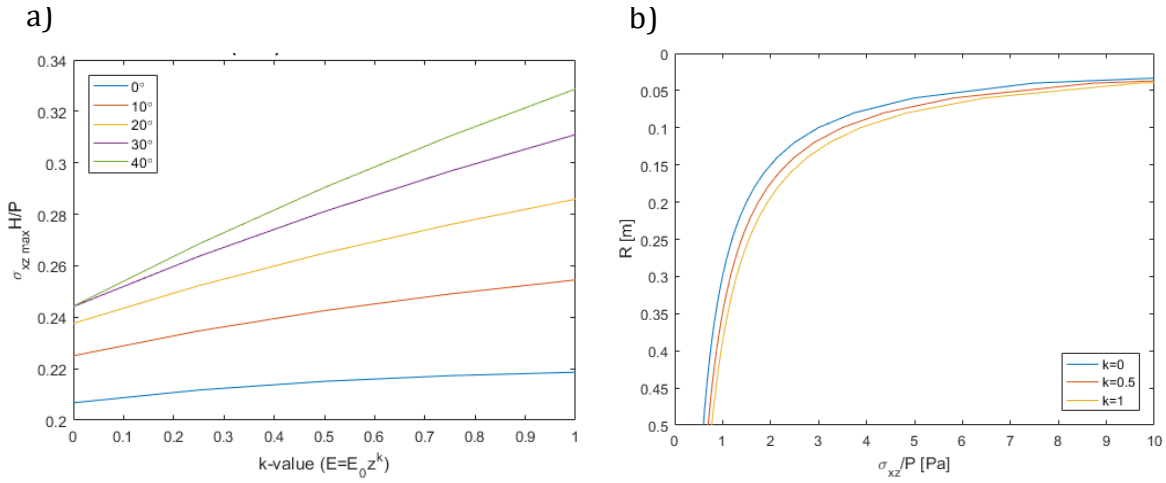

Figure 21. (a) Maximum shear stress, for a given weak layer depth H and line load P. (b) Stress decrease with depth directly below the line load.

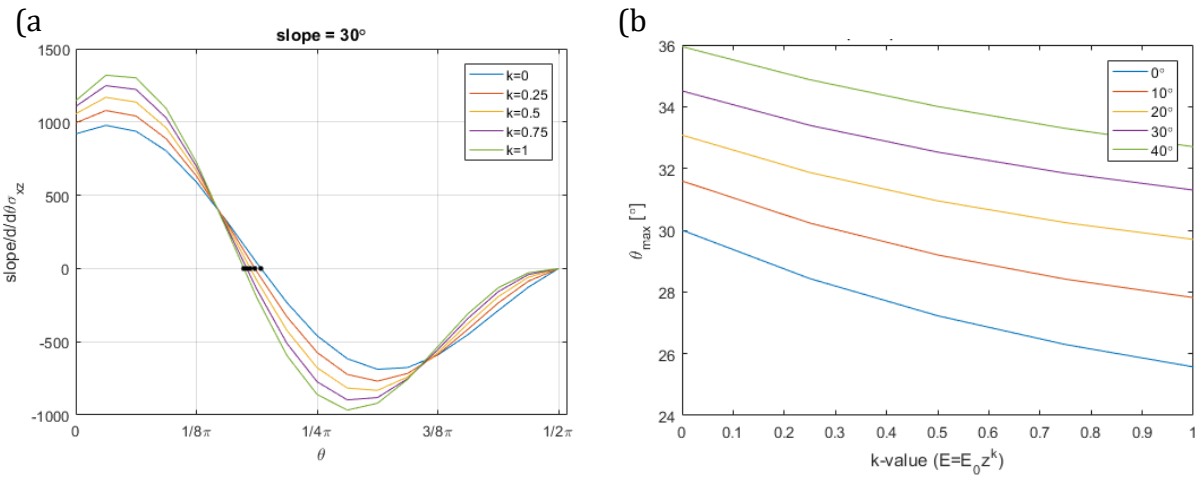

Figure 22. (a) Different locations of points of maximums stress at the weak layer. (b) Location of the maximum stress depending on the k-value and the slope angle. A lower theta represents also a shorter distance to the weak layer (R).

Figure 20 displays the shear stress along the structural weakness in a snowpack resulting from an external load, calculated using the method from Borstad (unpublished) for different k-values and various slope angles. Considering these graphs some remarks can be made: First, a homogeneous solution always underestimates the stress when the slab increases in hardness. In other words, the stress at depth is always higher for slabs where the hardness increases according to the power law, with respect to a homogeneous slab. Secondly, what stands out is that the difference between the homogeneous case (k=0) and an increasing hardness with depth (k>0) becomes more pronounced while moving up in slope angle. Therefore, the larger the slope angle, the more important the consideration of a non-homogeneous snowpack. This is highlighted in figure 21a. It summarizes the shear stress calculations varying with both the slope angle and the k-value for the points of maximum stress in the snowpack. The shear stress is plotted for an arbitrary weak layer depth and line load. On the left side with lower k-values, the lines per slope angle are relatively close together, whereas they move further apart with increasing k-value. However, the deeper the weak layer, the less variance. The difference between k=0 and k=1 becomes negligible beyond a certain depth (figure 21b). This is in accordance with the stress measurements in the field by Schweizer and Camponovo (2001). Furthermore, the peak in the graphs of figure 20 represents the maximum stress possible at the weak layer, and the corresponding θ is the location of the point of maximum stress. This point moves along the weak layer with changes in slope angle and k-value. When the hardness increases downward in the snowpack, the point of maximum shear stress moves further upslope towards the z-axis, closer to being directly under the load at the surface (figure 22).

Using snow pit data

The additional stress at the weak layer, induced by a skier or other load at the surface, was calculated for each set of field measurements (appendix 3). An example is shown in figure 23 where the k-value was only slightly different from the homogeneous case, too small to be demonstrated by the kh-value. This was often the case and only a few snow profiles show a significant difference between the homogeneous and non-homogeneous solution. The largest difference was found for snow pit 20160212, which has a difference

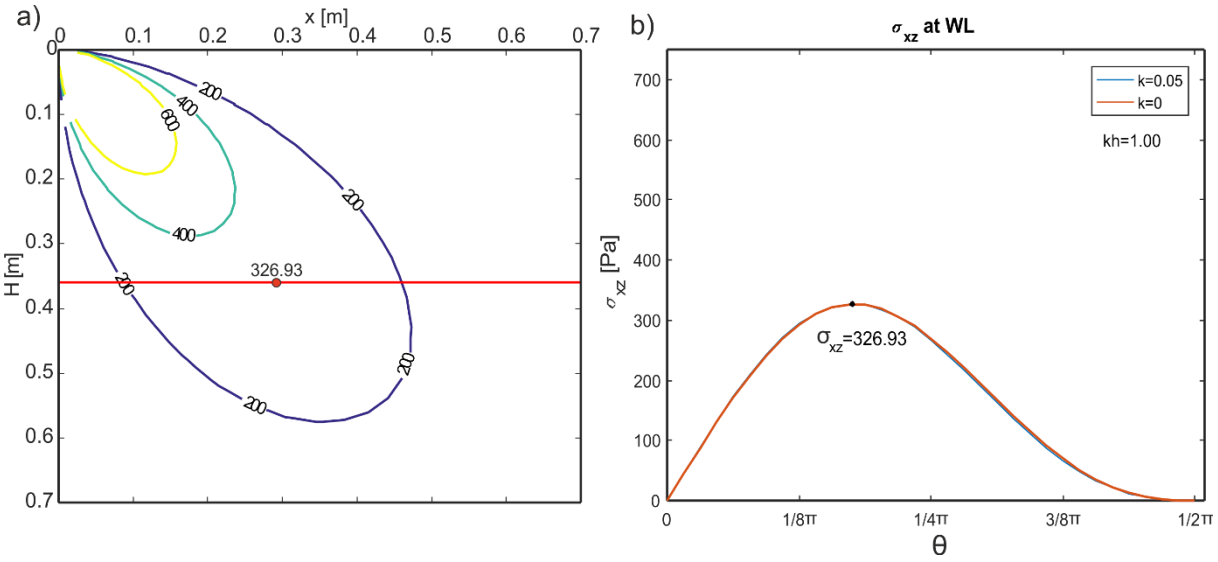

Figure 23. Shear stress at the weak layer for snow pit 20160303 (appendix 2), calculated using the non-homogeneous solution of Borstad (unpublished). a) the stress bulb below the load, and b) the stress at the weak layer. The peak shear stress at location θ on the weak layer is 326.93 Pa. For this case, the difference in maximum shear stress between a homogeneous slab and a non-homogeneous slab was negligible (kh=1.00).

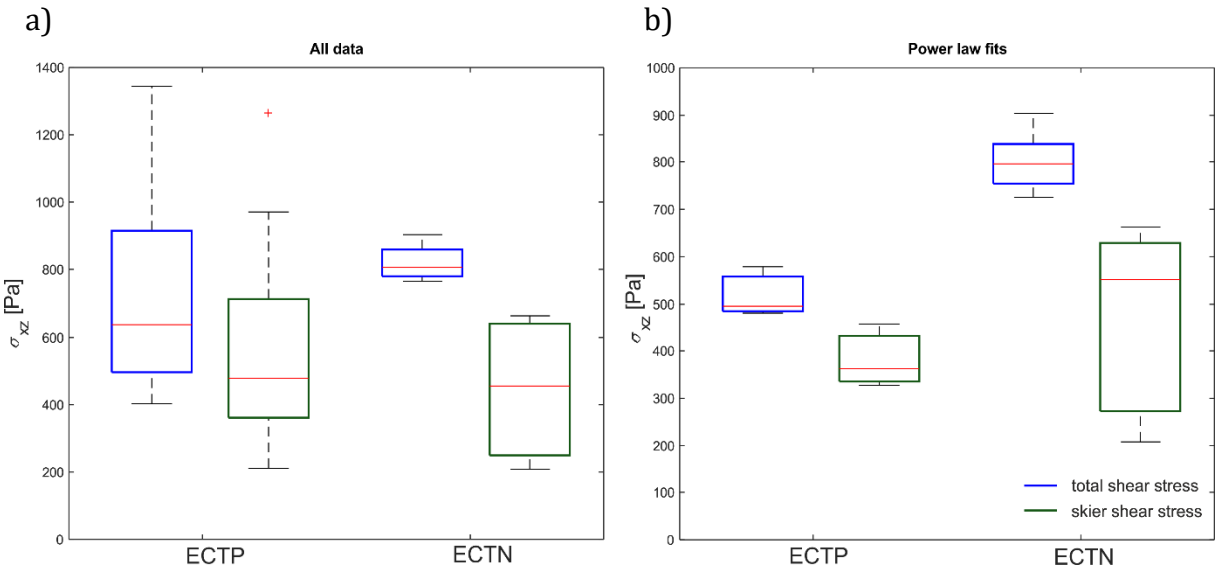

Figure 24. Distribution of the calculated shear stresses per observed ECT score for a) all data, and b) data for which the power law was the better fit (only 10 data points).

of 168.12 Pa (appendix 3). Figure 24a summarizes the resulting maximum shear stress, for all snow pits sorted by ECT score, for the stress induced by an additional load and for both the additional load and the gravitational shear stress. It appears that a wide range of stresses can lead to each of the ECT scores and no evident link between the shear stress and stability is demonstrated. The median of the all data boxplots for the additional load has an increased value for ECTP and is the lowest for ECTN. However, for all the other plots, the trend is the opposite (figure 24a and b). The total stress for the power law fits shows the most pronounced stress difference between propagating and non-propagating

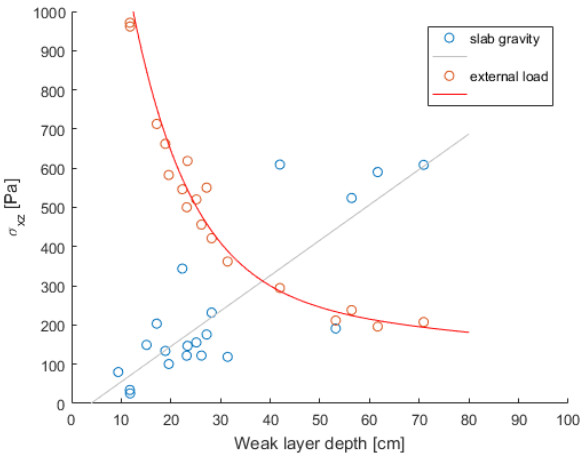

Figure 25. Shear stress induced by slab gravity and the external load, calculated for each data point.

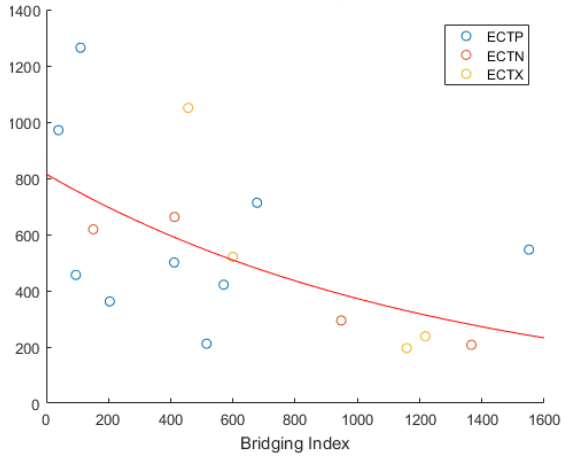

Figure 26. The relation between the maximum shear stress and the bridging index of the slab.

fractures. It must be kept in mind that the for the power law fits only 2 data points were available for ECTX, 5 for ECTN, and 3 for ECTP.

The significance of the additional load with respect to the slab gravity depends on the thickness of the slab (figure 25). The stress from the external load decreases exponentially with depth, whereas the stress due to the weight of the slab increases linearly (equation 11). Where the two trendlines intersect, the weight of the slab becomes more substantial compared to the added load, for most of the snow pits. The ratio of the two shear stresses did not show a relation with the ECT scores. In addition, the calculated stresses were compared to the bridging index of the slab (figure 26). A weak relation can be found between the stress and the BBI. In general, the higher the bridging index the lower the stress.

Shear strength and stability index

The shear strength of the weak layer was obtained with the equation of Höller and Fromm (2010) and is shown in figure 27. The stability index, defined with this shear strength and the calculated shear stress, shows a clear distribution between ECTP and ECTN scores (figure 28a). On average, propagating fractures have a reasonably lower stability index than fractures that did not propagate during the stability tests. When the ECT scores are ranked according to stability, a weak trend can be found (figure 28b), which confirms the correlation between the numerical stability index and the field observations. The results of the stability index applied to our data was also compared to the hardness ratio between the

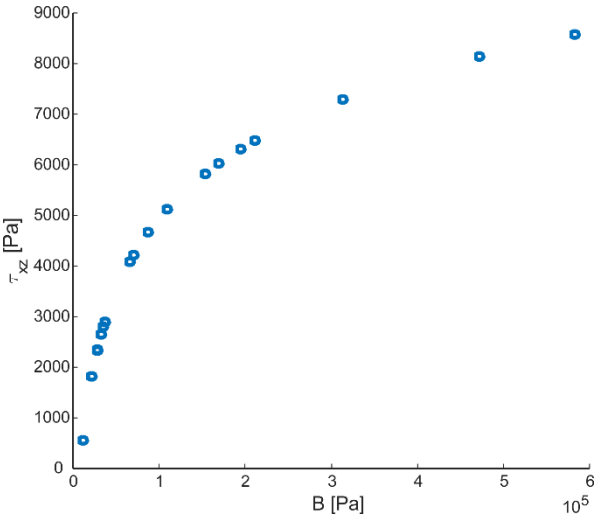

Figure 27. The shear strength from the the blade hardness according to the relation from Höller and Fromm (2010).

slab average and the weak layer, and the slab base and the weak layer (figure 29). The ratio of average slab hardness and weak layer hardness display a very weak correlation with the stability index, whereas for the ratio between the slab base hardness and the weak layer hardness this trend with the stability index is absent. The stability index values are relatively high, and in only one occasion the stability index was lower than 1 (appendix 3), for 20160317, which corresponds to a stability test score of ECTP 1.

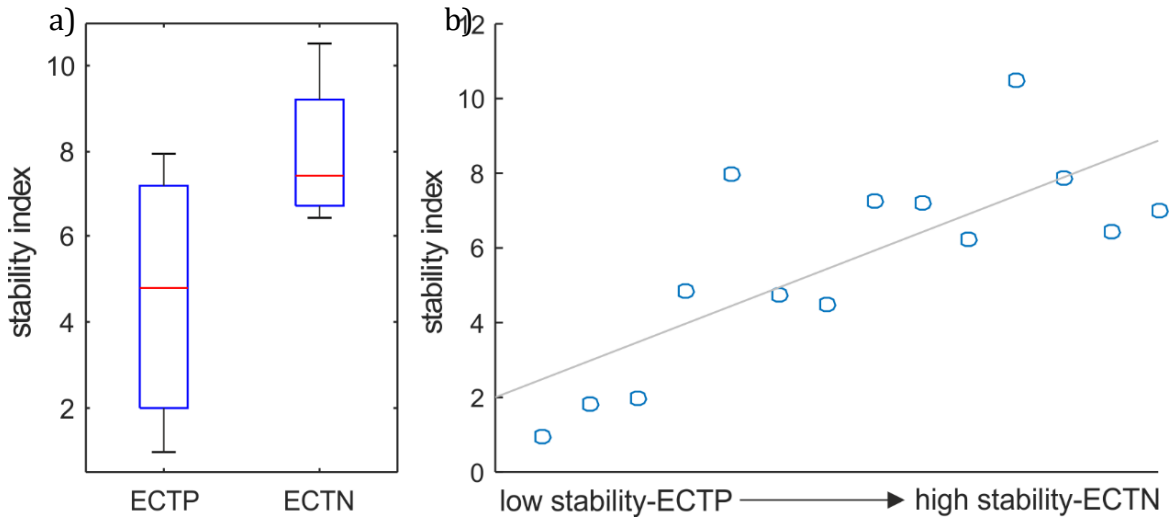

Figure 28. a) boxplot of the stability index ordered by ECT score. b) The stability index versus the ECT scores ranked by stability.

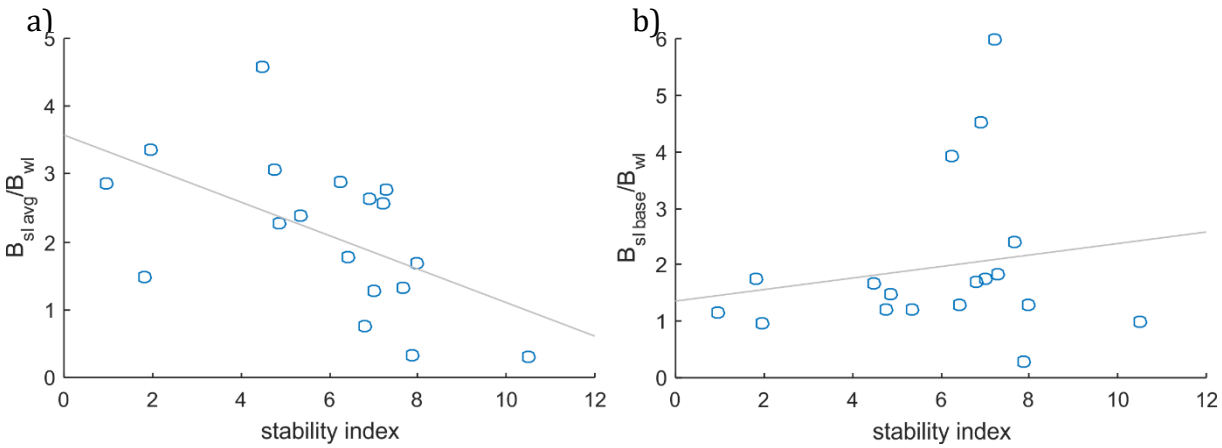

Figure 29. The stability index compared with a) the ratio between the average slab hardness and the weak layer hardness, and b) the ratio between the hardness of the base of the slab and the hardness of the weak layer.

5. DISCUSSION

5.1 Field observations

Thin-blade hardness

It is clear that the blade hardness provides more detailed and useful data than the hand hardness test. This data is crucial for the stress calculations. Hardness differences within individual layers, that would be neglected with the hand hardness method, can be recorded in detail. However, when measuring the hardness at a constant interval of 2 cm (as done for this study), smaller layers and important layers might be overlooked. Measurements with a smaller interval are difficult to execute and affect the hardness of the measurements above and below. Therefore, it is suggested to measure important layers that are thinner than 2 cm in addition to the normal interval to improve the integrity of the data.

Like in various previous studies (Mellor 1975; Shapiro et al. 1997; Borstad & McClung 2011), the results of this study indicate that hardness gives a much better correlation with several important snowpack properties and stability, with respect to the density (figure 15, 16, and 18). Propagation was most frequently observed below soft, thin slabs, within a range of densities. Therefore, hardness is more useful as an index property. Moreover, the thin-blade hardness gauge is easy to use and requires less actions than measuring the density for each layer. Another advantage is that only relative hardness is needed for stress calculations. Therefore, measurements from gauges that do not have exactly the same size blade can still be used.

The field observations and previous studies (Schweizer & Jamieson, 2001; Schweizer et al., 2003) indicate that the hardness ratio between the slab and the substrate plays an important role in the propagation of fractures across the weak layer or interface. The highest blade hardness ratios were found for propagating fractures (figure 16) which corresponds to previous research (e.g. van Herwijnen & Jamieson, 2007). The usefulness of hardness related parameters underlines the importance of hardness. It is impossible to obtain data for the hardness ratio without a well-functioning hardness gauge and it shows the need to adapt the thin-blade hardness gauge as a standard piece of equipment in avalanche research and forecasting.

The bridging index correlates reasonably well with the ECT scores (figures 15c) and a weak relation with the shear stress can be observed (figure 26). The results are in agreement with the findings of Thumlert and Jamieson (2014) and show that the bridging index is a useful and simple index that can help stability evaluation. However, our bridging index values cannot be directly compared to the index and thresholds from Thumlert and Jamieson (2014) because of the difference in method, i.e. the use of more accurate hardness data.

5.2 Stress calculations

General constraints of the method

The methods used for this paper encounter some complications. First, the amount of data used in this study is limited and was insufficient to draw some of the conclusions with a large certainty. Secondly, the best fit regressions of hardness assigned to the snowpack will ignore any peaks and valleys in the original profile. Layers with a significantly larger hardness will distribute the stress more parallel to the layering and less downwards. Therefore, the shear stress will be overestimated when the snow pack contains many small layers with deviating hardness values, such as ice layers. Also, the method used is only suitable for a slab with soft over hard snow up to a homogeneous slab. For a hard over soft slab, an exponential approach would be better and a different calculation would be needed. The exponential model cannot be solved analytically and requires a numerical solution.

Furthermore, many assumptions had to be made to obtain a manageable equation for the stress. The force of a skier is represented as a horizontal line load acting vertically down at the surface. In real life, a skier is often orientated with respect to the slope and the area of the skis that touches the snow surface varies. Therefore, the maximum stress exerted by a skier might be underestimated. In addition, for real life situations, the depth of ski penetration must be considered. The top layers will be compressed to a certain amount depending on the hardness, and as a result, the stress is not applied at the very top of the snowpack. However, according to Schweizer et al. (1995) the effect of compaction can be ignored for most snow pits as it has a significant effect on very soft snow only.

Finally, properties of the weak layer itself and the snowpack below the weak layer were not taken into account in this study. The underlying snow layers might, however, have a significant influence on the stress concentration in the weak layer (van Herwijnen & Jamieson, 2007; Habermann et al., 2008). Correspondingly, Monti et al. (2016) found a significant increase is stress in the weak layer for snow packs with a hard substratum, the substratum acts as a stress concentrator.

Stress and fracture propagation

The models show that the resulting shear stress at the weak layer after loading is significantly higher for a soft slab with increasing hardness downward in the snowpack (power law regression, $k>0$), than for a slab with a uniform hardness ($k=0$). The stress cannot dissipate layer-parallel (bridging) because of the absence of hard layers, and is transferred deeper downwards into the snowpack (figure 19). For this case, simple stress calculations using only a homogenous slab always underestimate the stress at the weak layer. For a snowpack with hard layers on top and a decrease in stress downwards through the slab, it is expected that the homogeneous approach overestimates the shear stress. The exponential law gives a much better fit than the power law in the case of a hard over soft slab. Even though the exponential case was not solved, the results of the stress calculations where the exponential law was the better fit are still of value. They show the maximum shear stress possible, because bridging of the hard layer in the upper part of the slab can only lead to a stress reduction. It would be valuable to calculate the stresses with the exponential law in future research in order to cover a wider range of hardness profiles with a larger certainty.

The importance of the difference between hard over soft slab versus soft over hard slab for stress calculations and evaluations was already recognized in previous literature. Schweizer and Camponovo (2001) showed that a soft slab enables the skier induced deformation to reach the weak layer efficiently. Furthermore, Schweizer et al. (1995) stated that a hard upper-layer causes bridging and the stress will be more spread out horizontally. The method used for this paper, where different regressions are fit to the hardness, provides the possibility to account for the different hardness profiles, in contrast to methods where the effect of layer order is not taken into account (e.g. Monti et al., 2016).

The deviating results for the good power law fits (figure 24b) might be an effect of the limited dataset (9 profiles, 3 ECTP, 5 ECTN, 2 ECTX). The uncertainty is so large that both an increase and decrease of stress are possible while moving from ECTP to ECTN, for the skier induced shear stress. The large spread of the results can also be due to other factors which have to be taken into account. Many aspects can lead to an unstable snowpack regardless of the stress. The results of the individual snow pits (appendix 2) also show that a significant increase in hardness downwards (k>0) does not necessarily lead to propagation. Other factors that play a role in fracturing are for example deformation energy, the presence, depth, or strength of a weak, and type of crystals in the weak layer. It is therefore not adequate to look solely at the shear stress.

Shear stress decreases exponentially with depth. Therefore, it is unlikely to trigger a very deep weak layer as a skier. Similarly, the deeper the slab, the higher the bridging index. Figure 16 shows that most propagating fractures were found below shallow slabs, regardless of the slab properties. This is in agreement with the findings of van Herwijnen and Jamieson (2007), who found that skier-triggered avalanches most frequently happened in snowpacks with a slab between 20 and 30 cm thick.

Stability index

Without a stability index, the stress calculations are of minor value. The stability index correlates much better with the ECT scores than the shear stress alone (figure 24 and 28). It correlates well with the ECTP of ECTN and is consistent with the stability evaluation in the field. Most profiles tested were rather stable, therefor high results of the stability index were expected. The only unstable result of the stability index was the one of the only snow pit that was assessed in the field as unstable (20160317). So, the stability index successfully discriminated between stable and unstable snowpacks. However, our dataset was too small to assure the integrity of this stability index. The limited amount of data complicated the comparison with other methods, therefore, we are unable to conclude that this stability index is an improvement with respect to previous studies. Furthermore, deviations can occur because of the method of calculating the shear strength of the weak layer. Field measurements of weak layer strength, using for example a shear frame, would give more accurate results.

Very soft snow

Very soft upper layers (B<5N) often give deviating results and are therefore left out of the attempts to correlate stress to ECT scores. The calculations resulted in very high shear stresses but the ECT's show that the slab was not cohesive enough to propagate, with often Q3 failure. Deformation around the shovel has a large impact and the snow and

stress from the loading steps leads to internal collapse of the layer. Snow of very low hardness and low density might act as a granular material rather than a cellular material (Kirchner et al., 2001). Consequently, some glide between grains and crystal rearrangement might occur, leading to compaction. Compaction is more important for these very soft layers and could avoid stress transmission to deeper layers (Schweizer et al., 1995).

Redefining weak snow profiles

According to the results from the calculations and previous work on bridging of hard layers (Camponovo & Schweizer, 1996; Schweizer, 1993; Schweizer & Jamieson, 2001; Thumlert & Jamieson, 2014), we can redefine stable and unstable snow profiles of Schweizer and Wiesinger (2001), figure 5. Schweizer and Wiesinger defined profiles 1, 5, 7 and 9 as potentially unstable, 6 and 10 as stable, and 2, 3, 4, and 8 as undefined. Our results contradict the increase in hardness as indication for stability: a hard layer near the surface of the snowpack indicates a stable snowpack. Moreover, Habermann et al. (2008) showed that a decreasing hardness does not only lead to a decrease in the stress below an external load, but also in a decrease in the propagation propensity of the shear fracture below the slab. Similarly, according to Schweizer and Jamieson (2001), profiles 1, 4 and 6 are most common in avalanches in Swiss and Canadian datasets. The redefinition of stable and unstable snow profiles is based on the amount of bridging, hardness contrast between the layers, and the depth of the weak layer.

The results for 3 different weak layer positions are shown in figure 30. Overall, profiles 1, 4, 6, 7, and 8 are potentially unstable, whereas profiles 5, and 10 can be regarded as more stable. 2, 3, and 9 are undefined. The real stability depends of course also on the strength and the type of crystals in the weak layer. Furthermore, the instability of snow profiles 1, 3, 4, 6, 7, and 8 might be overestimated when the top layers consists of very soft snow, because of the effect of compaction.

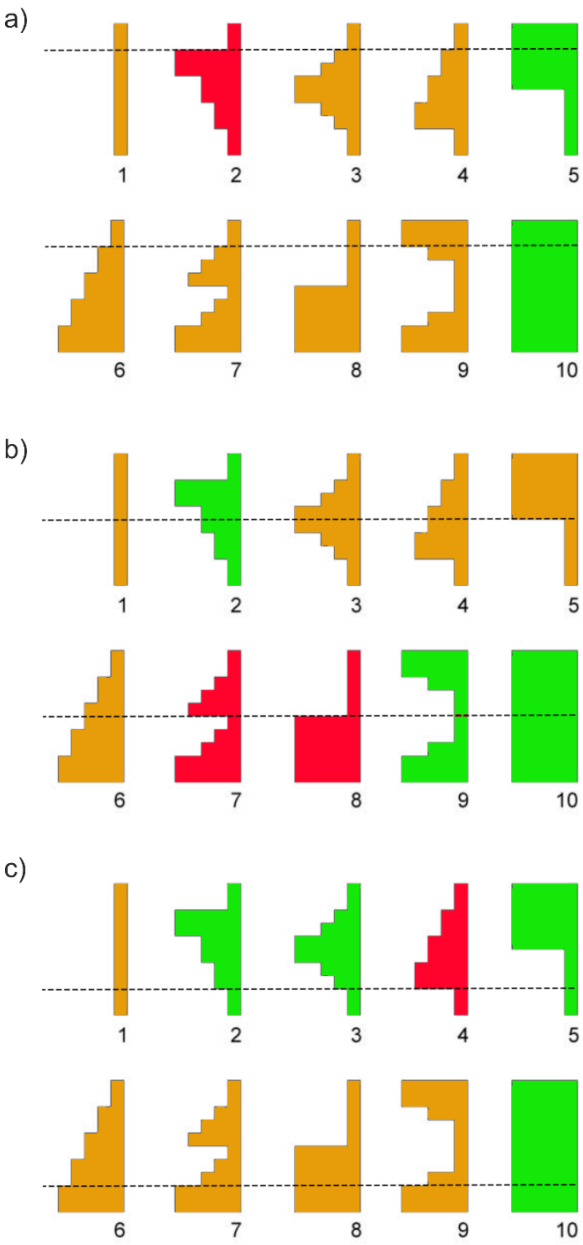

Figure 30. Classification of stable and unstable snow profiles for 3 weak layer positions, shallow a), medium b), and deep c). The classification was based on bridging and hardness contrasts. Green represents most likely stable, orange is potentially unstable, and red is potentially very unstable. Modified from Schweizer and Wiesinger (2001).

6. CONCLUSION

Standard snow pit data from the field was used to calculate shear stress using a non-homogeneous slab hardness as an index for the snow mechanical properties. Outcomes of field measurements and calculations were compared to ECT scores and linked to the snow pit measurements. In 48% of the investigated snow profiles, soft over hard snow was found, and the power law solution provided a good representation of the hardness profile. For the other 52%, the use of an exponential model would be more appropriate.

It was shown that hardness is a useful parameter that correlates well with ECT outcomes. Using blade hardness data for stability evaluation is a promising method for avalanche forecasters. The use of the thin-blade hardness gauge has many advantages over the use of density. Hardness is easy to measure in the field, more precise and requires less actions. Previous studies found that hardness correlates well to various mechanical properties, like the elastic modulus, in contrast to snow density. Properties that are crucial for stress calculations. The detailed hardness data allows us to execute stress calculations with a non-homogeneous approach. It was shown that homogeneous approach underestimates the stress for a soft over hard slab. The difference between a homogeneous and non-homogeneous snowpack becomes more considerable with an increasing slope angle.

No direct relation was found between the stress and the stability obtained from ECT's and field observations. A connection between shear stress and weak layer strength calculated from blade hardness provides the necessary information to improve stability evaluation. The stability index was successful in discriminating between stable and unstable for the given dataset, but the dataset was not sufficient. A much larger dataset is needed to make better correlations and to draw more solid conclusions. Shear frame experiments would improve the shear strength values and thus also the stability index. However, obtaining shear strength from blade hardness appears to be a good and easy solution in the absence of shear frame data. In addition, a study of hardness profiles of crown fractures and a study of hardness profiles specifically considering unstable slopes would be very useful to better define stable and unstable hardness profiles.

Regarding the real-life situation, the results suggest that it is more likely to trigger and avalanche while skiing on a snowpack with gradually increasing hardness, and less likely with decreasing hardness due to layer parallel stress dissipation (considering that all other factors, e.g. nature of the weak layer, are the same for both cases).

7. REFERENCES

Bader, H.P. & Salm, B., 1990. On the mechanics of snow slab release. *Cold Regions Science and Technology*, 17(3), pp.287–300.

Biot, M.A., 1941. General Theory of Three-Dimensional Consolidation. *Journal of Applied Physics*, 12(2), pp.155–164.

Biot, M.A., 1956. Theory of deformation of a porous viscoelastic anisotropic solid. *Journal of Applied Physics*, 27(5), pp.459–467.

Biot, M.A., 1955. Theory of elasticity and consolidation for a porous anisotropic solid. *Journal of Applied Physics*, 26(2), pp.182–185.

Booker, J.R., 1985. the Behaviour of an Elastic Non-Homogeneous. *International Journal for Numeriacal and Analytical Methods in Geomechanics*, 9, pp.353–367.

Borstad, C.P., 2016. Line load solution on a sloping , non-homogeneous half space. *Unpublished*.

Borstad, C.P. & McClung, D.M., 2011. Thin-blade penetration resistance and snow strength. *Journal of Glaciology*, 57(202), pp.325–336.

Boussinesq, J., 1878. Équilibre d'élasticité d'un sol isotrope sans pesanteur, supportant différents poids. *CR Math. Acad. Sci. Paris*.

Burmister, D.M., 1945. The general theory of stresses and displacements in layered soil systems. II. *Journal of Applied Physics*, 16(3), pp.126–127.

Campbell, C. & Jamieson, B., 2007. Spatial variability of slab stability and fracture characteristics within avalanche start zones. *Cold Regions Science and Technology*, 47(1–2), pp.134–147.

Camponovo, C. & Schweizer, J., 1996. Measurements on skier triggering. *International Snow Science Workshop*, pp.100–103.

Camponovo, C. & Schweizer, J., 2001. Rheological measurements of the viscoelastic properties of snow. *Annals of Glaciology*, 32, pp.44–50.

Canadian Avalanche Association, 2014. *Observation Guidelines and Recording Standards for Weather, Snowpack and Avalanches*,

Colbeck, S.C., 1982. An overview of seasonal snow metamorphism. *Reviews of Geophysics*, 20(1), pp.45–61.

DeVito, C., Tupy, A. & Gonzales, B., 2013. A Snow Stratigraphy Comparison with the Ramsonde and Thin-Blade Penetrometer. *International Snow Science Workshop Grenoble – Chamonix Mont-Blanc*, pp.1052–1059.

Eckerstorfer, M. & Christiansen, H.H., 2011. The "High Arctic Maritime Snow Climate" in Central Svalbard. *Arctic, Antarctic, and Alpine Research*, 43(1), pp.11–21.

Fierz, C. et al., 2009. The international classification for seasonal snow on the ground. *IHP-VII Technical Documents in Hydrology*, 83(1), p.90.

Föhn, P.M.B., 1987. The stability index and various triggering mechanisms. *IAHS Publ.*, 162(162), pp.195–214.

Fukue, M., 1977. Mechanical performance of snow under loading. *PhD thesis, McGill University.*

Geldsetzer, T. & Jamieson, B., 2000. Estimating dry snow density from grain form and hand hardness. *International Snow Science Workshop*, (January), pp.121–127.

Giannakopoulos, A.E. & Suresh, S., 1997. Indentation of solids with gradients in elastic properties: Part I. Point force. *International Journal of Solids and Structures*, 34(19), pp.2357–2392.

Greene, E. et al., 2010. Snow, Weather, and Avalanches: Observation Guidelines for Avalanche Programs in the United States. *The American Avalanche Association*.

Habermann, M., Schweizer, J. & Jamieson, J.B., 2008. Influence of snowpack layering on human-triggered snow slab avalanche release. *Cold Regions Science and Technology*, 54(3), pp.176–182.

Haefeli, R., 1939. Schneemechanik; Mit Hinweisen auf die Erdbaumechanik. *Eidgenösissche Technische Hochschule in Zürich*, 3, p.243.

Heierli, J., Gumbsch, P. & Zaiser, M., 2008. Anticrack nucleation as triggering mechanism for snow slab avalanches. *Science*, 321(1), pp.235–240.

van Herwijnen, A. & Jamieson, B., 2007. Snowpack properties associated with fracture initiation and propagation resulting in skier-triggered dry snow slab avalanches. *Cold Regions Science and Technology*, 50(1–3), pp.13–22.

Höller, P. & Fromm, R., 2010. The relationship between measured snow hardness and shear strength. *International Snow Science Workshop*, pp.431–434.

Jamieson, J.B. & Johnston, C.D., 1998. Refinements to the stability index for skier-triggered slab avalanches. *Annals of Glaciology*, 26, pp.296–302.

Kirchner, H.O.K. et al., 2001. Snow as a foam of ice: Plasticity, fracture and the brittle-to-ductile transition. *Philosophical Magazine A*, 81(9), pp.2161–2181.

McClung, D. & Schaerer, P.A., 2006. The Avalanche Handbook: 3rd Edition.

Mellor, M., 1975. A review of basic snow mechanics. *Snow Mechanics (Proceedings of the Grindelwald Symposium April 1974), IAHS Publ.\ no.\ 114*, pp.251–291.

Monti, F. et al., 2016. Snow instability evaluation: Calculating the skier-induced stress in a multi-layered snowpack. *Natural Hazards and Earth System Sciences*, 16(3), pp.775–788.

Narita, H., 1980. Mechanical behaviour and structure of snow under uniaxial tensile stress. *Journal of Glaciology*, 26(94), pp.275–282.

Norsk Meteorologisk Institutt, 2016. Weather data. *www.met.no*.

Petrovic, J.J., 2003. Review Mechanical properties of ice and snow. *Journal of Materials Science*, 38(1), pp.1–6.

Pomeroy, J.W.W. & Brun, E., 1990. Physical Properties of Snow. *Snow Ecology: An*

Interdisciplinary Examination of Snow-Covered Ecosystems, 97, pp.45–126.

Quervain, de, M.R., 1950. Die Festigkeitseigenschaften der Schneedecke und ihre Messung. *Geofisica Pura e Applicata*, 18(1), pp.179–191.

Quervain, de, M.R., 1966. Problems of avalanche research. *Sym- posium at Davos 1965—Scientific Aspects of Snow and Ice Avalanches, IAHS Publ.*, 69, pp.1–8.

Reiweger, I., Gaume, J. & Schweizer, J., 2015. A new mixed-mode failure criterion for weak snowpack layers. *Geophysical Research Letters*, 42(5), pp.1427–1432.

Reiweger, I. & Schweizer, J., 2010. Failure of a layer of buried surface hoar. *Geophysical Research Letters*, 37(24), pp.1–5.

Salm, B., 1982. Mechanical properties of snow. *Reviews of Geophysics*, 20(1), pp.1–19.

Schweizer, J., 1998. Laboratory experiments on shear failure of snow. *Annals of Glaciology*, 26(1), pp.97–102.

Schweizer, J., 1999. Review of dry snow slab avalanche release. *Cold Regions Science and Technology*, 30(1–3), pp.43–57.

Schweizer, J. et al., 1995. Snow mechanics and avalanche formation: field experiments on the dynamic response of the snow cover. *Surveys in Geophysics*, 16(5–6), pp.621–633.

Schweizer, J., 1993. The influence of the layered character of snow cover on the triggering of slab avalanches. *Annals of Glaciology*, 18(January 1993), pp.193–198.

Schweizer, J. & Camponovo, C., 2001. The skier's zone of influence in triggering slab avalanches. *Annals of Glaciology*, 32(1), pp.314–320.

Schweizer, J. & Jamieson, J.B., 2000. Field observations of skier-triggered avalanches. *Proceedings International Snow Science Workshop, Big Sky, Montana, U.S.A.*, (October), pp.2–6.

Schweizer, J. & Jamieson, J.B., 2001. Snow cover properties for skier triggering of avalanches. *Cold Regions Science and Technology*, 33(2), pp.207–221.

Schweizer, J., Jamieson, J.B. & Schneebeli, M., 2003. Snow avalanche formation. *Reviews of Geophysics*, 41(4), p.1016.

Schweizer, J. & Wiesinger, T., 2001. Snow profile interpretation for stability evaluation. *Cold Regions Science and Technology*, 33(2–3), pp.179–188.

Shapiro, L.H. et al., 1997. Snow Mechanics: review of the state of knowledge and applications. *CRREL Report 97-3*, (August), p.43.

Sigrist, C., 2006. Measurement of fracture mechanical properties of snow and application to dry snow slab avalanche release. *PhD Thesis*, (16736), pp.1–158.

Simenhois, R. & Birkeland, K., 2007. An update on the Extended Column Test: New recording standards and additional data analyses. *Published in The Avalanche Review*, 26(2).

Simenhois, R. & Birkeland, K., 2006. The Extended Column Test: A field test for fractureminitiatuin and propagation. *Proceedings of the 2006 International Snow Science Workshop*.

Thumlert, S. & Jamieson, B., 2014. Stress measurements in the snow cover below localized dynamic loads. *Cold Regions Science and Technology*, 106, pp.28–35.

Wu, Q. et al., 2005. Dynamic compression of highly compressible porous media with application to snow compaction. *Journal of Fluid Mechanics*, 542(1), pp.281–304.

8. APPENDICES

Appendix 1

Table of field measurements. In red, the measurements that were left out of further calculations, either due to the presence of wet snow, or due to distortion by very soft upper layers.

Date	ECT	In	dw	ρ	B_{sl}/B_{su}	SBHI	BI	Bwl	k	R^2 PL	R^2 EX
20160204	ECTX	25	68	231	0.54	9.04	1088	70000	0.00	0.00	0.19
20160211	ECTP	31	20	235	1.32	28.63	636	312963	0.00	0.00	0.57
20160212	ECTX	33	18	185	0.44	19.29	429	472222	1.00	0.35	0.39
20160216	ECTP	42	30	235	1.18	31.48	1457	211111	0.00	0.00	0.90
20160218	ECTN	33	50	272	1.92	13.37	891	194444	0.02	0.00	0.01
20160219	ECTN	26	21	165	1.04	10.44	387	108889	0.11	0.00	0.00
20160223	ECTN	11	12	116	0.34	2.27	50	18519	0.00	0.00	0.68
20160225	ECTP	15	24	207	0.27	8.68	386	35185	0.00	0.00	0.46
20160226	ECTN	21	25	179	0.10	3.06	142	169444	1.00	0.53	0.95
20160303	ECTP	12	36	235	1.22	5	312	28333	0.05	0.01	0.02
20160312	ECTX	20	60	277	0.84	12.18	1218	153500	0.58	0.45	0.36
20160316	ECTP	10	54	211	6.33	5.72	515	37000	0.00	0.00	0.02
20160317	ECTP	21	28	133	0.19	2.03	95	11833	0.00	0.00	0.59
20160319	ECTN	23	77	224	0.00	10.78	1366	583333	1.00	0.73	0.91
20160322	ECTN	25	30	156	0.25	1.27	64	66333	1.00	0.61	-1.16
20160402	ECTP	20	30	245	2.88	11.41	570	65667	0.00	0.00	0.10
20160406	ECTP	20	10	254	0.04	6.61	110	32833	0.00	0.00	0.90
20160409	ECTX	12	20	252	0.44	7.30	243	57667	0.00	0.00	0.08
20160412	ECTX	15	26	244	6.11	13.85	600	87333	0.70	0.43	0.28
20160414	ECTP	11	32	202	0.32	3.83	204	28167	0.02	0.00	0.03
20160420	ECTP	12	12	143	0.11	1.93	39	21833	0.00	0.00	0.37

ECT Ect score
In Slope inclination
dw Depth of the weak layer, measured vertically down the snowpack
ρ Estimated slab density
B_{sl}/B_{su} Ratio between the blade hardness of the slab and the blade hardness of the substratum
Bwl Hardness of the weak layer
k Exponent of the power law regression fitted to the hardness profile
R^2 PL Goodness of the power law fit
R^2 EX Goodness of the exponential fit

Appendix 2

Location:	Svalbard, Larsbreen	Date:	--	Snowpit depth:	182 cm
Lat/Lng:	78.18911, 15.58322	Observer:	Franz Czech	Snowpack depth:	--

Elevation:	282 m	Wind:	Light, --	Profile includes Blade Hardness and SP2 Data
Slope:	25°	Blowing snow:	Light, --	
Aspect:	90° E	Precipitation:	Snow - Very Light	
Air temp.:	-9.2°C	Foot Pen. (PF):	--	
Sky:	Overcast	Ski Pen. (PS):	9 cm	250 N gauge

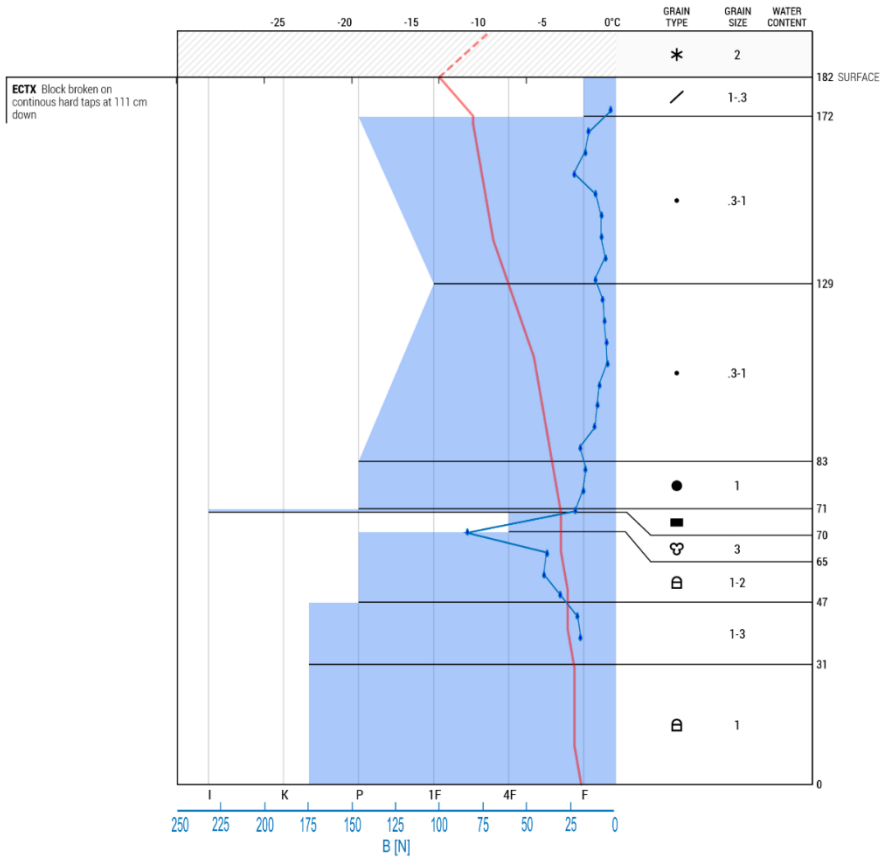

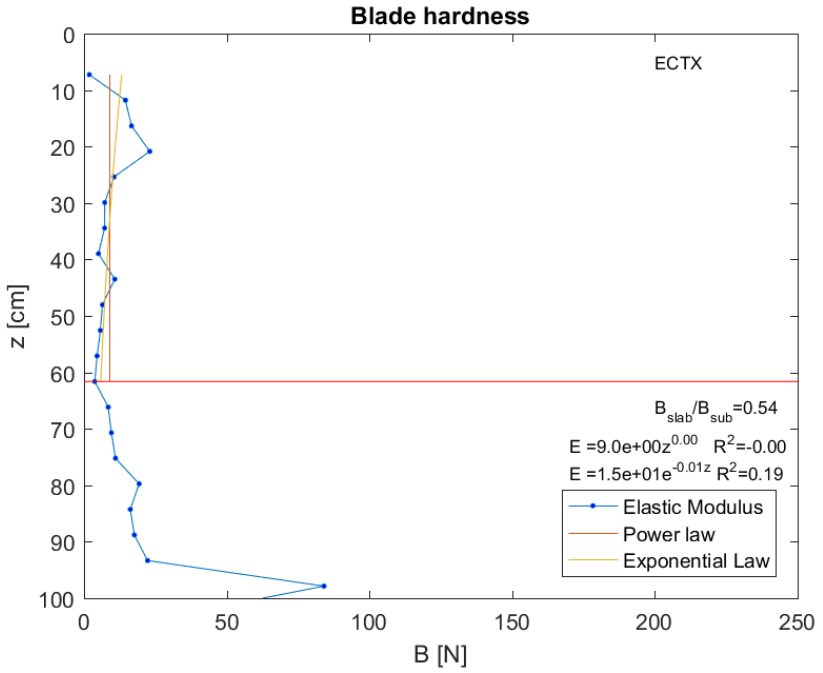

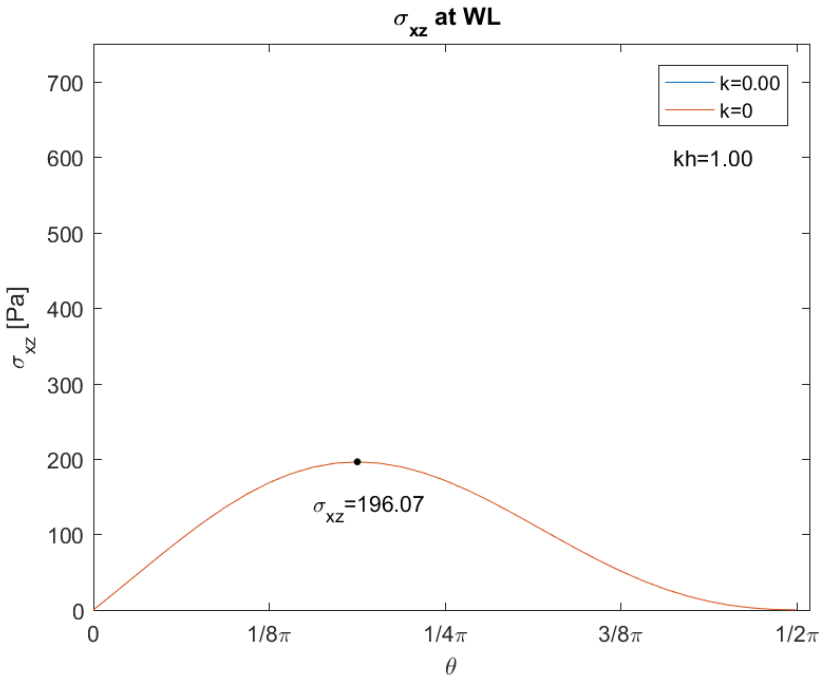

50

Location:	Svalbard, Breinosa	Date:	2016-02-11	Snowpit depth:	175 cm
Lat/Lng:	78.15147, 16.04880	Observer:	Markus Richter	Snowpack depth:	175 cm

Elevation:	481 m	Wind:	Light, 240° SWbW	Profile includes Blade Hardness and Avatech SP2 measurements.
Slope:	31°	Blowing snow:	Previous, --	
Aspect:	0° N	Precipitation:	Snow - Light	
Air temp.:	-12.1°C	Foot Pen. (PF):	0 cm	
Sky:	Overcast	Ski Pen. (PS):	0 cm	250 N gauge

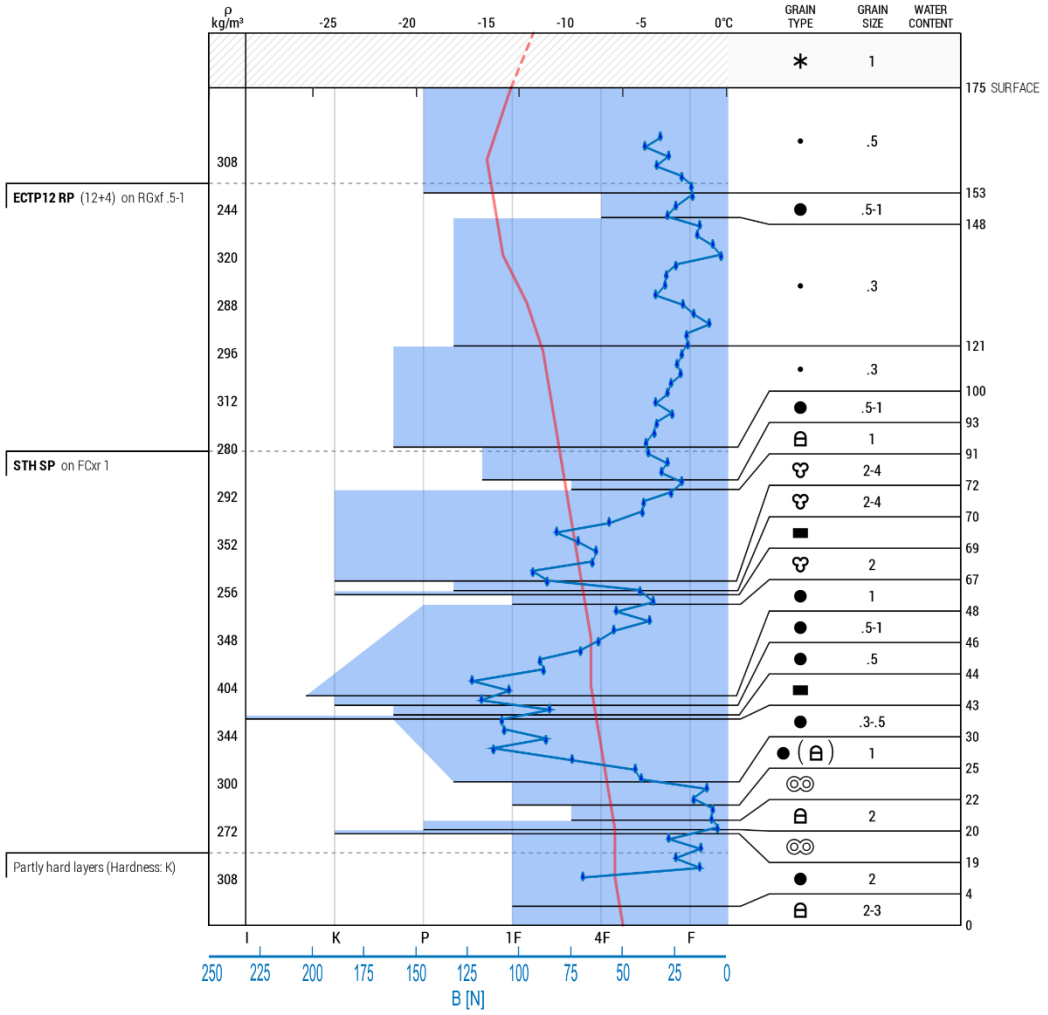

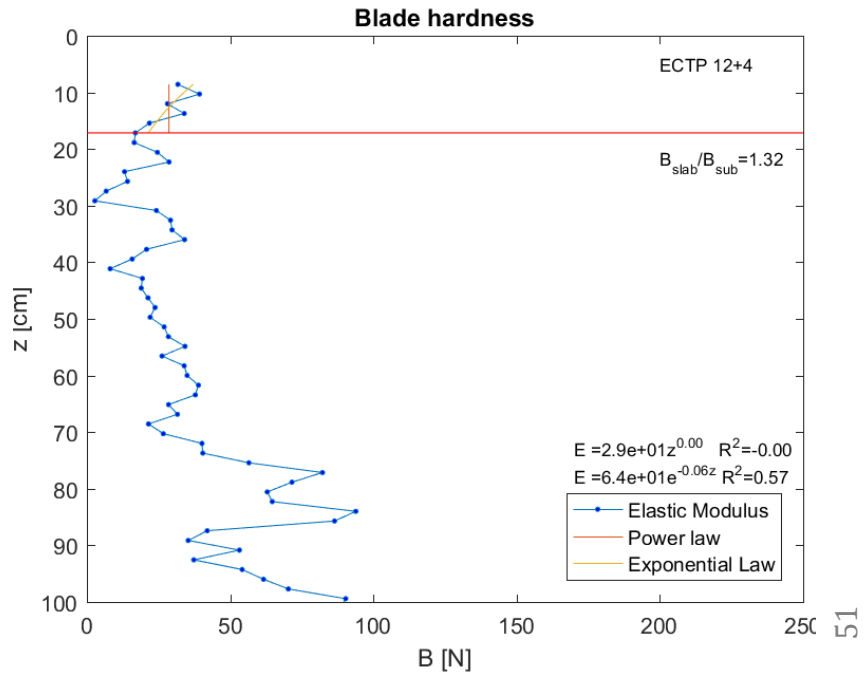

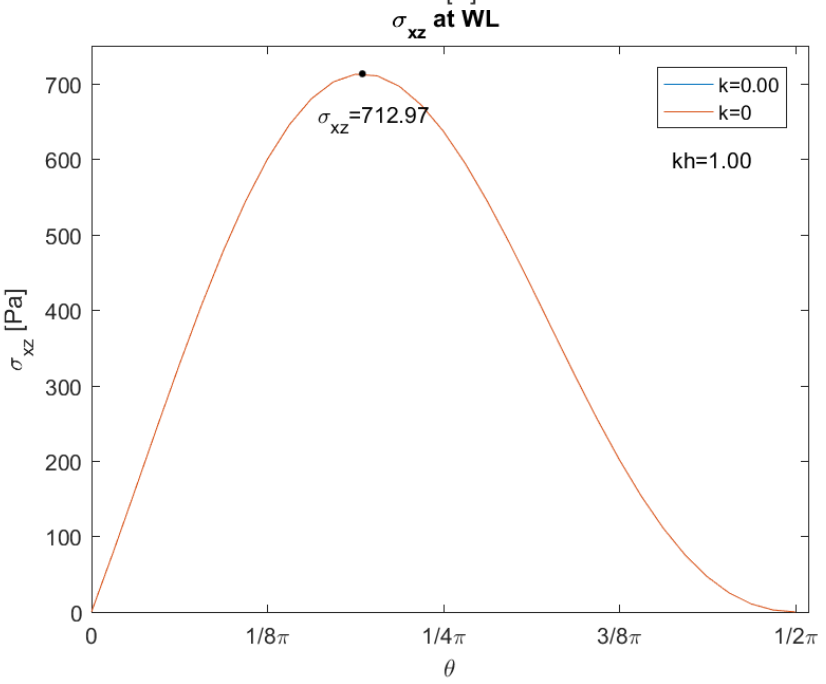

Location:	Svalbard, Sarkofagen	Date:	2016-02-12 12:30 pm	Snowpit depth:	130 cm
Lat/Lng:	78.19046, 15.57576	Observer:	Franz Czech	Snowpack depth:	130 cm

Elevation:	348 m	Wind:	Light, --	Snowpit contains Avatech SP2 and blade hardness measurements
Slope:	33°	Blowing snow:	Light, --	
Aspect:	90° E	Precipitation:	No Precipitation	
Air temp.:	-13.5°C	Foot Pen. (PF):	11 cm	
Sky:	Broken	Ski Pen. (PS):	--	250 N gauge

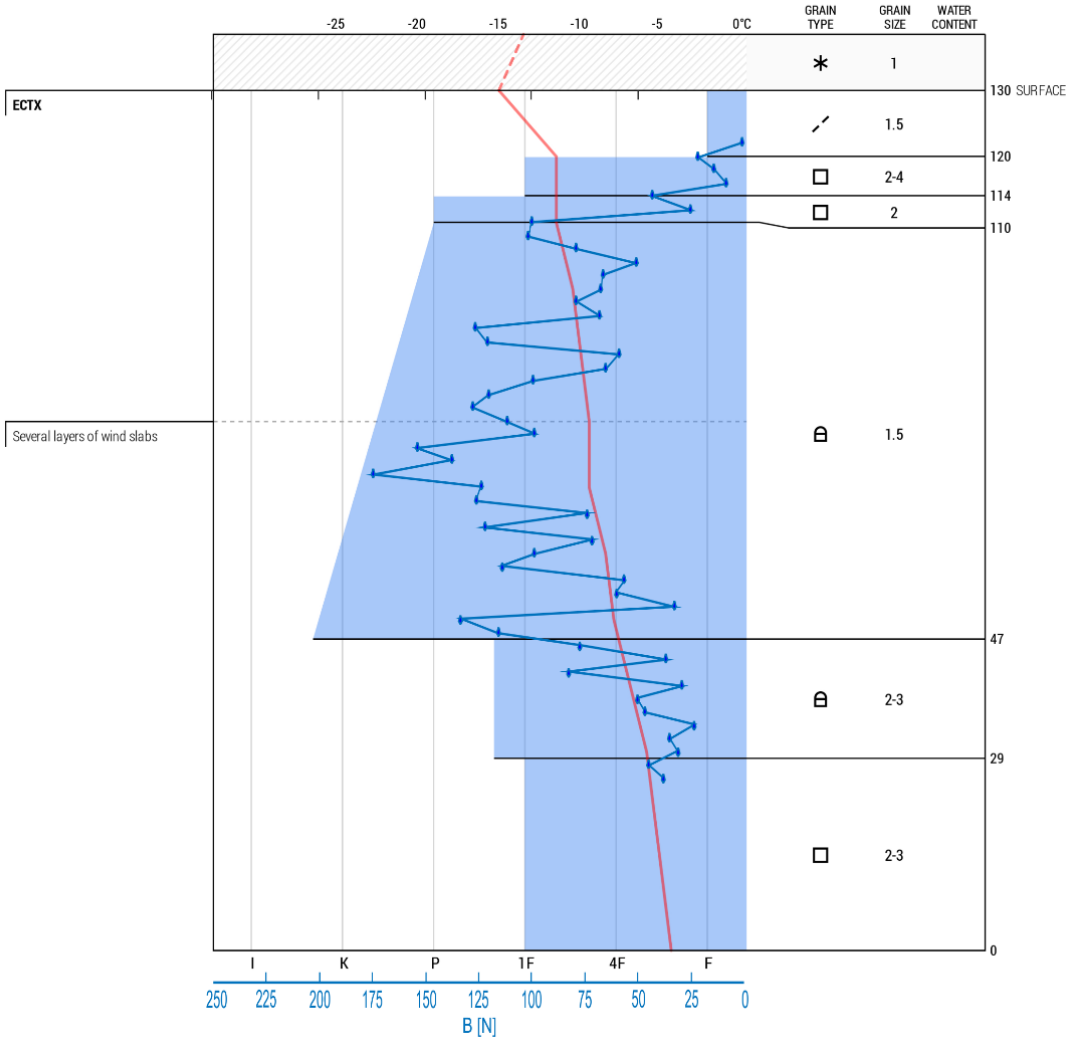

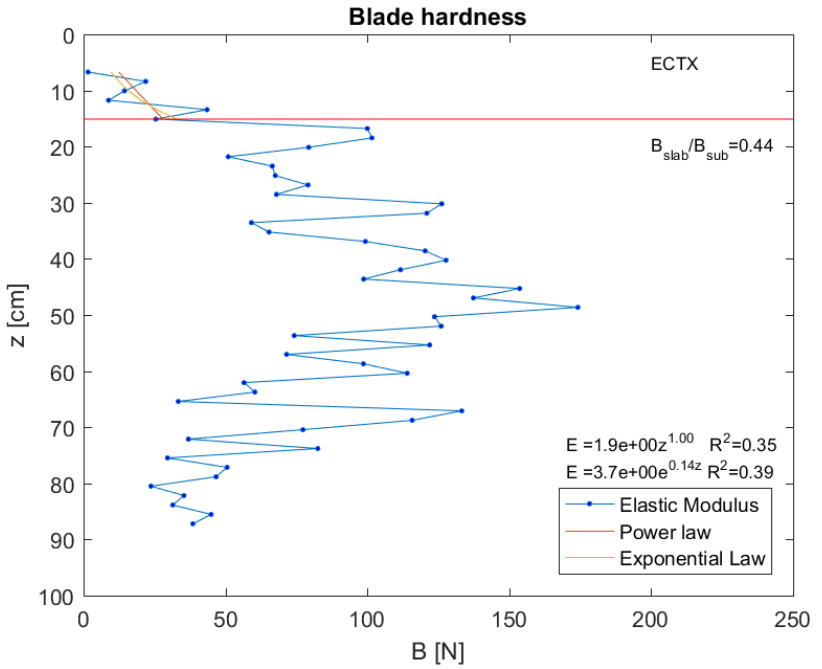

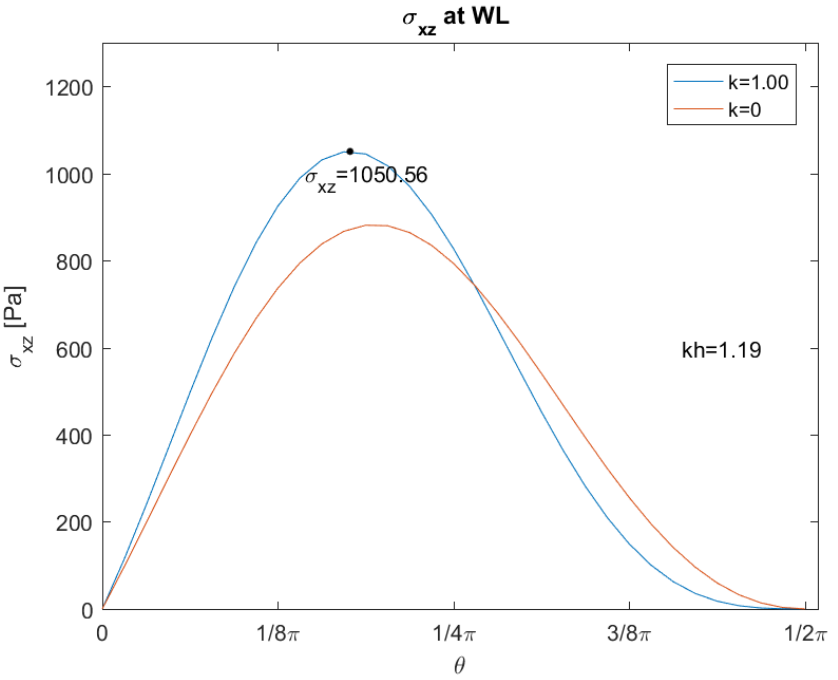

Location:	Svalbard, Trollsteinen	Date:	2016-02-16 12:45 pm	Snowpit depth:	156 cm
Lat/Lng:	78.16566, 15.56900	Observer:	Franz Czech	Snowpack depth:	156 cm

Elevation:	-32,768 m	Wind:	Calm, --	Snowpit contains Blade Hardness and SP2 Data
Slope:	42°	Blowing snow:	None, --	
Aspect:	315° NW	Precipitation:	Snow - Light	
Air temp.:	-7.3°C	Foot Pen. (PF):	25 cm	
Sky:	Overcast	Ski Pen. (PS):	--	250 N gauge

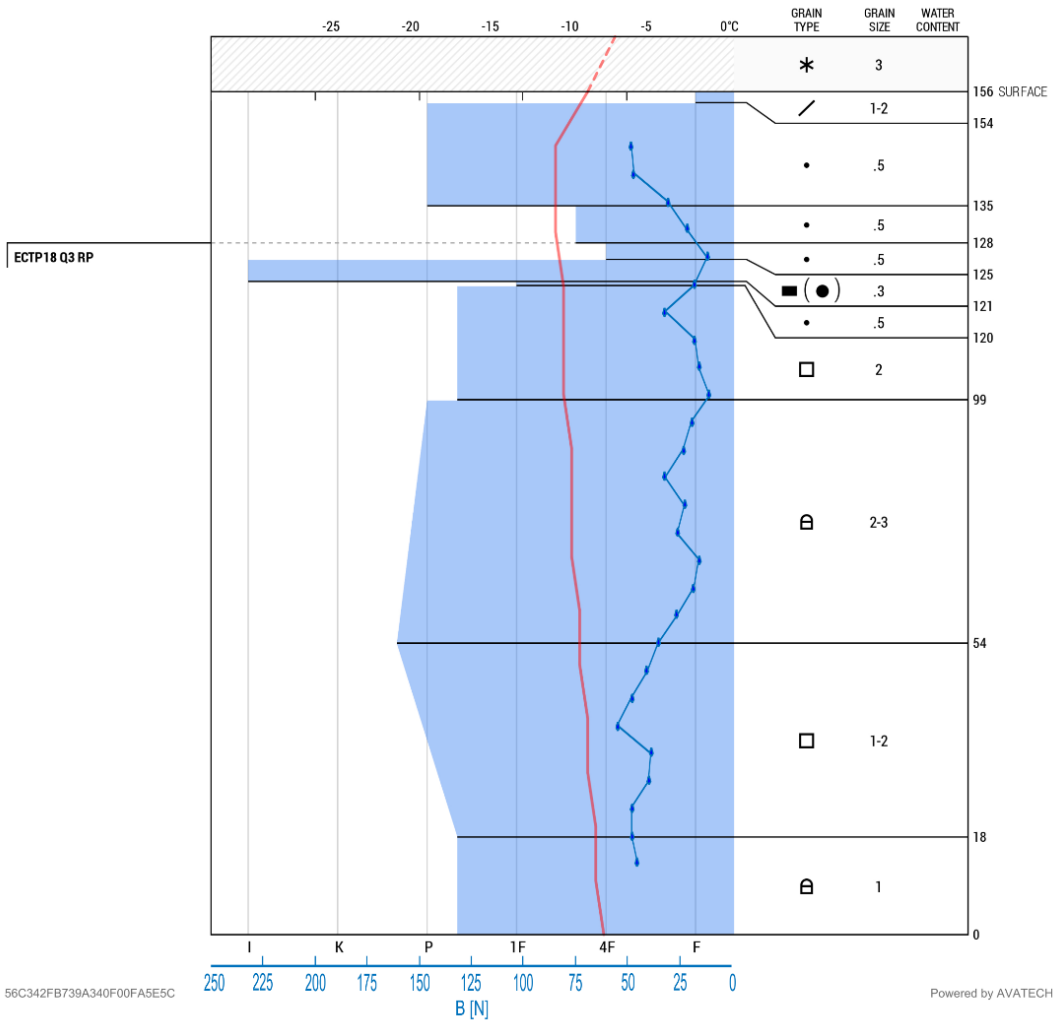

56C342FB739A340F00FA5E5C

Powered by AVATECH

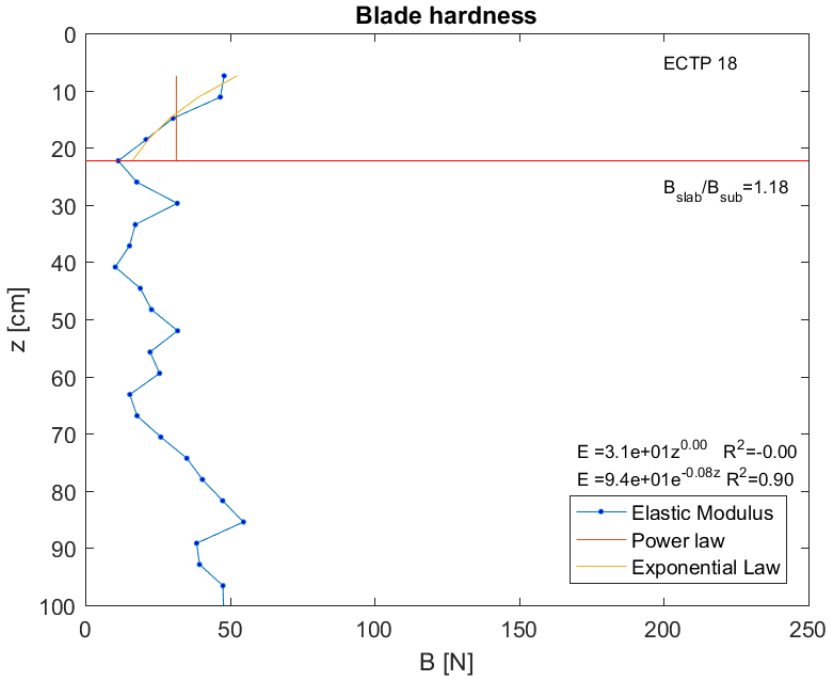

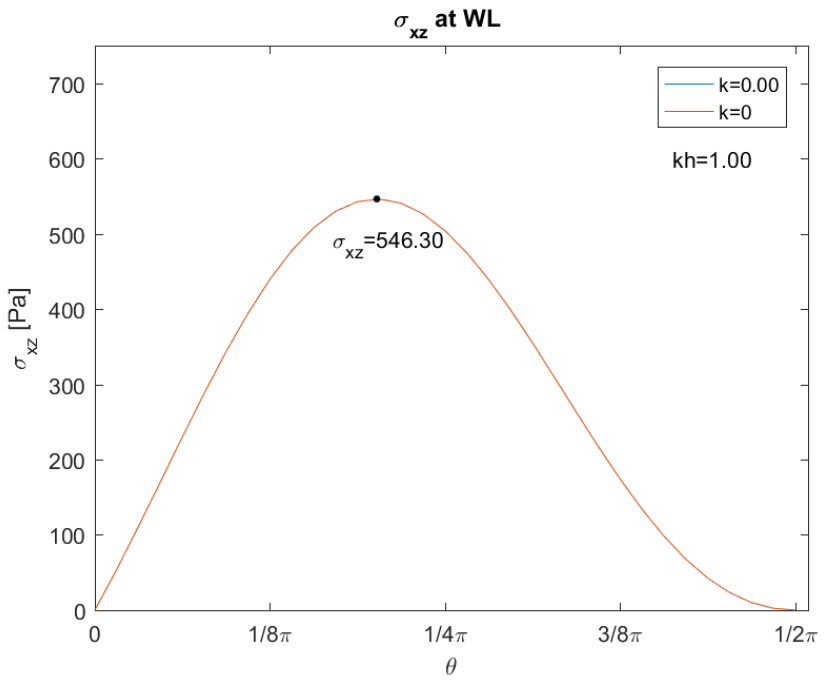

Location:	Svalbard, Tropfsteinen	Date:	2016-02-18 12:30 pm	Snowpit depth:	102 cm
Lat/Lng:	78.16574, 15.56917	Observer:	Franz Czech	Snowpack depth:	102 cm

Elevation:	807 m	Wind:	Light, 135° SE	Snowsuit contains SP2 and Hardness Blade Data	
Slope:	33°	Blowing snow:	Light, 135° SE		
Aspect:	315° NW	Precipitation:	Snow - Very Light		
Air temp.:	-5.0°C	Foot Pen. (PF):	21 cm		
Sky:	Broken	Ski Pen. (PS):	--	250 N gauge	

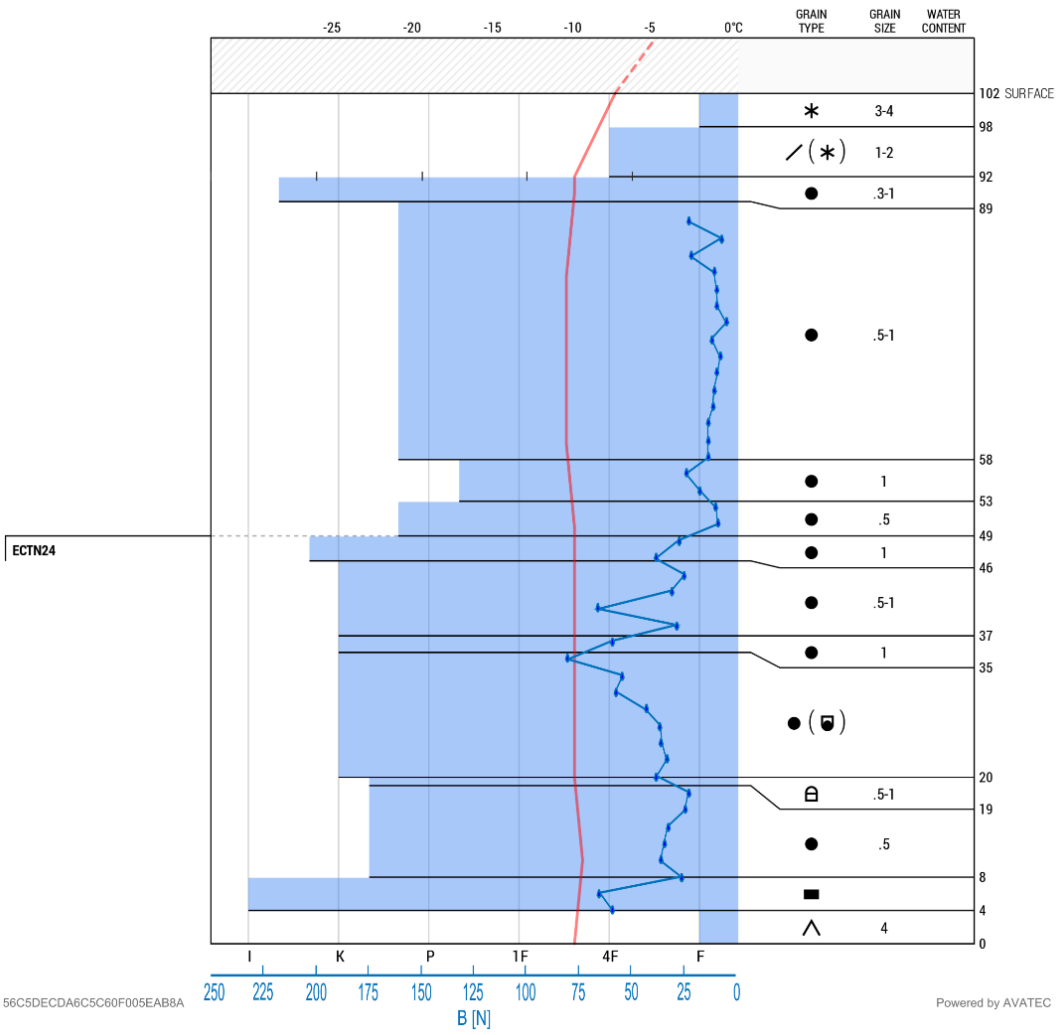

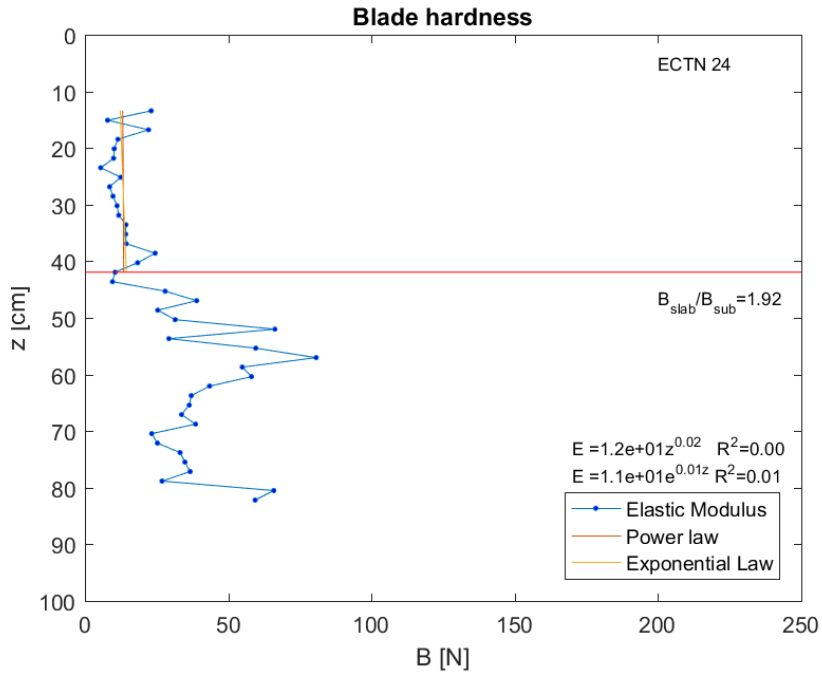

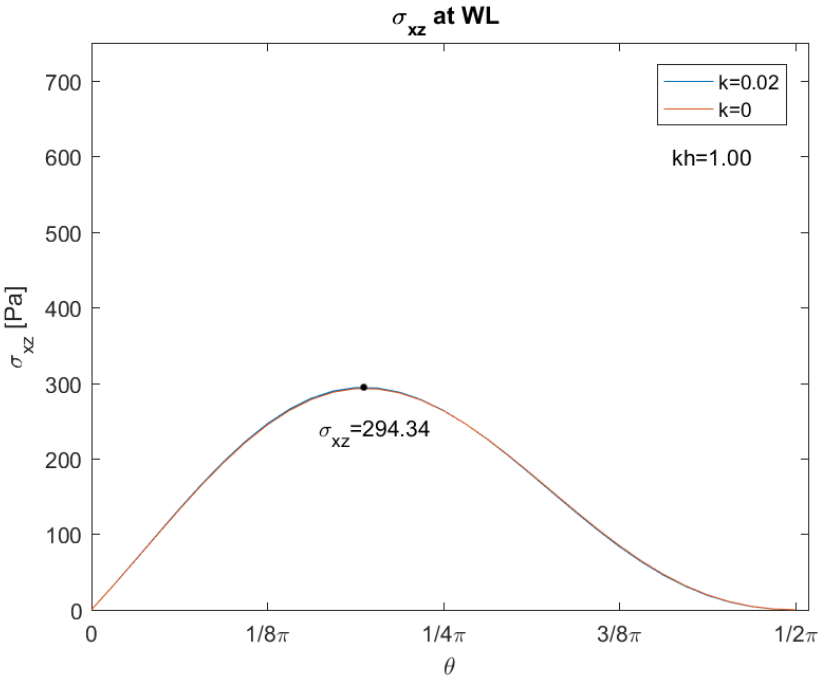

Location:	Svalbard, Breinosa	Date:	2016-02-19 12:00 pm	Snowpit depth:	143 cm
Lat/Lng:	78.14340, 16.04803	Observer:	Laura Swinkels	Snowpack depth:	--

Elevation:	587 m	Wind:	Moderate, 270° W	Hardness and SP2 measurements were done on site
Slope:	26°	Blowing snow:	Moderate, 270° W	
Aspect:	270° W	Precipitation:	No Precipitation	
Air temp.:	-7.2°C	Foot Pen. (PF):	15.5 cm	
Sky:	Few	Ski Pen. (PS):	--	250 N gauge

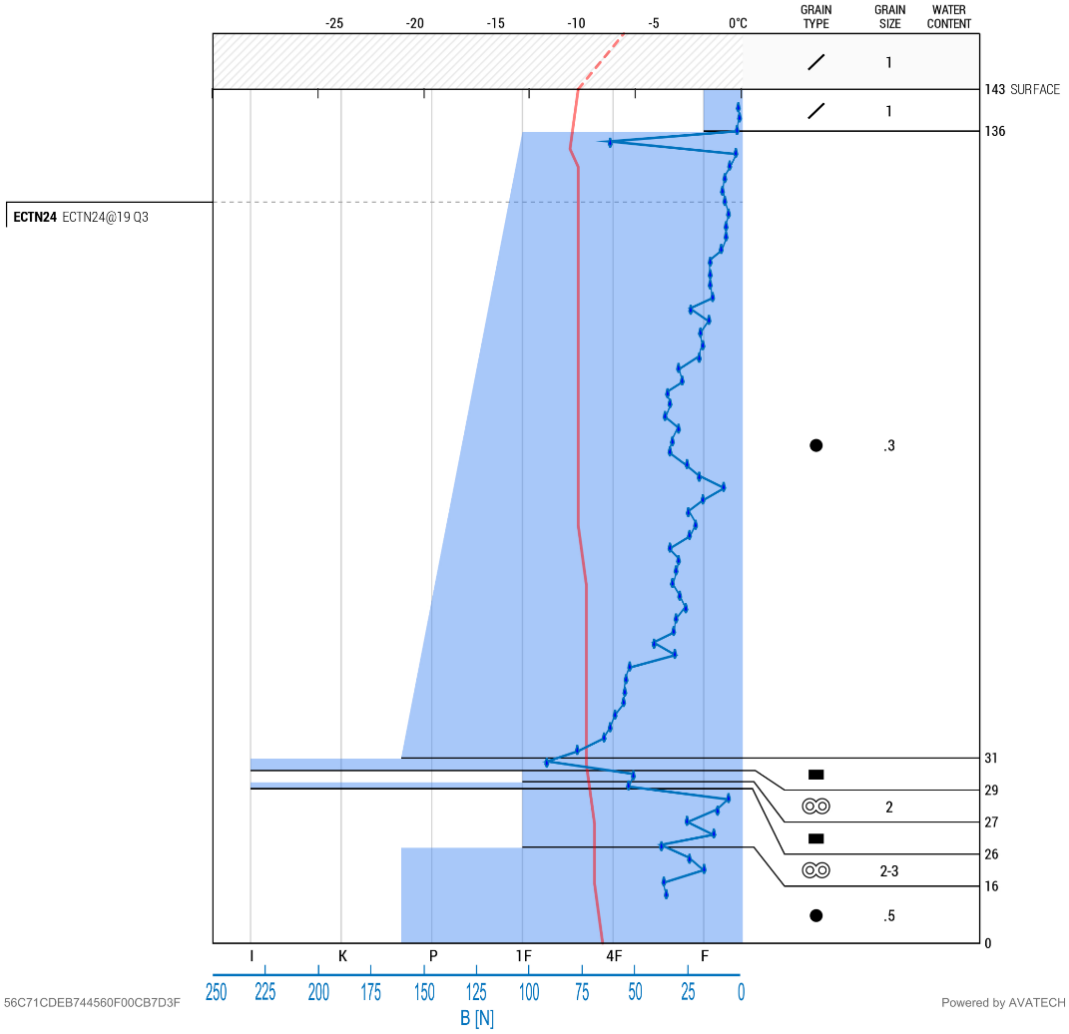

56C71CDEB744560F00CB7D3F

Powered by AVATECH

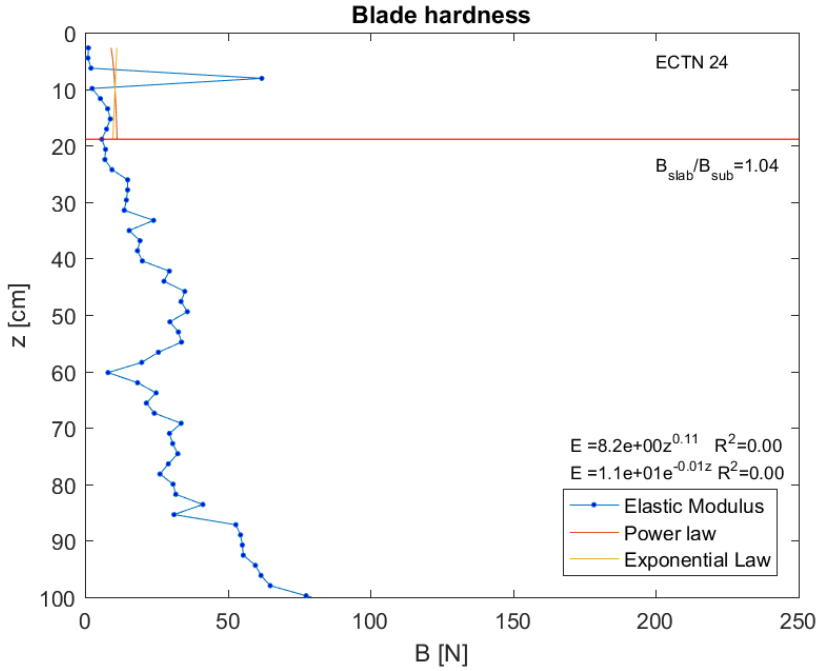

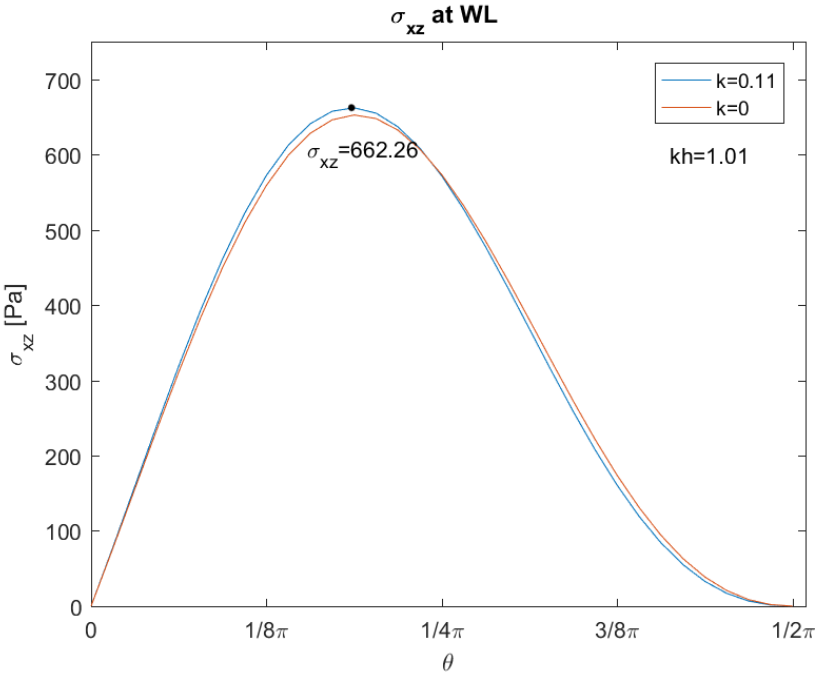

Location:	Breinosa, Svalbard	Date:	2016-02-23 11:45 am	Snowpit depth:	175 cm
Lat/Lng:	78.15097, 16.04227	Observer:	Laura Swinkels	Snowpack depth:	--

Elevation:	467 m	Wind:	Moderate, 45° NE	
Slope:	11°	Blowing snow:	Moderate, 45° NE	
Aspect:	315° NW	Precipitation:	Snow - Light	
Air temp.:	-3.3°C	Foot Pen. (PF):	--	
Sky:	Overcast	Ski Pen. (PS):	--	250 N gauge

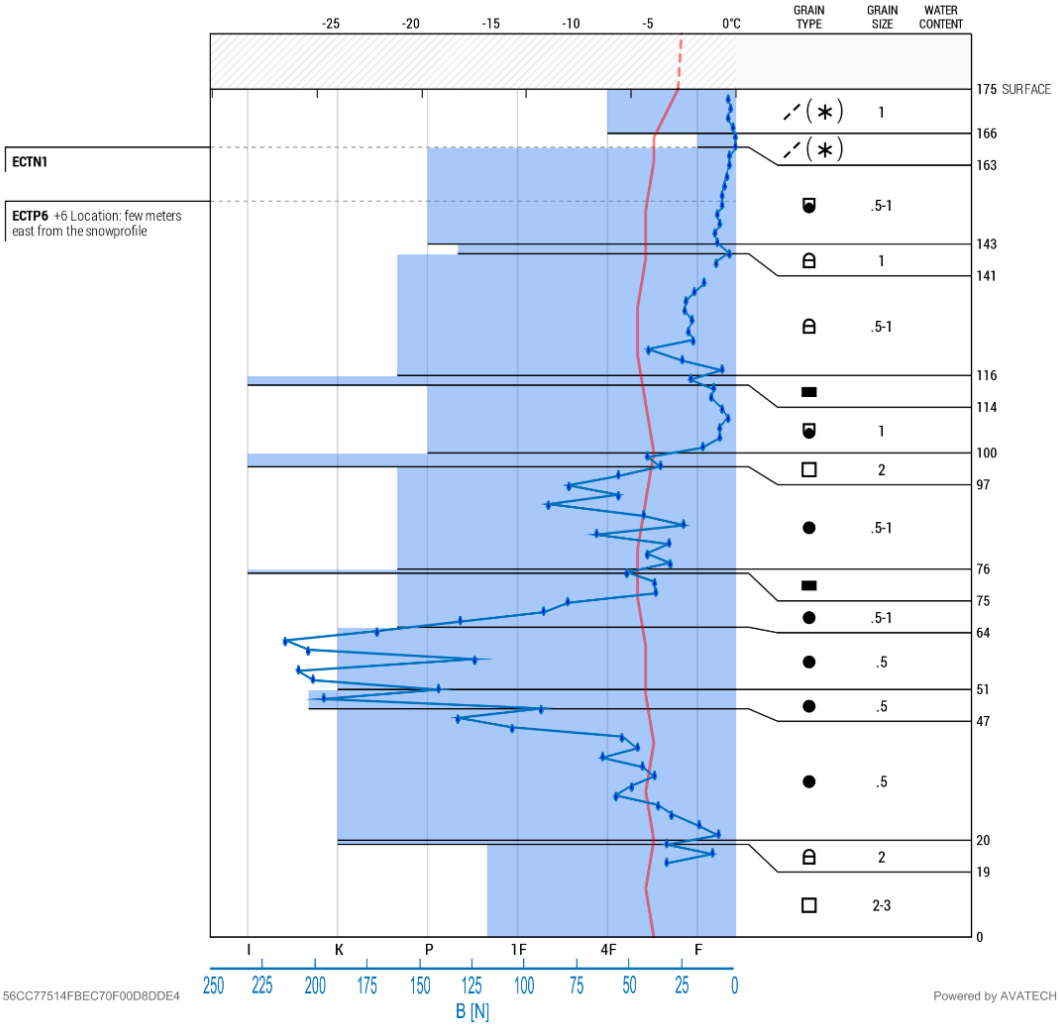

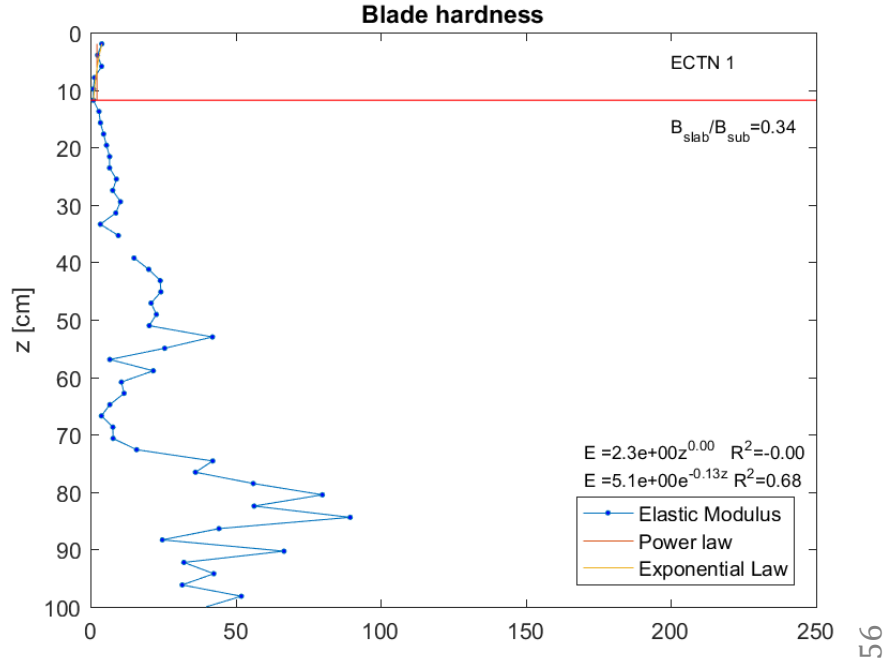

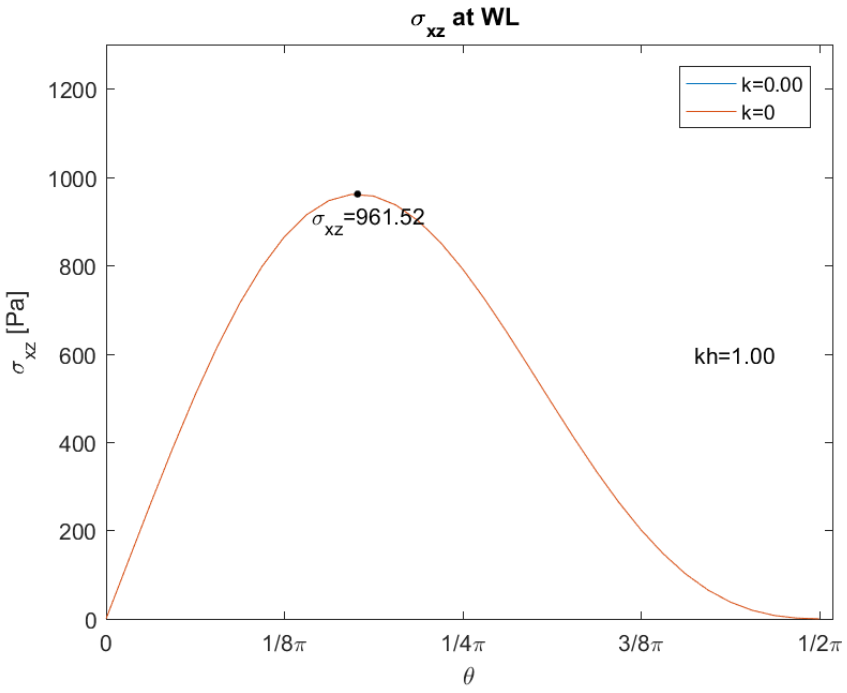

Location:	Bolterdalen, Svalbard	Date:	2016-02-25 9:30 am	Snowpit depth:	86 cm
Lat/Lng:	78.15006, 16.04382	Observer:	Laura Swinkels	Snowpack depth:	--

Elevation:	471 m	Wind:	Moderate, 90° E	Blade hardness measurements and SP2 probings were done on site. After the ECT shovel shear of the remaining block resulted in fractures at the faceted layer from 45-46 and at 39 with just using little force.
Slope:	15°	Blowing snow:	Moderate, 90° E	
Aspect:	0° N	Precipitation:	Snow - Very Light	
Air temp.:	-8.3°C	Foot Pen. (PF):	5 cm	
Sky:	Broken	Ski Pen. (PS):	--	250 N gauge

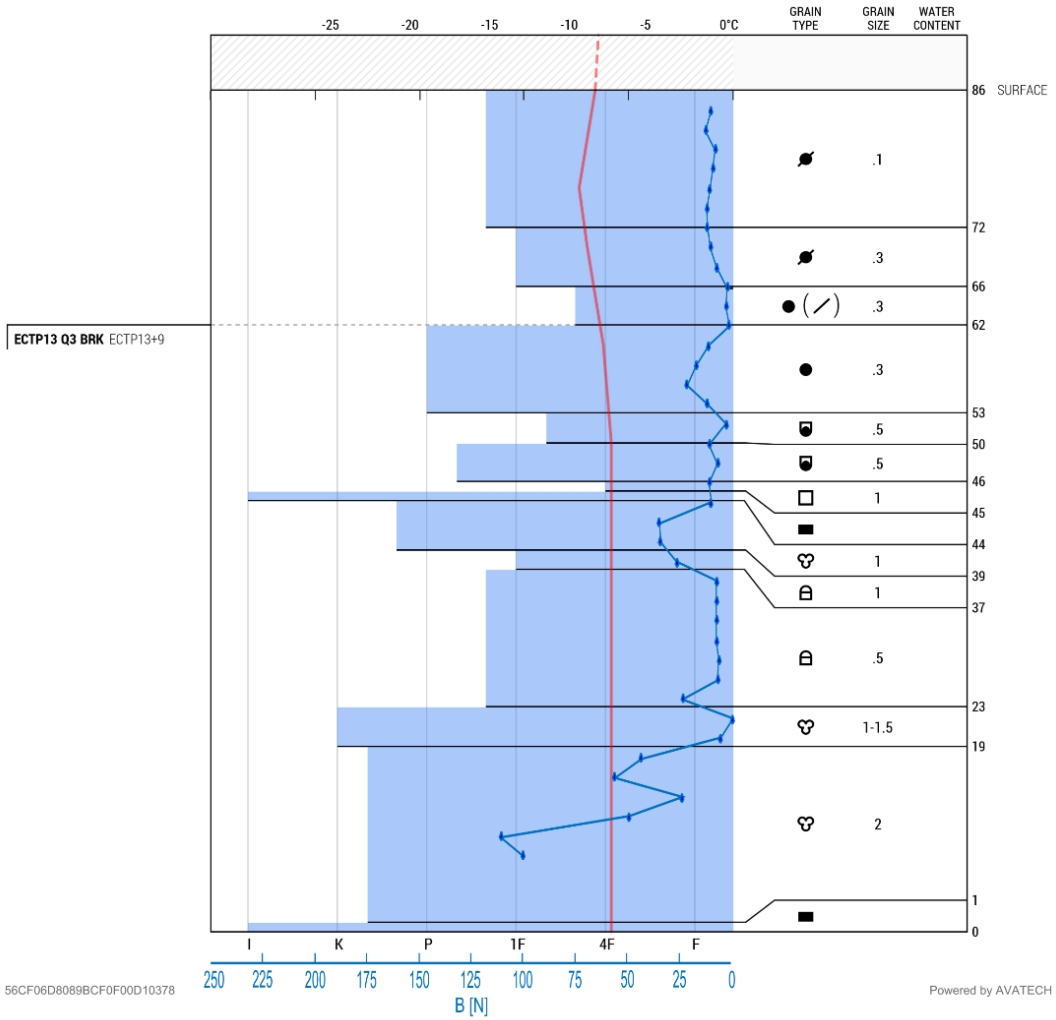

56CF06D8089BCF0F00D10378

Powered by AVATECH

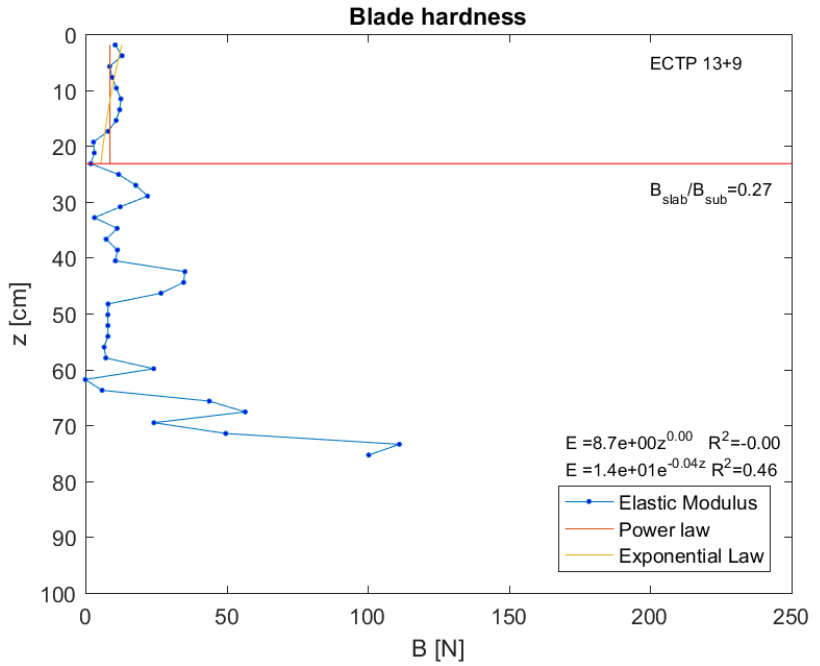

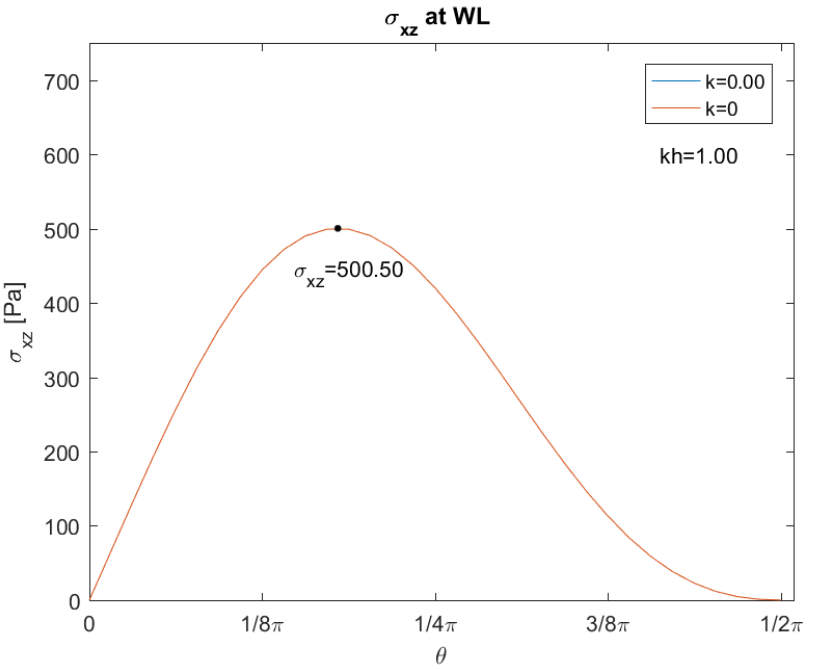

Location:	Larsbreen, Svalbard	Date:	2016-02-26 5:20 pm	Snowpit depth:	79 cm
Lat/Lng:	78.18057, 15.58411	Observer:	Laura Swinkels	Snowpack depth:	--

Elevation:	500 m	Wind:	Calm, --	
Slope:	21°	Blowing snow:	None, --	
Aspect:	270° W	Precipitation:	No Precipitation	
Air temp.:	-14.0°C	Foot Pen. (PF):	20 cm	
Sky:	◯ Clear	Ski Pen. (PS):	--	250 N gauge

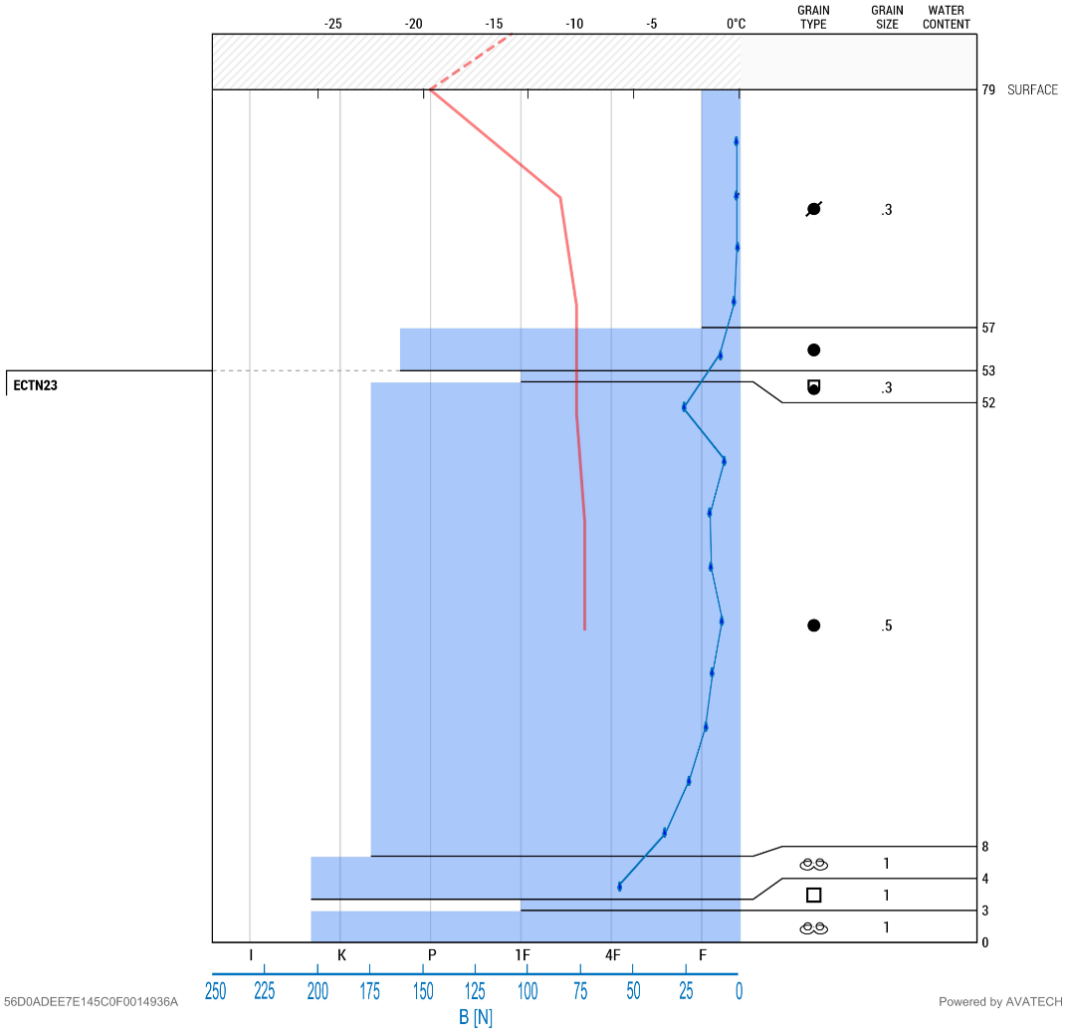

56D0ADEE7E145C0F0014936A

Powered by AVATECH

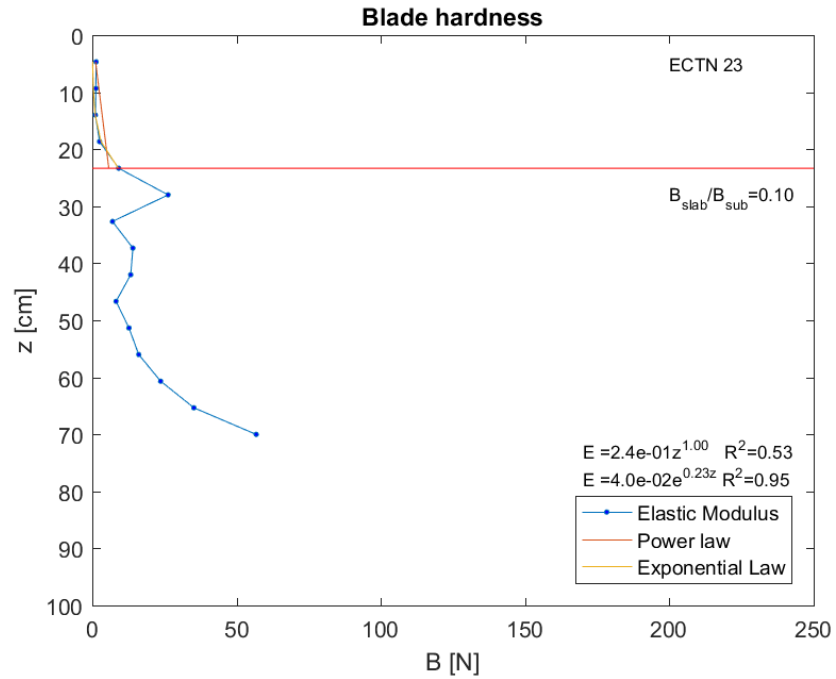

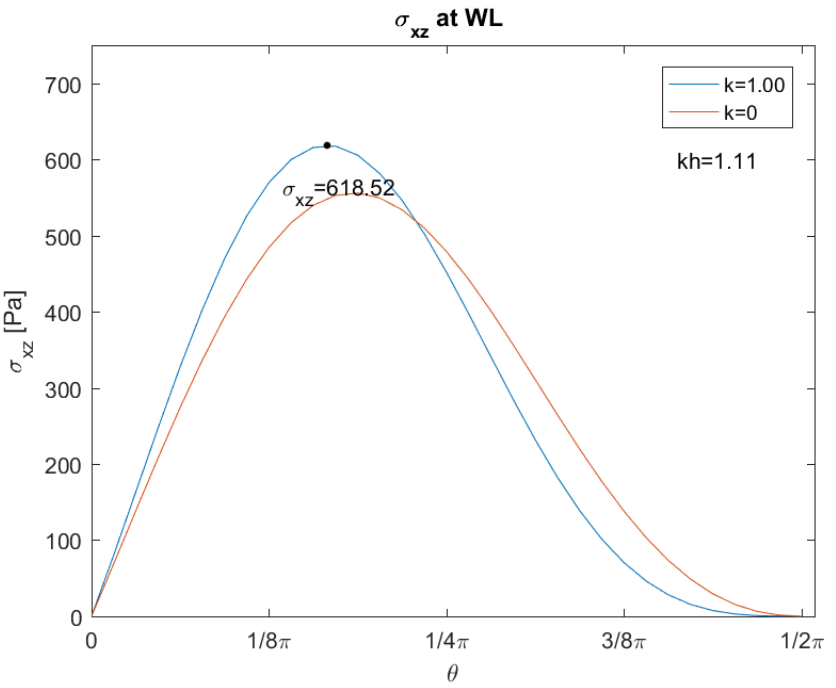

Location:	Kjølen, Tromsø	Date:	2016-03-03 1:30 pm	Snowpit depth:	120 cm
Lat/Lng:	69.71846, 18.83124	Observer:	Laura Swinkels	Snowpack depth:	--

Elevation:	463 m	Wind:	Moderate, 190° SbW	
Slope:	12°	Blowing snow:	Light, 190° SbW	
Aspect:	60° NEbE	Precipitation:	No Precipitation	
Air temp.:	-7.5°C	Foot Pen. (PF):	11 cm	
Sky:	Scattered	Ski Pen. (PS):	--	50 N gauge

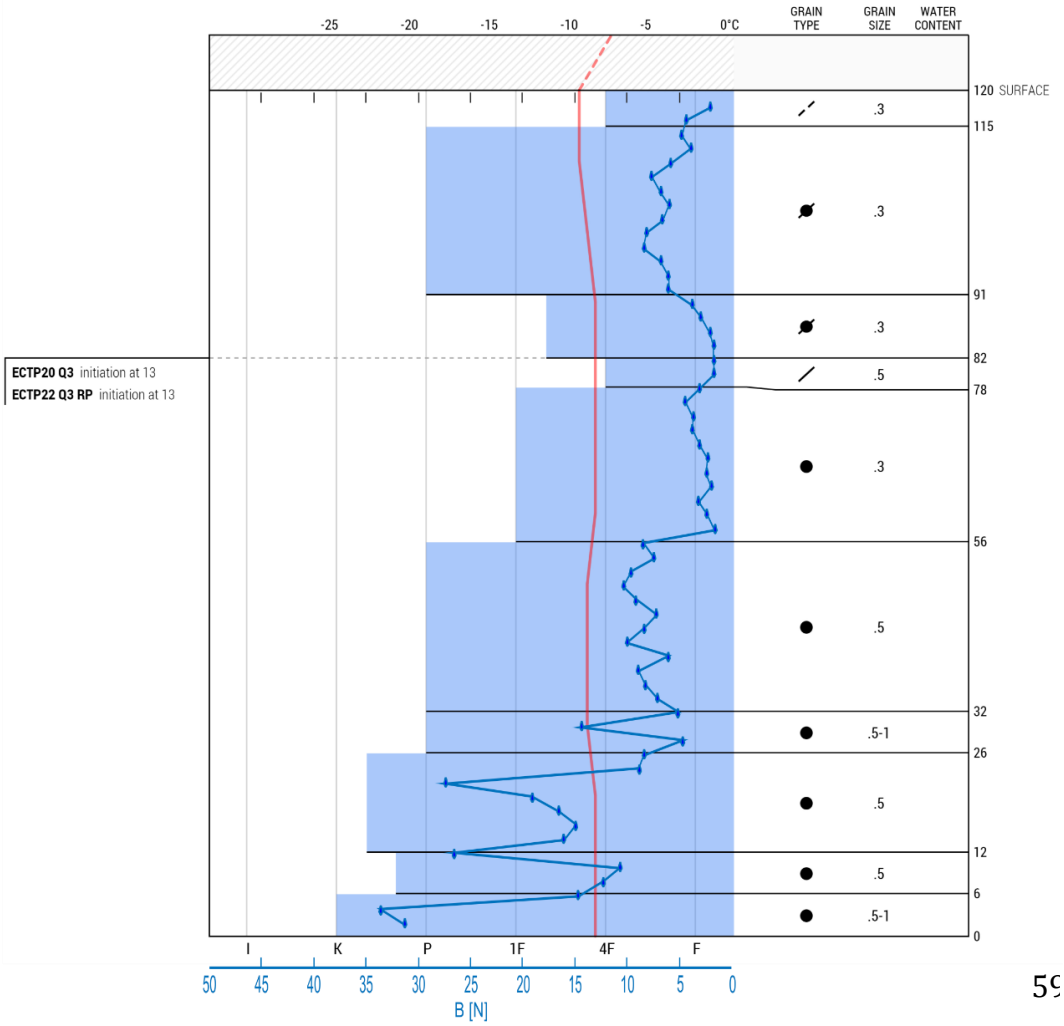

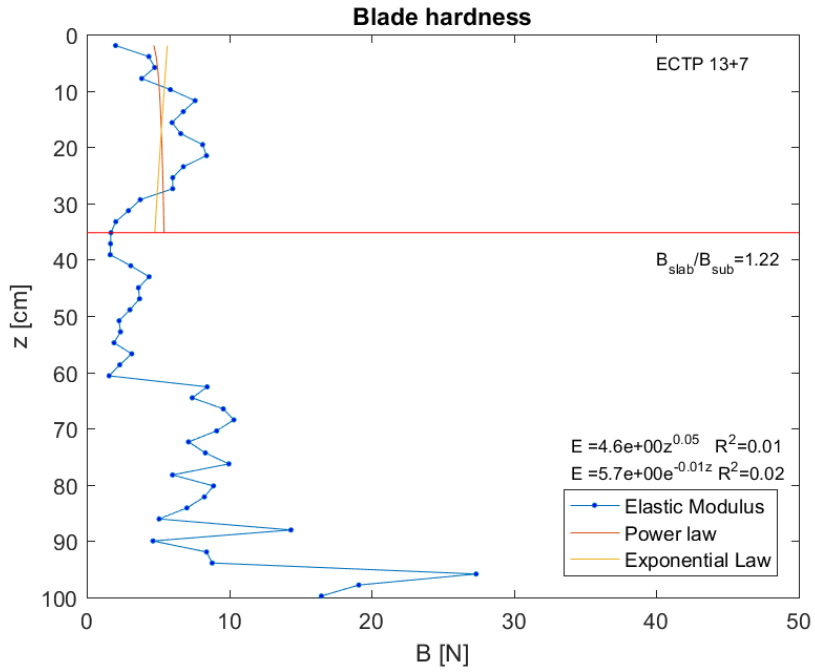

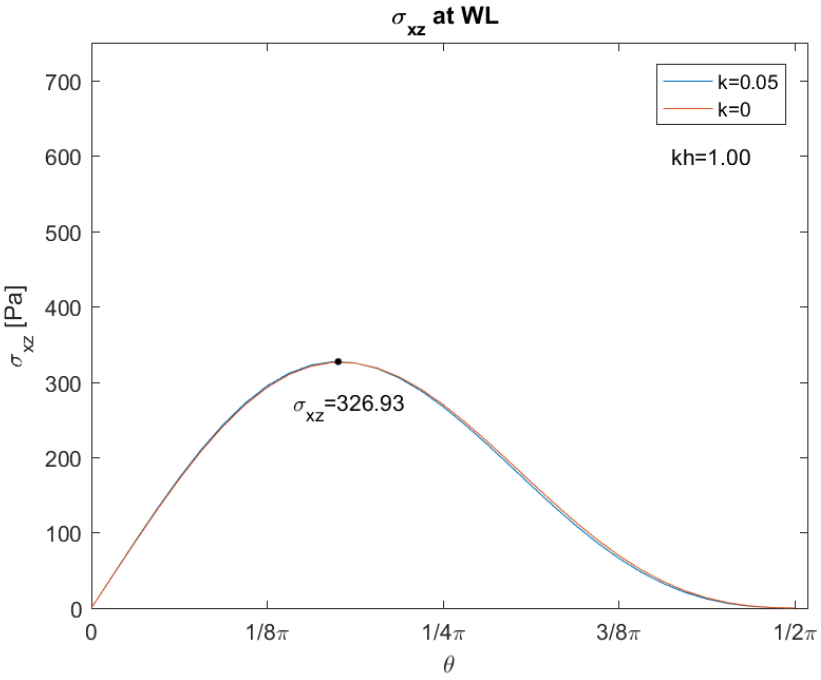

59

Location:	Fagerfjellet near Tromsø	Date:	2016-03-12	Snowpit depth:	138 cm
Lat/Lng:	69.55961, 19.24891	Observer:	Laura Swinkels	Snowpack depth:	138 cm

Elevation:	730 m	Wind:	Moderate, 225° SW	50 N gauge	
Slope:	20°	Blowing snow:	Moderate, 225° SW		
Aspect:	323° NWbN	Precipitation:	No Precipitation		
Air temp.:	1.0°C	Foot Pen. (PF):	14 cm		
Sky:	Overcast	Ski Pen. (PS):	--		

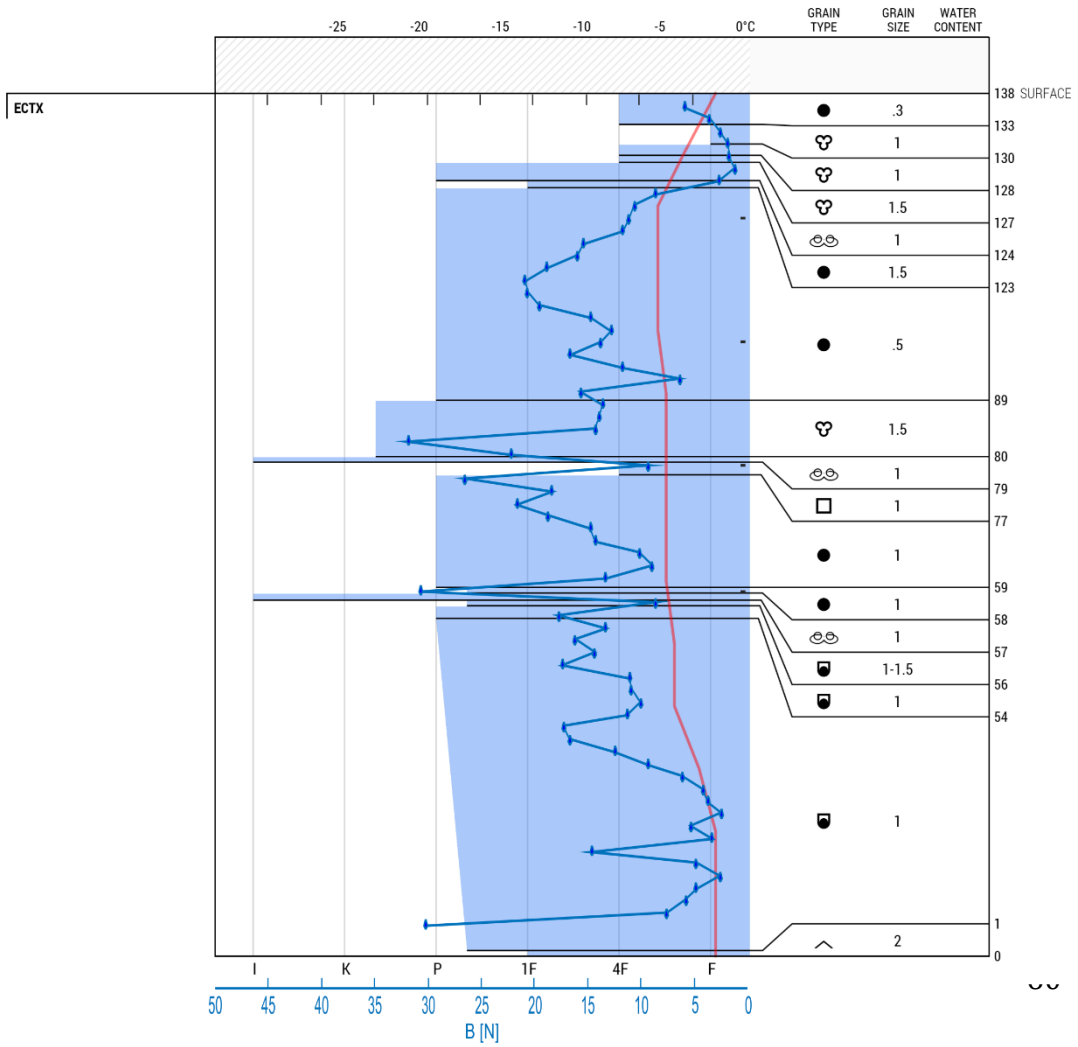

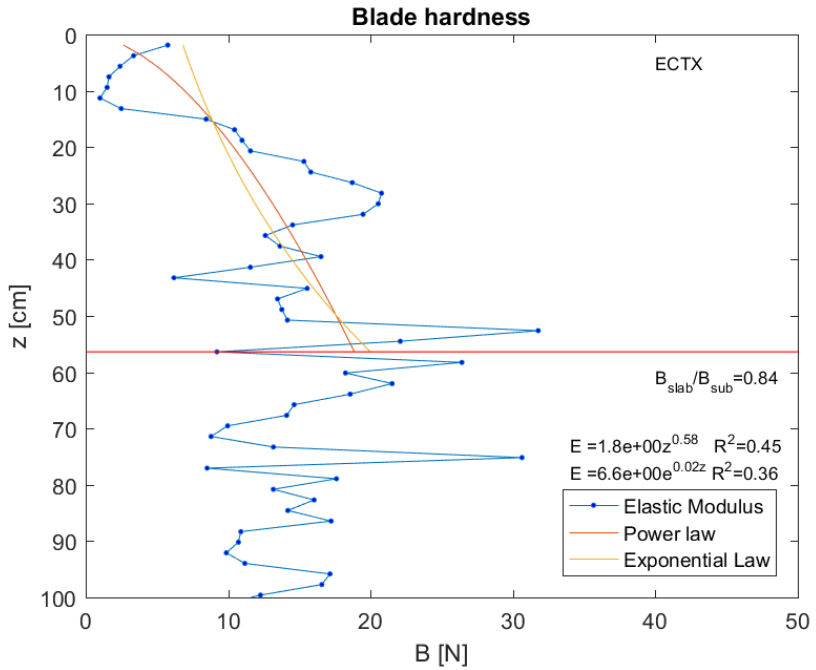

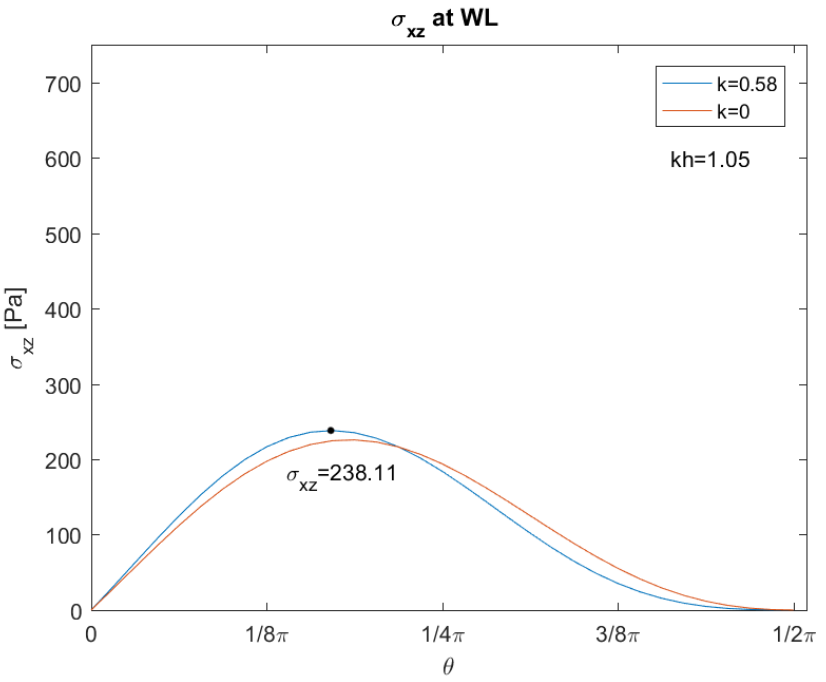

Location:	Blåtinden, Balsfjorden	Date:	2016-03-16	Snowpit depth:	90 cm
Lat/Lng:	69.38479, 19.33199	Observer:	Laura Swinkels	Snowpack depth:	90 cm

Elevation:	547 m	Wind:	Strong, 270° W		
Slope:	10°	Blowing snow:	Moderate, 270° W		
Aspect:	186° SbW	Precipitation:	Snow - Moderate		
Air temp.:	-4.0°C	Foot Pen. (PF):	24 cm		
Sky:	Overcast	Ski Pen. (PS):	--	50 N gauge	

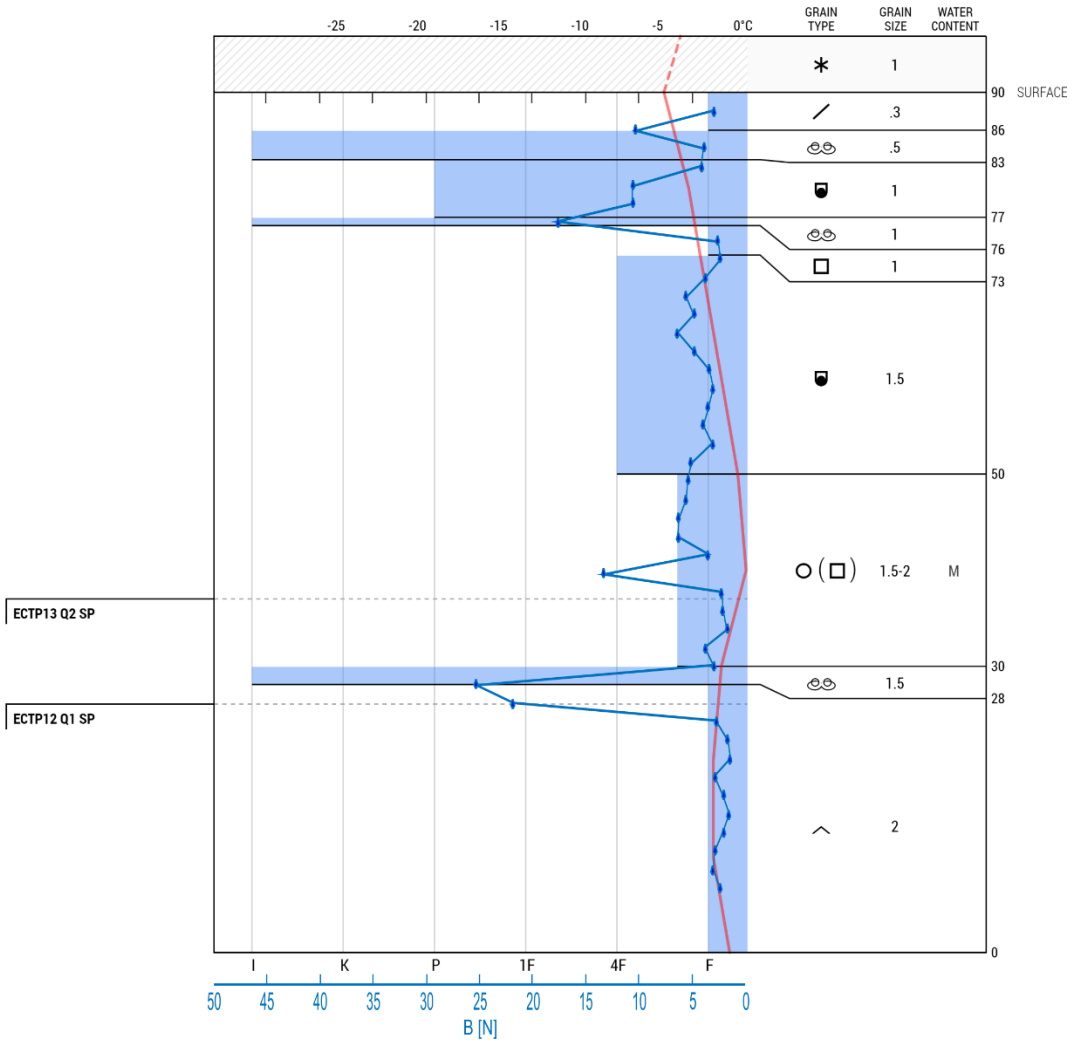

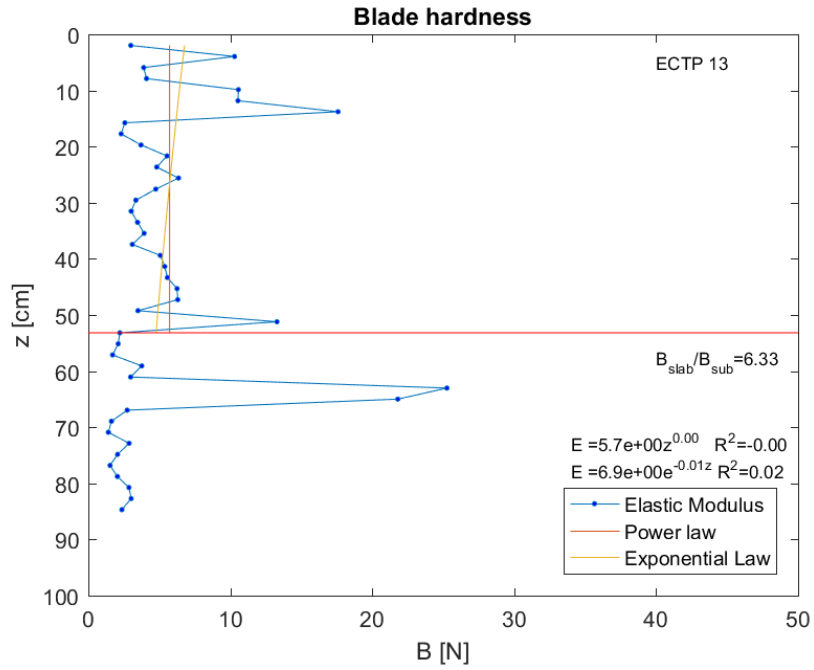

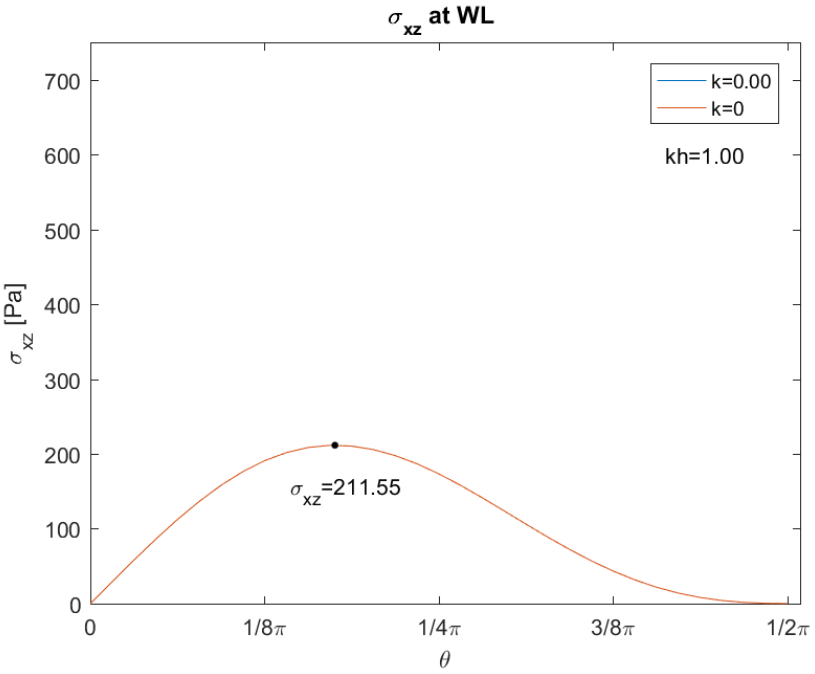

Location:	Strupen, Troms	Date:	2016-03-17	Snowpit depth:	169 cm
Lat/Lng:	69.70236, 18.87039	Observer:	Laura Swinkels	Snowpack depth:	169 cm

Elevation:	124 m	Wind:	Moderate, 180° S		
Slope:	21°	Blowing snow:	Moderate, 180° S		
Aspect:	140° SE	Precipitation:	Snow - Moderate		
Air temp.:	-6.5°C	Foot Pen. (PF):	28 cm		
Sky:	Scattered	Ski Pen. (PS):	--	50 N gauge	

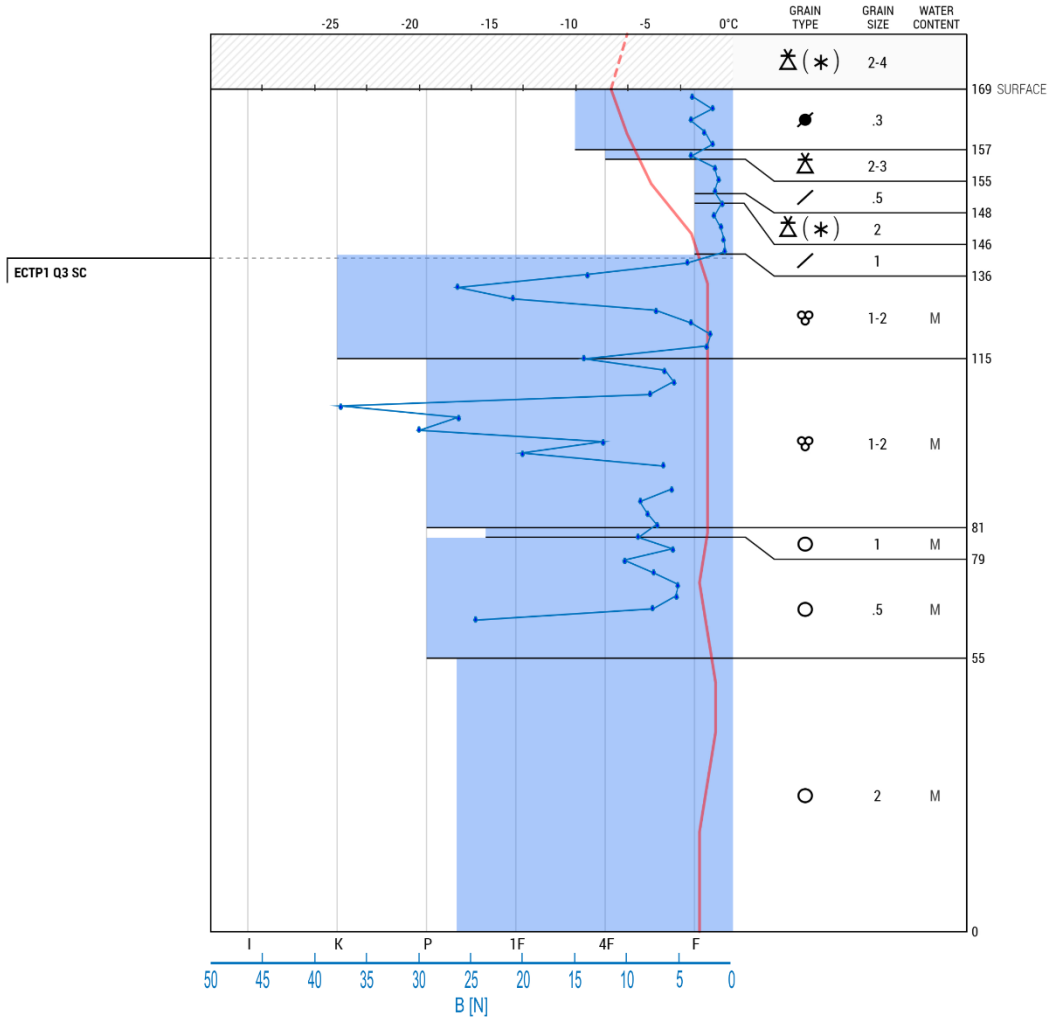

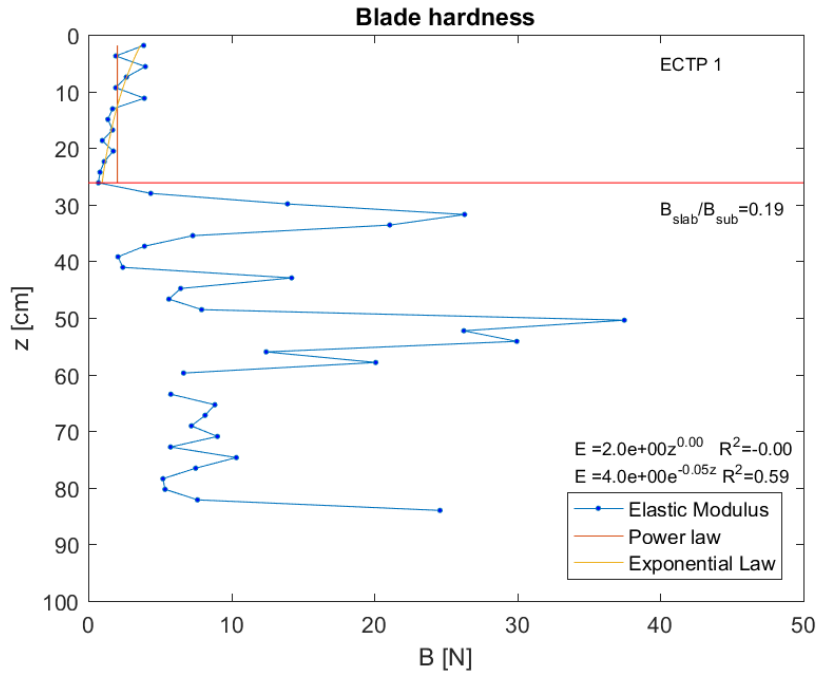

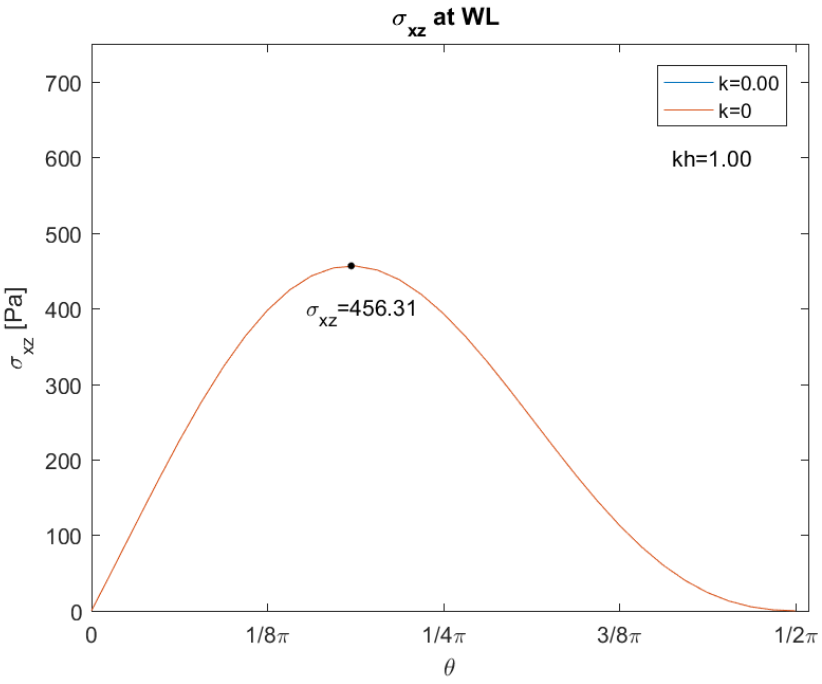

Location:	Hatten, Balsfjorden	Date:	2016-03-19	Snowpit depth:	160 cm
Lat/Lng:	69.38410, 19.32977	Observer:	Laura Swinkels	Snowpack depth:	195 cm

Elevation:	530 m	Wind:	Light, 20° NNE	
Slope:	23°	Blowing snow:	Light, 20° NNE	
Aspect:	190° SbW	Precipitation:	Snow - Very Light	
Air temp.:	-7.5°C	Foot Pen. (PF):	--	
Sky:	Few	Ski Pen. (PS):	--	50 N gauge

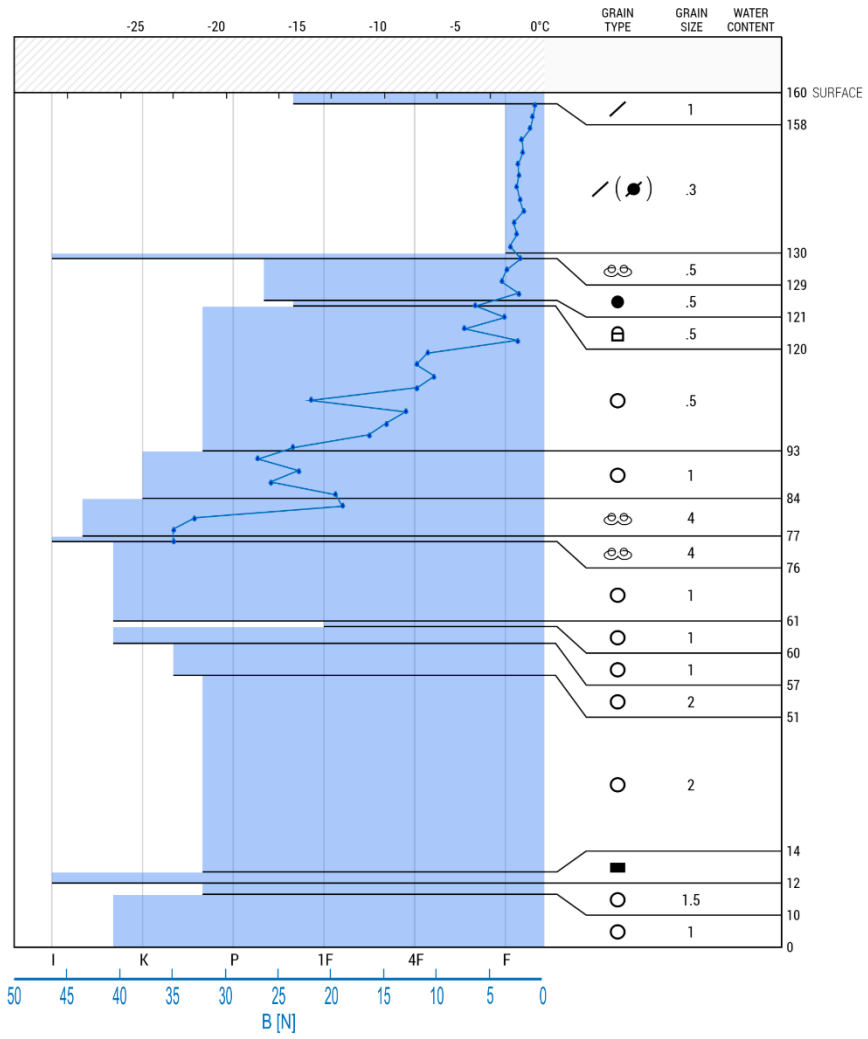

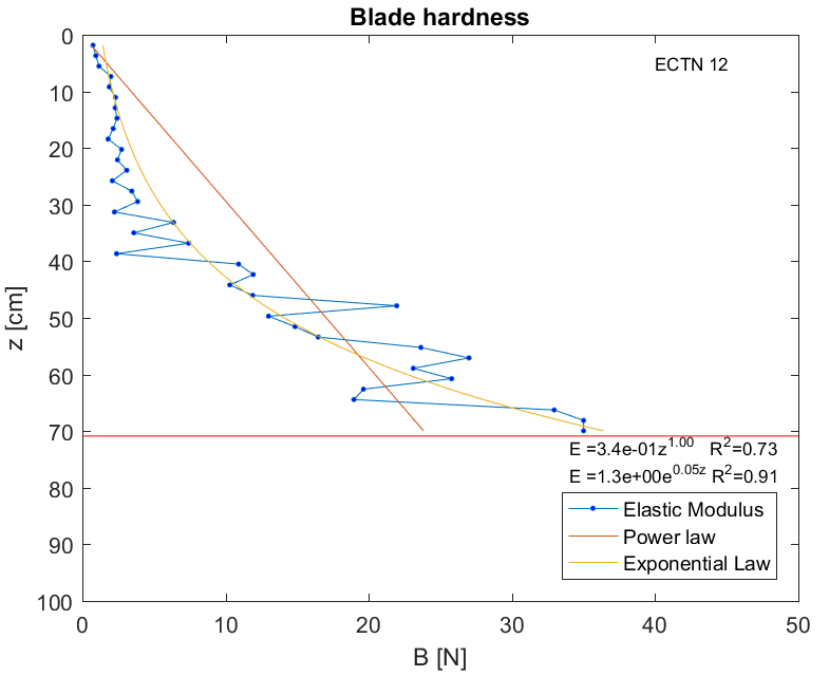

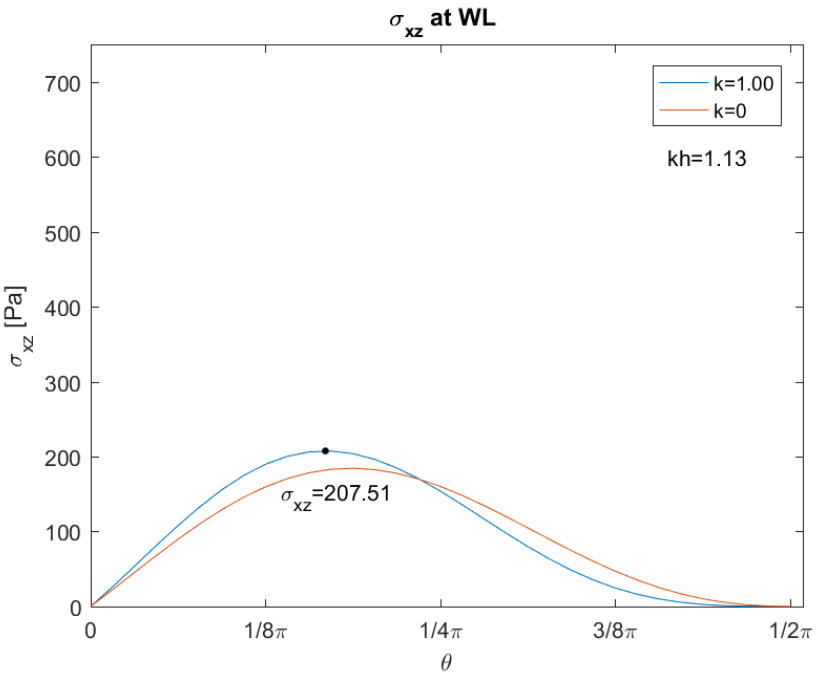

Location:	Storsteinnestindan, Kvaløya	Date:	2016-03-22	Snowpit depth:	110 cm
Lat/Lng:	69.65810, 18.52695	Observer:	Laura Swinkels	Snowpack depth:	180 cm

Elevation:	283 m	Wind:	Calm, 20° NNE	
Slope:	25°	Blowing snow:	None, --	
Aspect:	130° SE	Precipitation:	No Precipitation	
Air temp.:	-7.5°C	Foot Pen. (PF):	28 cm	
Sky:	Few	Ski Pen. (PS):	--	50 N gauge

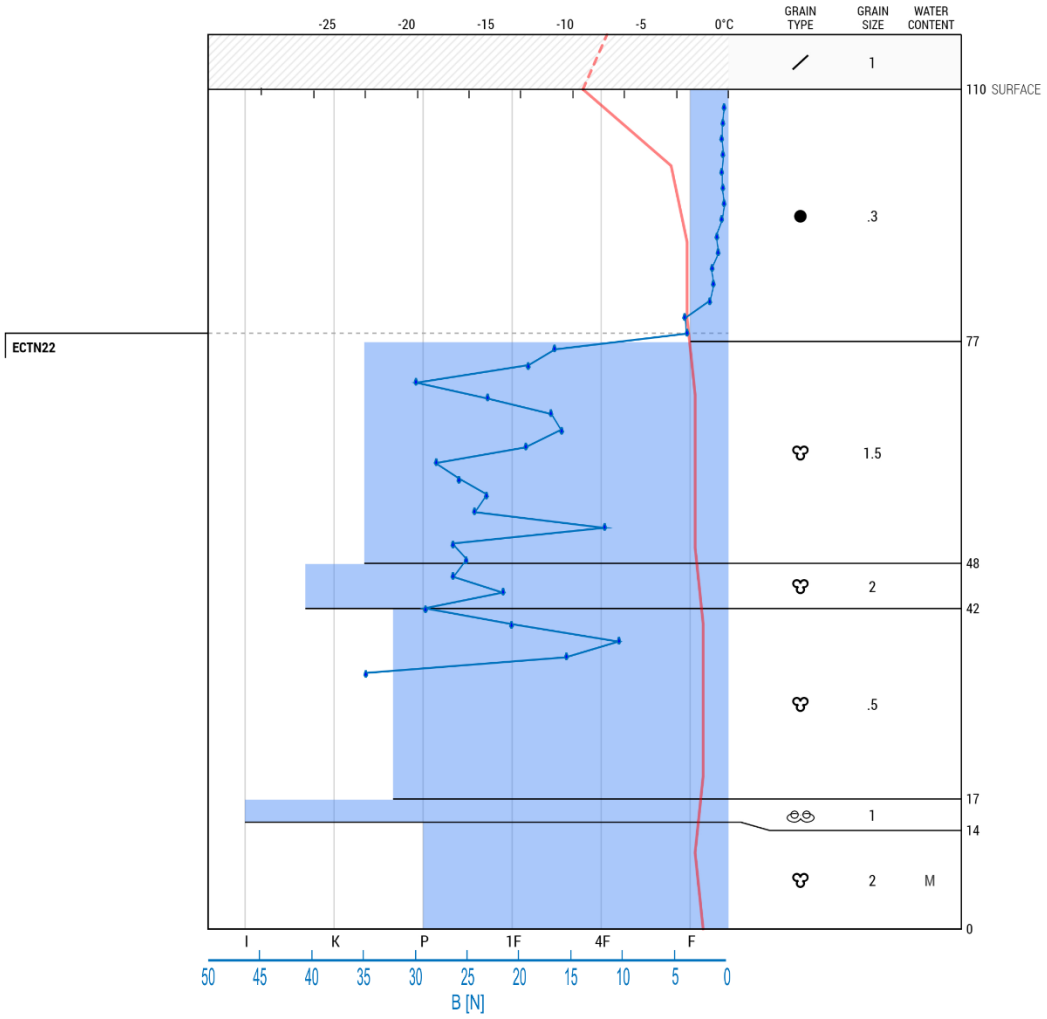

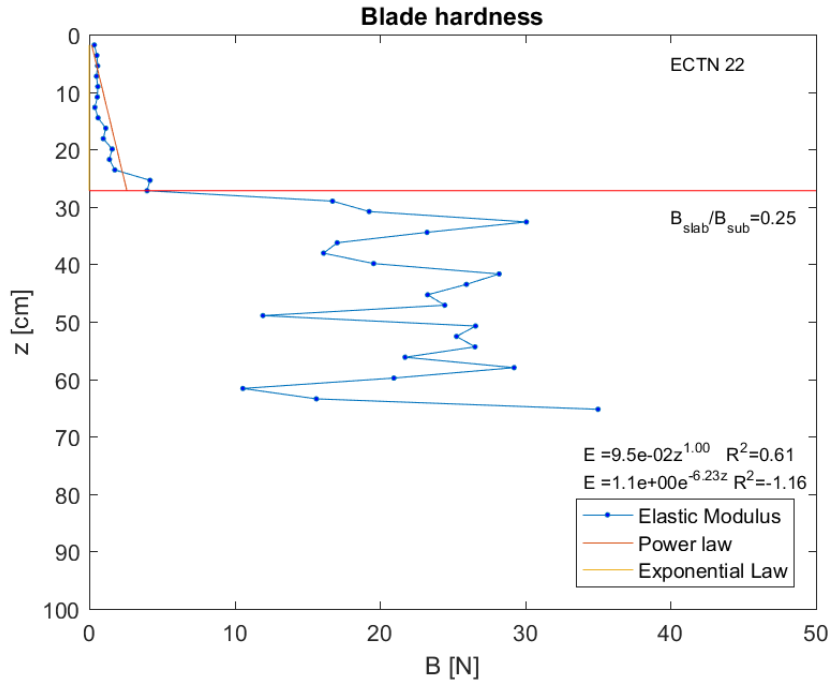

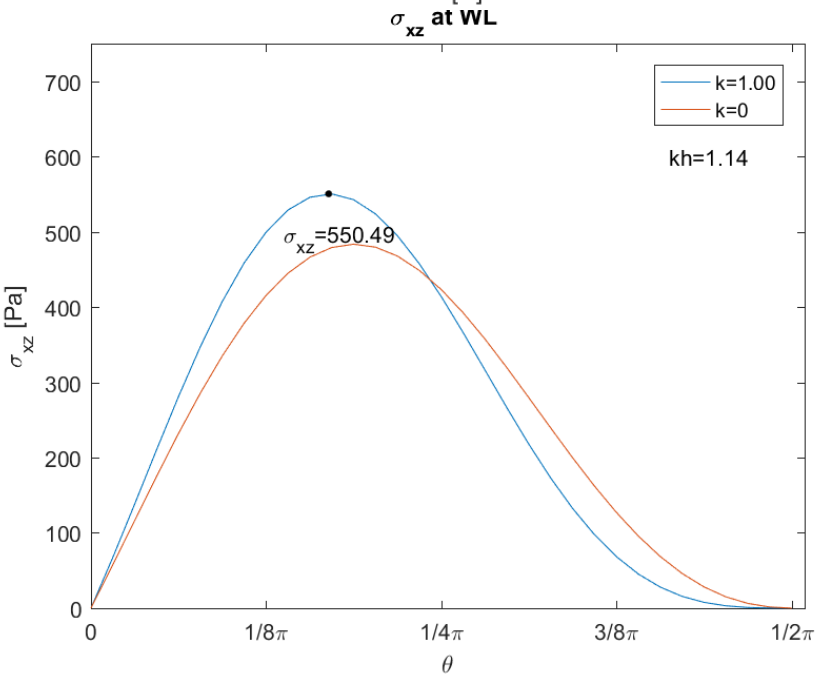

Location:	Saltdalen	Date:	2016-04-02	Snowpit depth:	120 cm
Lat/Lng:	69.48476, 19.37502	Observer:	Laura Swinkels	Snowpack depth:	120 cm

Elevation:	630 m	Wind:	Light, 180° S	
Slope:	20°	Blowing snow:	None, --	
Aspect:	330° NWbN	Precipitation:	No Precipitation	
Air temp.:	-3.0°C	Foot Pen. (PF):	--	
Sky:	◯ Clear	Ski Pen. (PS):	--	50 N gauge

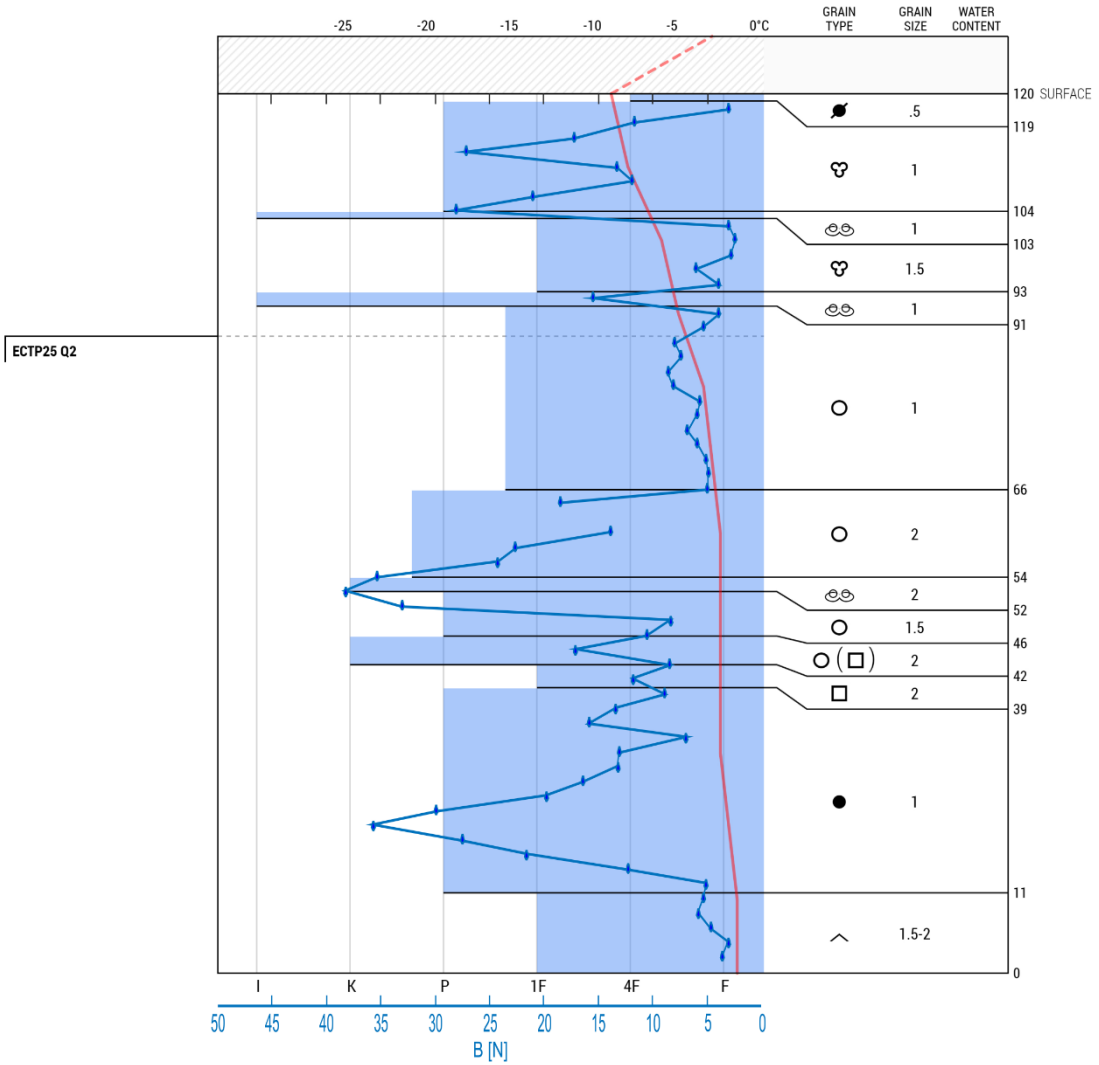

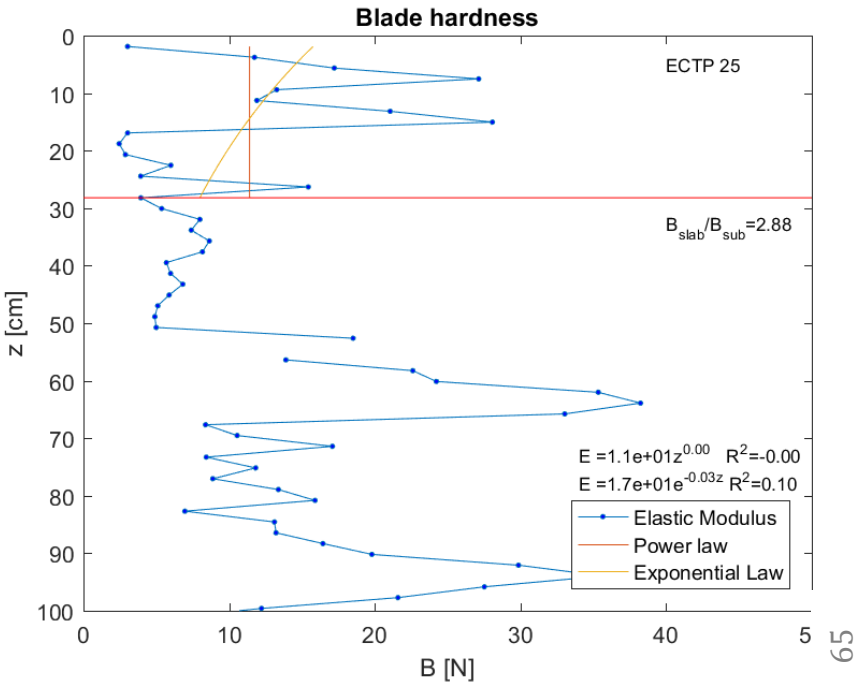

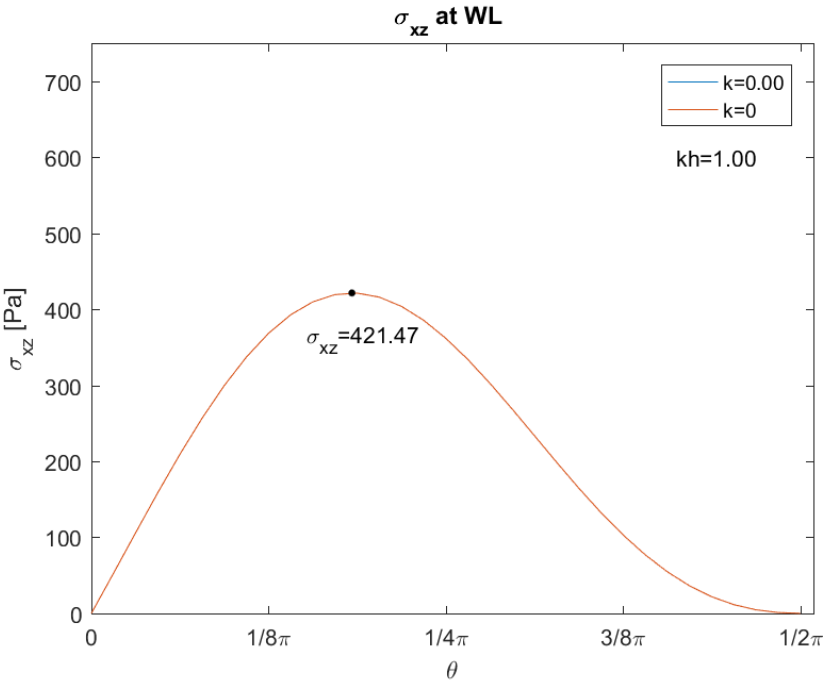

Location:	--	Date:	2016-04-06	Snowpit depth:	90 cm
Lat/Lng:	69.62447, 18.99966	Observer:	Laura Swinkels	Snowpack depth:	170 cm

Elevation:	630 m	Wind:	Light, 140° SE	50 N gauge
Slope:	20°	Blowing snow:	None, --	
Aspect:	35° NEbN	Precipitation:	No Precipitation	
Air temp.:	-4.5°C	Foot Pen. (PF):	5 cm	
Sky:	◯ Clear	Ski Pen. (PS):	--	

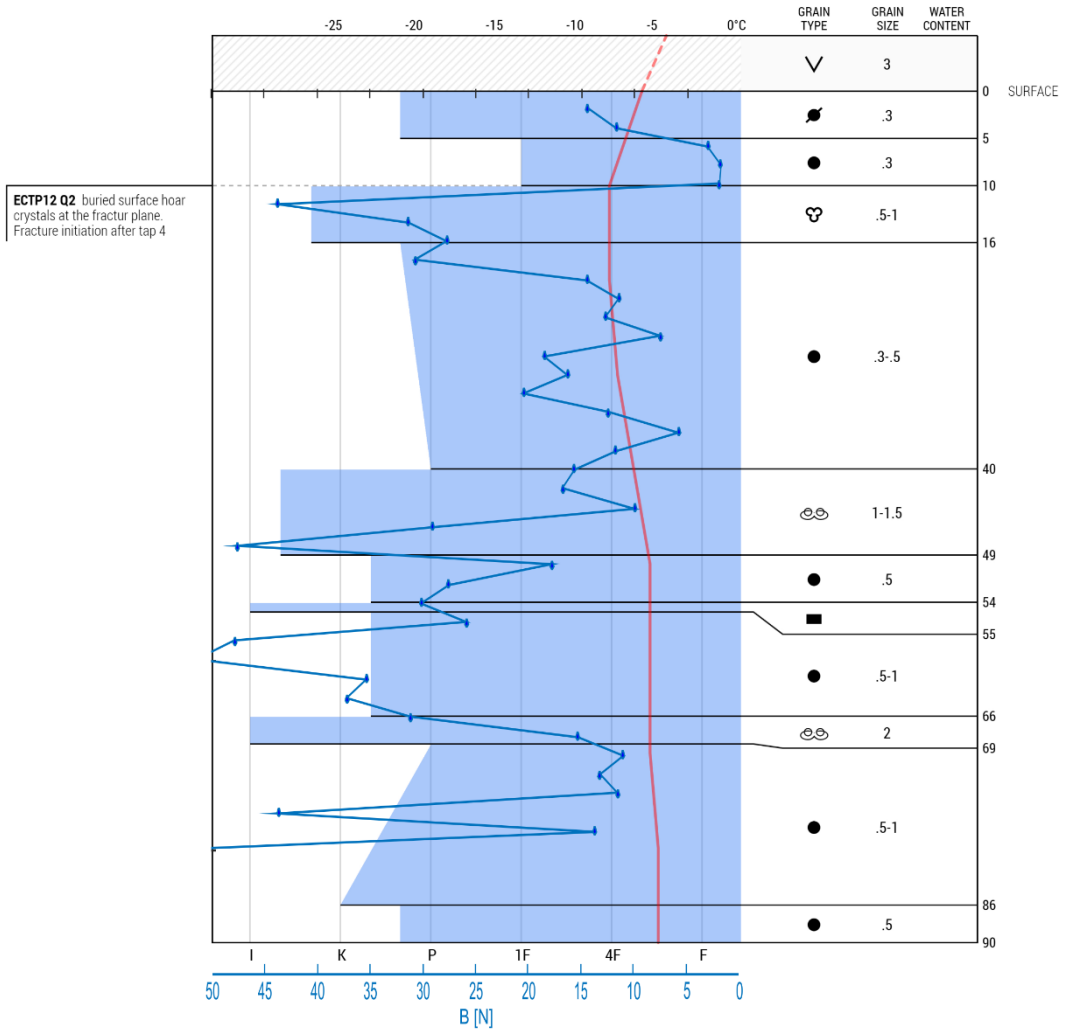

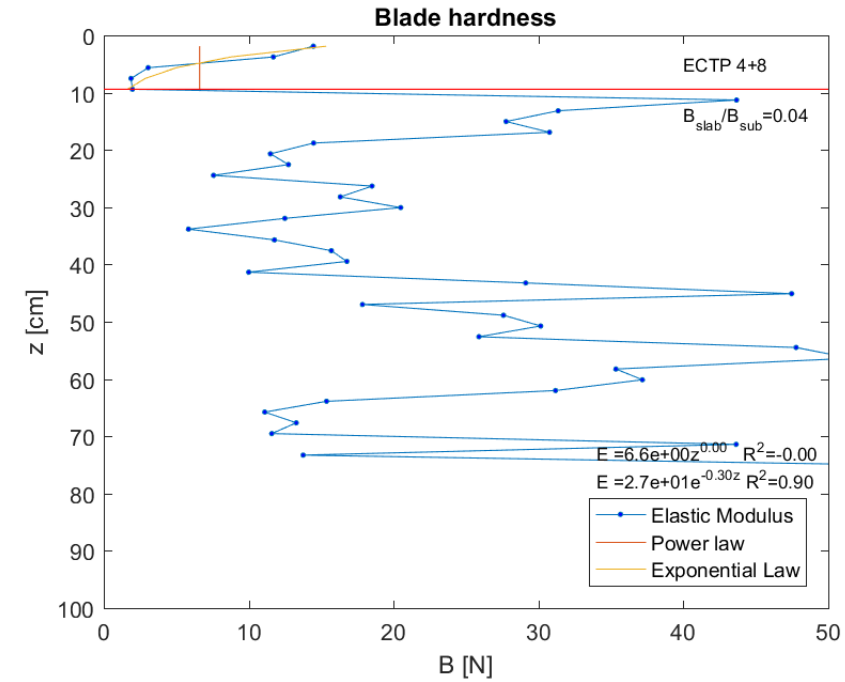

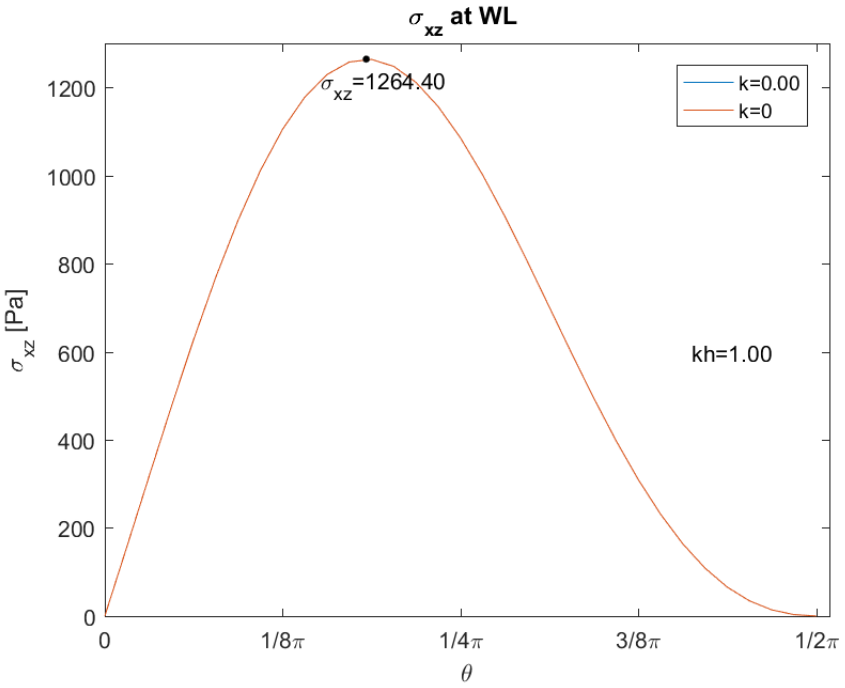

Location:	Nordfjellet, Tromsø	Date:	2016-04-09	Snowpit depth:	84 cm
Lat/Lng:	69.65738, 19.06866	Observer:	Laura Swinkels	Snowpack depth:	84 cm

Elevation:	625 m	Wind:	Moderate, 170° SbE	50 N gauge
Slope:	12°	Blowing snow:	None, --	
Aspect:	300° NWbW	Precipitation:	Snow - Very Light	
Air temp.:	-2.0°C	Foot Pen. (PF):	1 cm	
Sky:	Overcast	Ski Pen. (PS):	--	

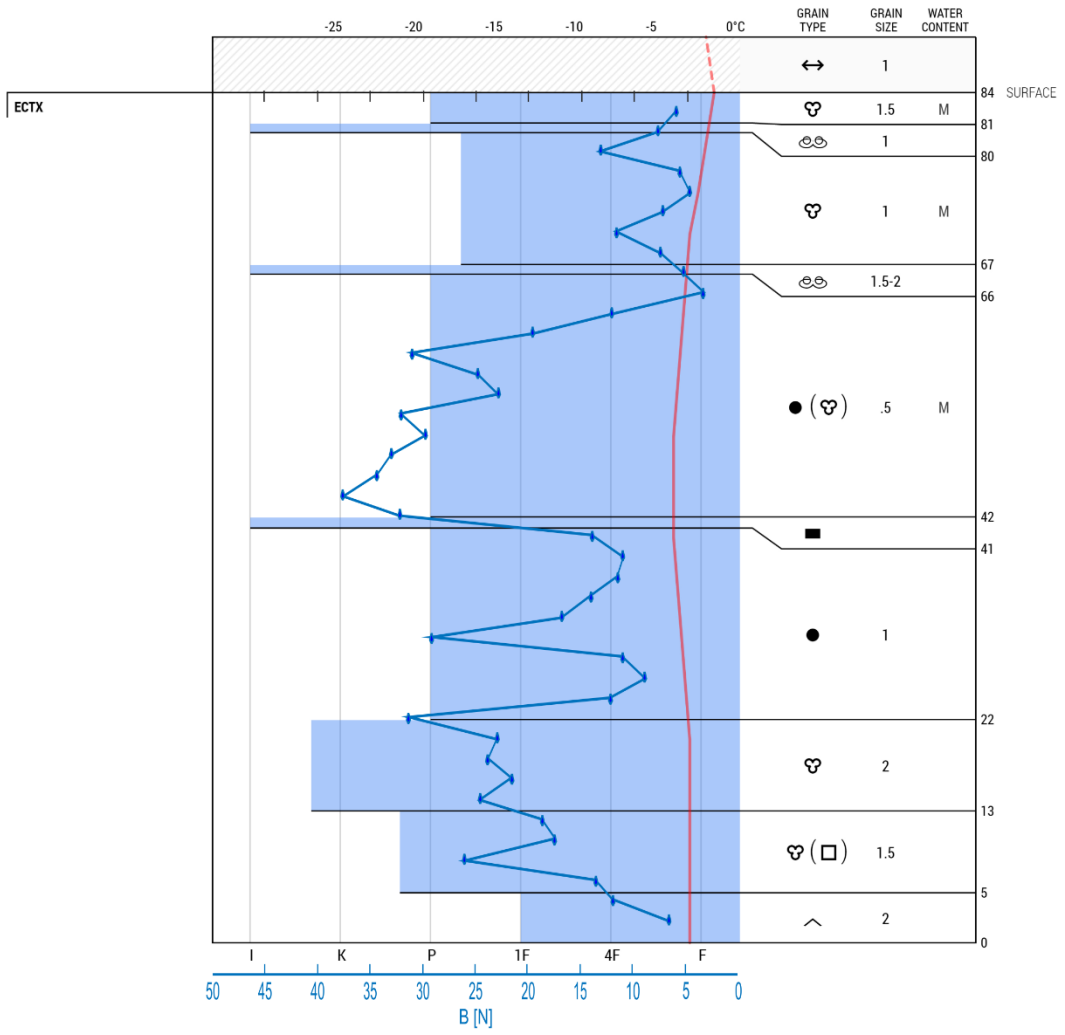

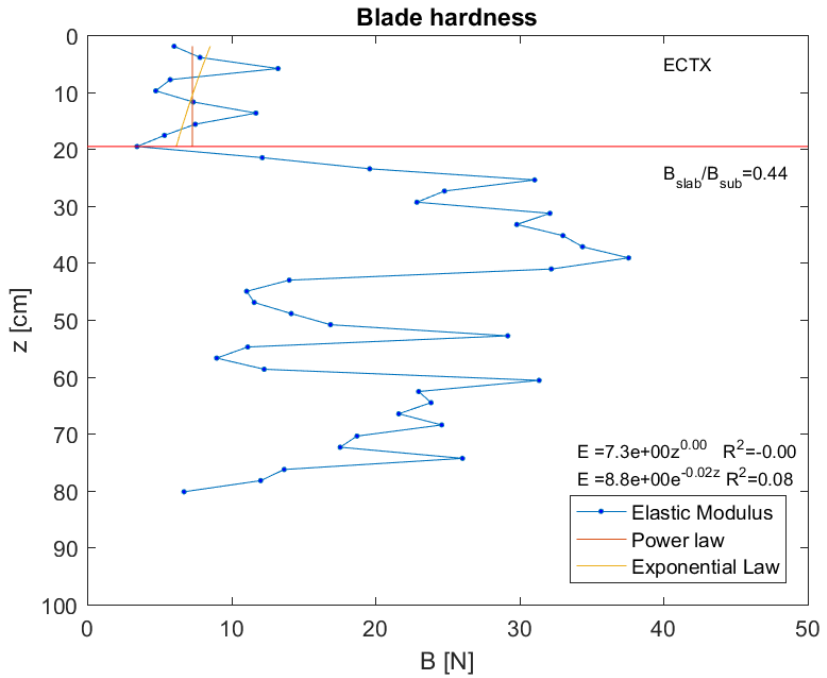

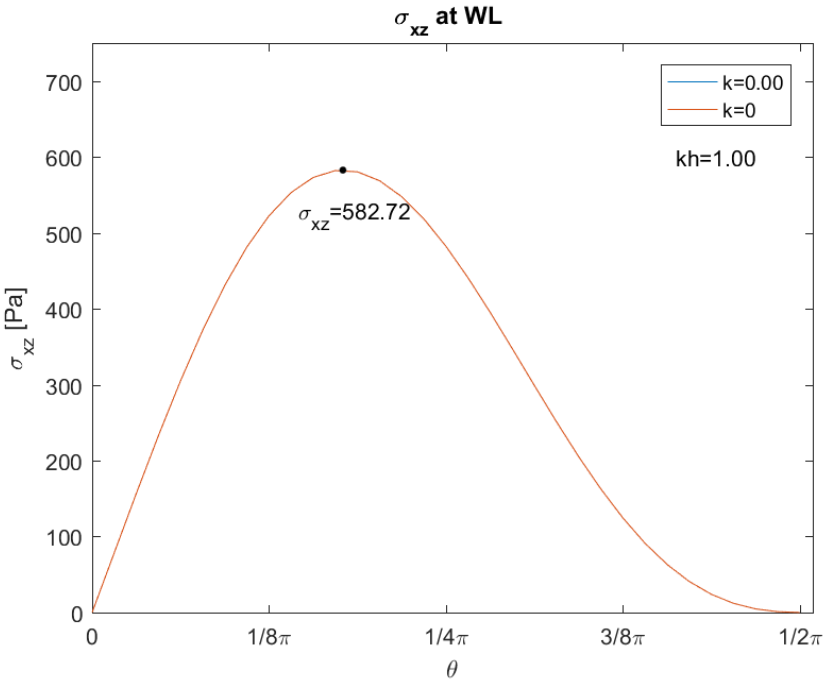

Location:		Date:	--	Snowpit depth:	83 cm
Lat/Lng:	69.65738, 19.06843	Observer:	Laura Swinkels	Snowpack depth:	170 cm

Elevation:	620 m	Wind:	Strong, 350° NbW	
Slope:	15°	Blowing snow:	Light, 350° NbW	
Aspect:	310° NW	Precipitation:	Snow - Moderate	
Air temp.:	-5.5°C	Foot Pen. (PF):	3 cm	
Sky:	Obscured	Ski Pen. (PS):	--	50 N gauge

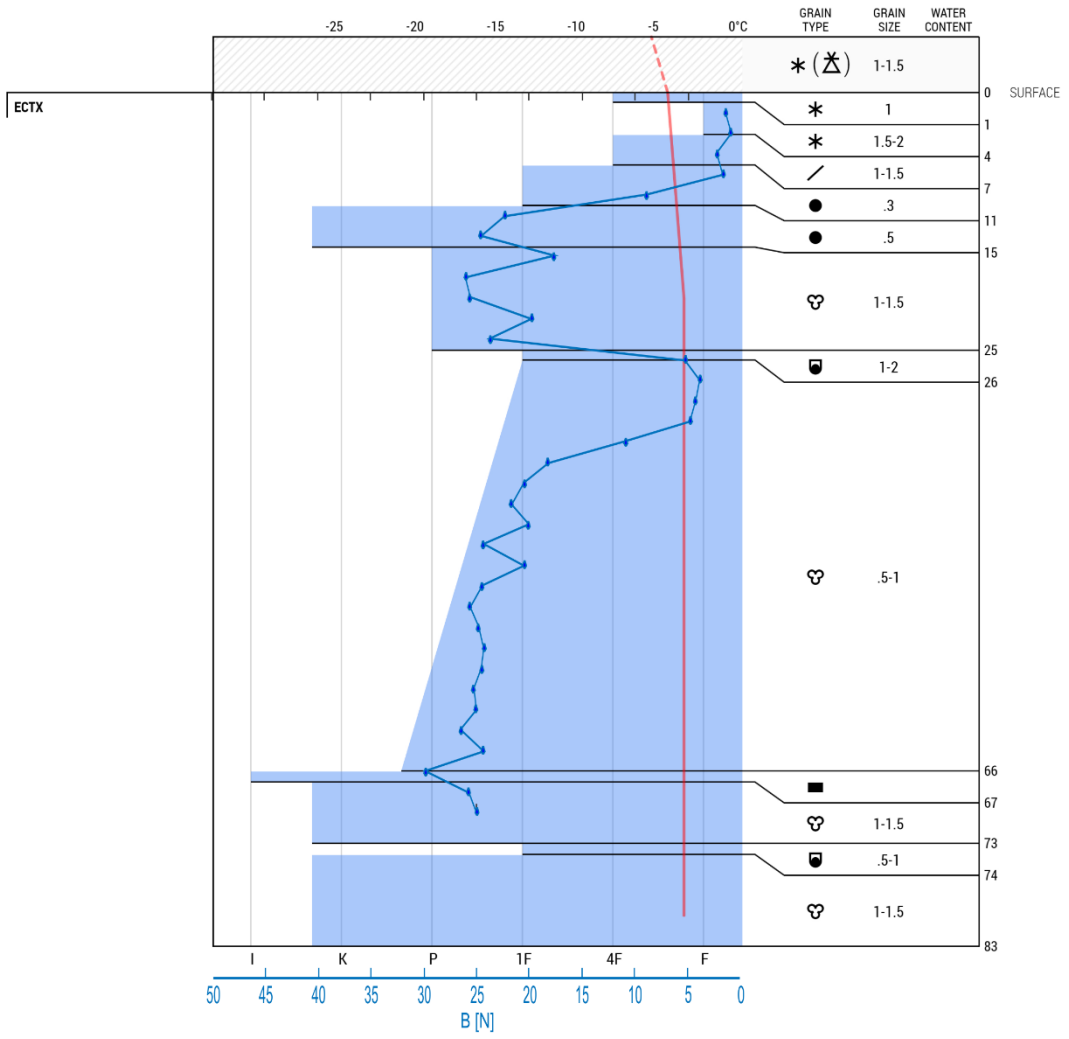

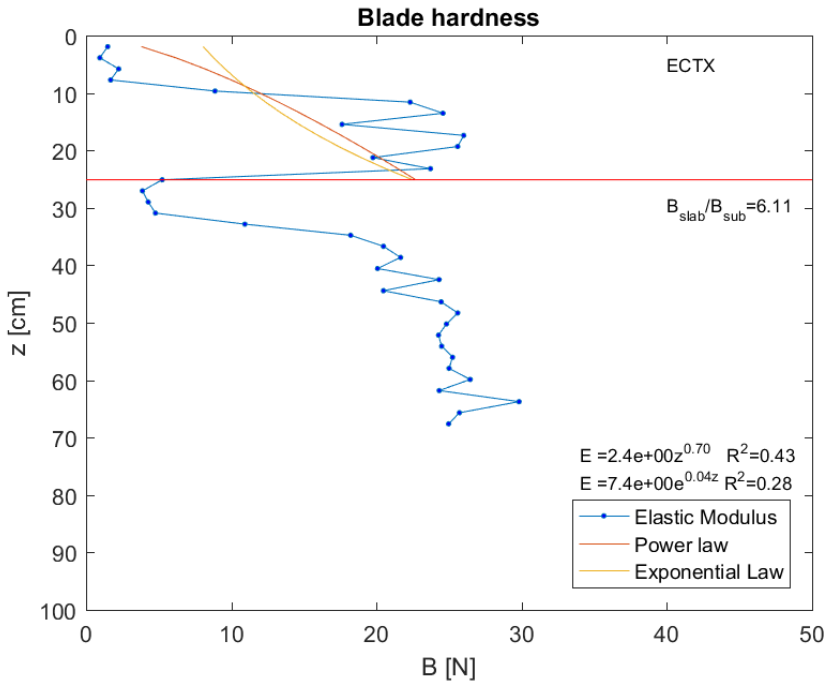

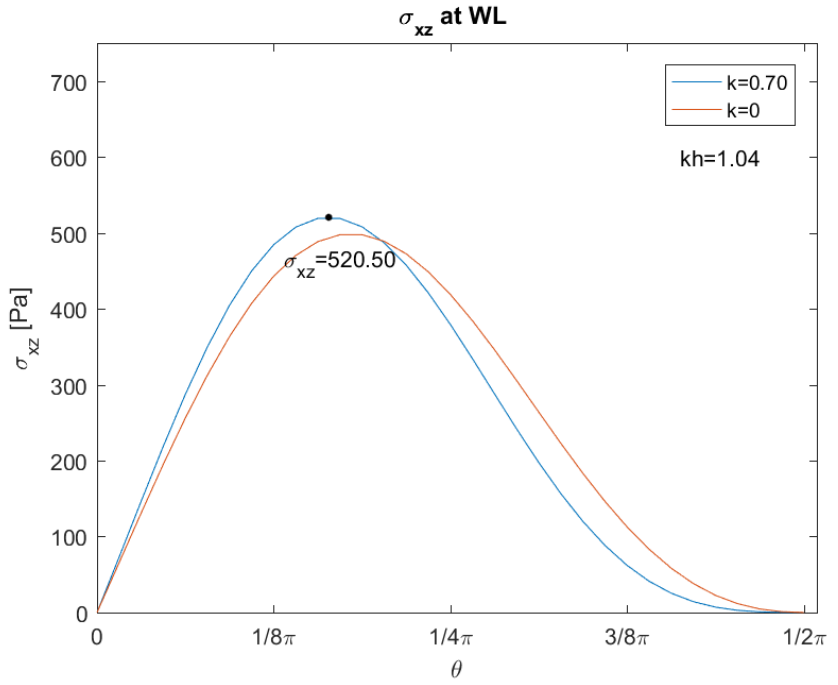

Location:	Nordfjellet, Tromsø	Date:	2016-04-14	Snowpit depth:	102 cm
Lat/Lng:	69.66243, 19.07175	Observer:	Laura Swinkels	Snowpack depth:	102 cm

Elevation:	535 m	Wind:	Moderate, 180° S	
Slope:	11°	Blowing snow:	Moderate, 180° S	
Aspect:	350° NbW	Precipitation:	No Precipitation	
Air temp.:	-6.5°C	Foot Pen. (PF):	15 cm	
Sky:	Overcast	Ski Pen. (PS):	--	50 N gauge

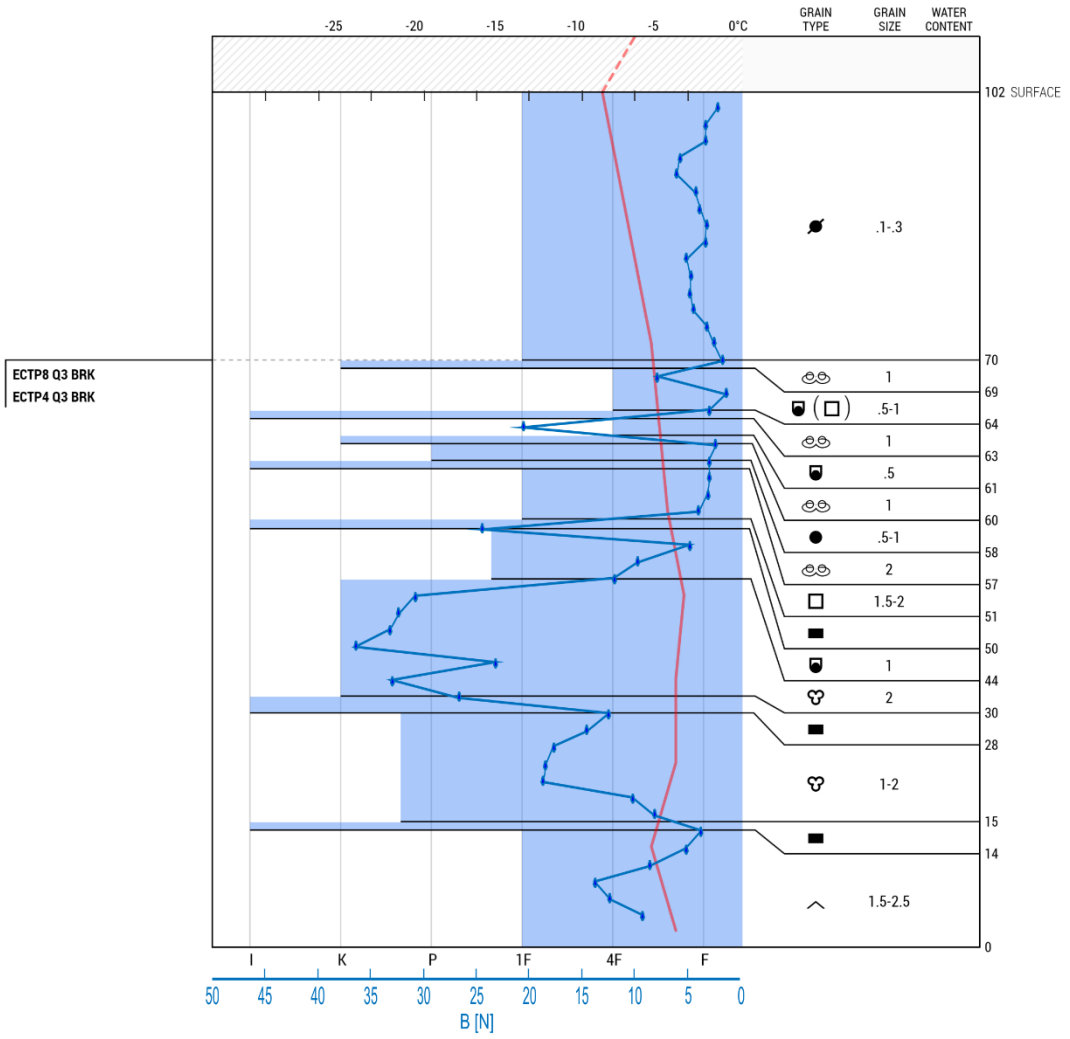

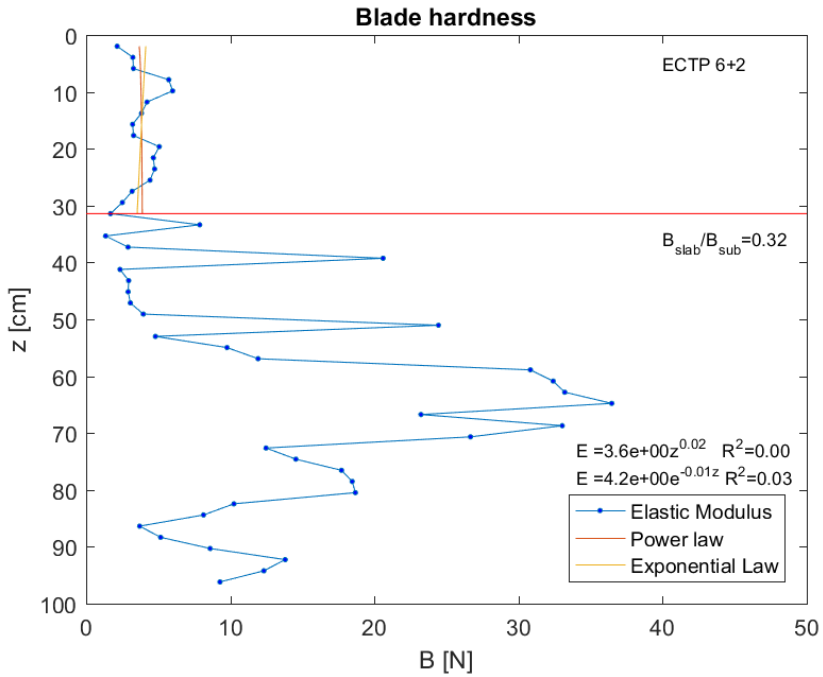

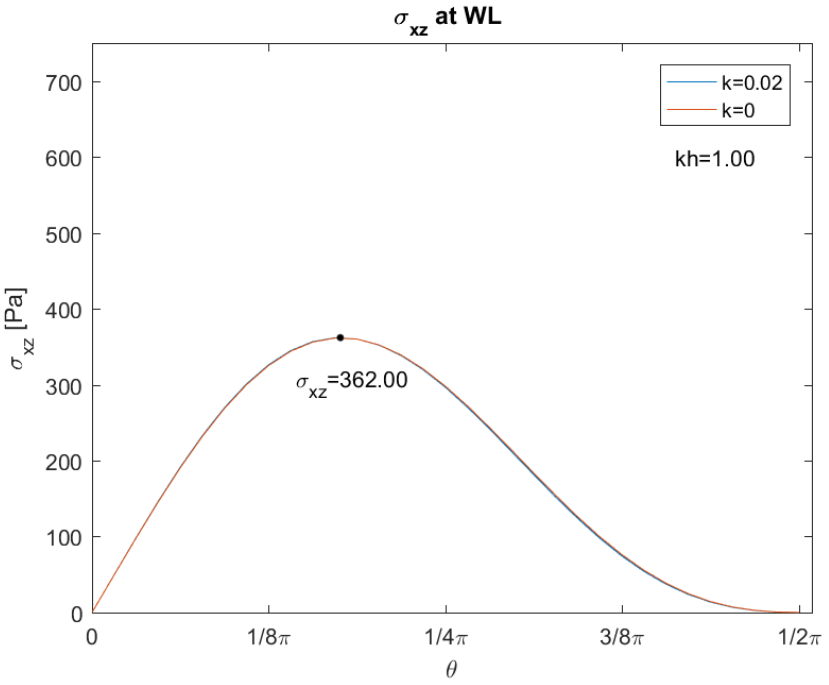

Location:	Rødtinden, Kvaløya	Date:	--	Snowpit depth:	80 cm
Lat/Lng:	69.70292, 18.74604	Observer:	Laura Swinkels	Snowpack depth:	180 cm

Elevation:	482 m	Wind:	Light, 170° SbE		
Slope:	12°	Blowing snow:	None, --		
Aspect:	220° SW	Precipitation:	No Precipitation		
Air temp.:	0.5°C	Foot Pen. (PF):	12 cm		
Sky:	Few	Ski Pen. (PS):	--	50 N gauge	

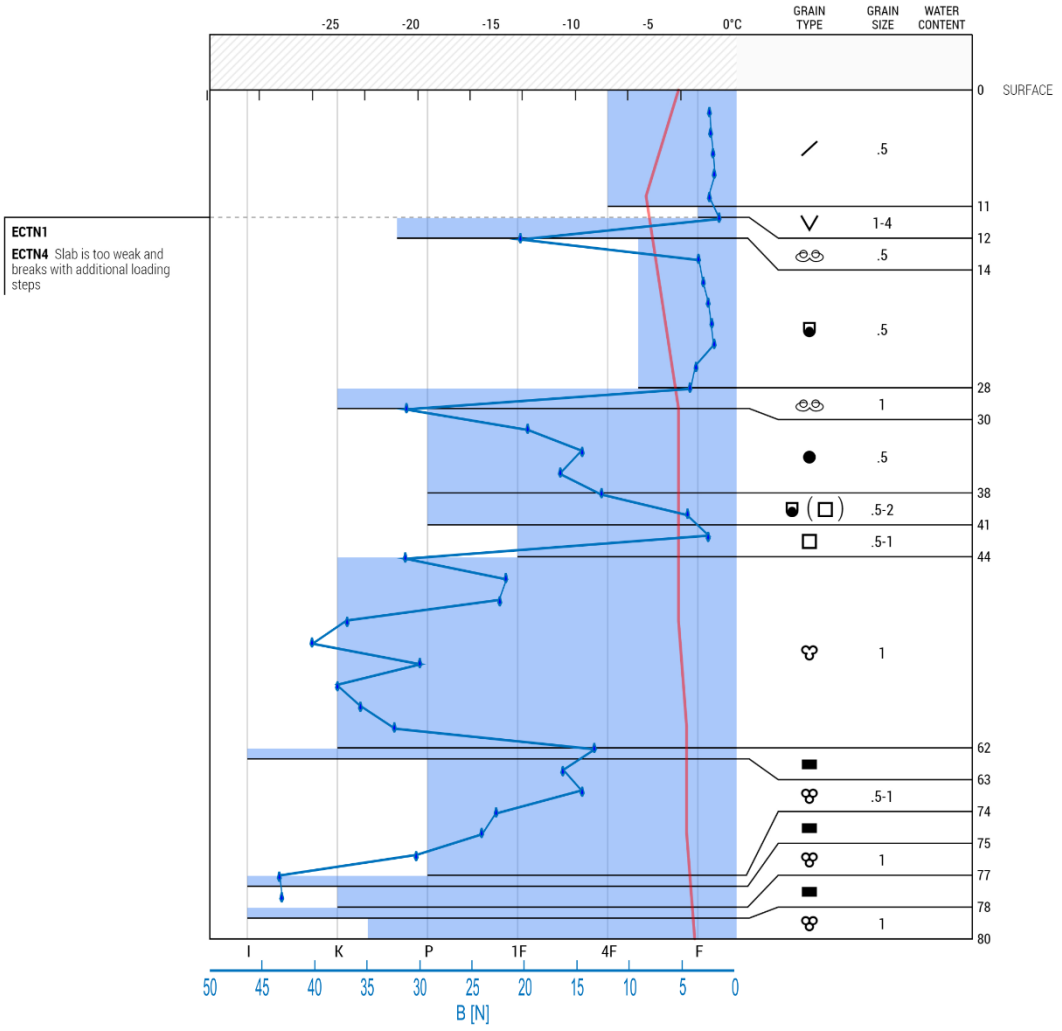

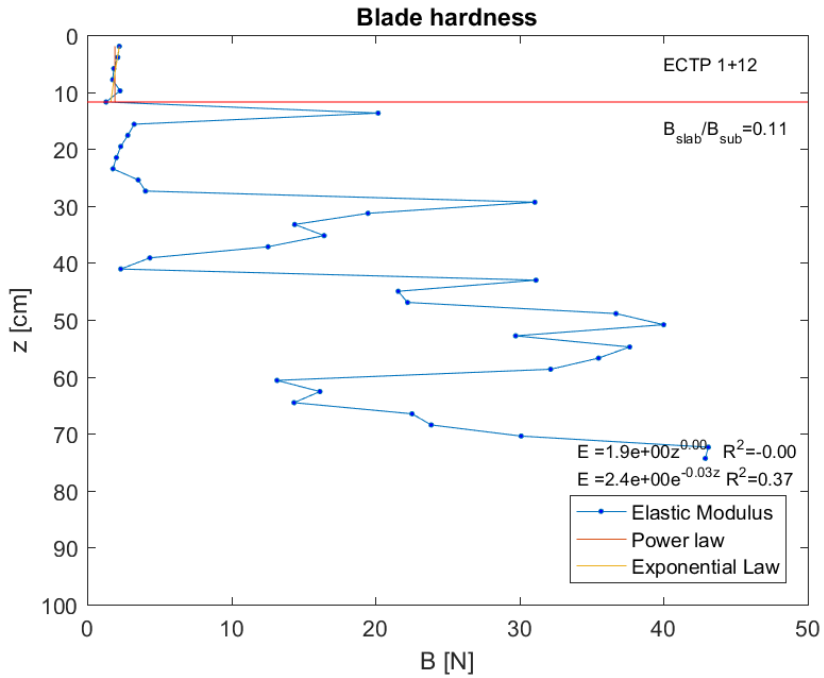

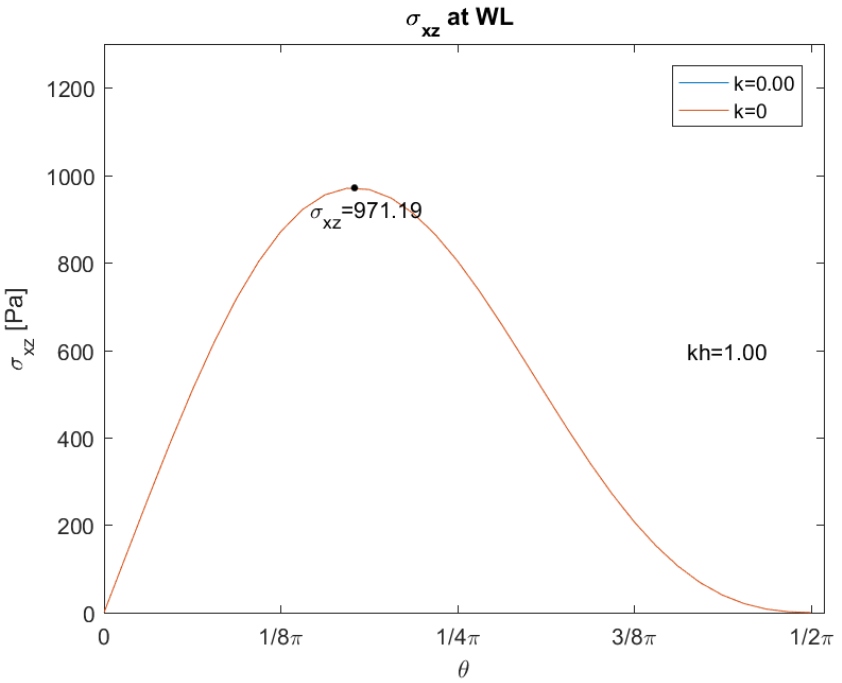

Appendix 3

Table of calculated parameters for each snow pit.

Date	k	Θ_{max}	Θ_{k0max}	σ_{wlmax}	$\sigma_{wlk0max}$	σ diff	σ_g	σ_{tot}	kh	S
20160204	0.00	0.59	0.59	196.07	196.07	0.00	590.22	786.29	1.00	5.36
20160211	0.00	0.60	0.60	712.97	712.97	0.00	203.55	916.52	1.00	7.96
20160212	1.00	0.55	0.61	1050.56	882.44	168.12	149.22	1199.77	1.19	6.78
20160216	0.00	0.63	0.63	546.30	546.30	0.00	343.91	890.21	1.00	7.28
20160218	0.02	0.61	0.61	294.34	293.06	1.28	609.41	903.75	1.00	6.99
20160219	0.11	0.58	0.59	662.26	652.65	9.61	133.93	796.19	1.01	6.43
20160225	0.00	0.56	0.56	500.50	500.50	0.00	121.84	622.34	1.00	4.49
20160226	1.00	0.52	0.55	618.52	556.06	62.46	146.87	765.39	1.11	7.88
20160303	0.05	0.55	0.56	326.93	326.31	0.62	168.78	495.71	1.00	4.74
20160312	0.58	0.54	0.56	238.11	225.81	12.30	524.01	762.11	1.05	7.65
20160316	0.00	0.55	0.55	211.55	211.55	0.00	191.15	402.69	1.00	7.20
20160317	0.00	0.58	0.58	456.31	456.31	0.00	122.22	578.54	1.00	0.96
20160319	1.00	0.53	0.58	207.51	184.39	23.12	608.57	816.08	1.13	10.51
20160402	0.00	0.58	0.58	421.47	421.47	0.00	231.74	653.20	1.00	6.25
20160406	0.00	0.58	0.58	1264.40	1264.40	0.00	80.08	1344.48	1.00	1.97
20160412	0.70	0.51	0.56	520.50	498.71	21.80	155.59	676.09	1.04	6.90
20160414	0.02	0.55	0.55	362.00	361.77	0.23	118.77	480.77	1.00	4.86
20160420	0.00	0.56	0.56	971.19	971.19	0.00	34.23	1005.43	1.00	1.80

Θ_{max} Angle between the z-axis (fig. 7) and the point of maximum shear stress at the weak layer

Θ_{k0max} Angle with respect to the z-axis for the homogeneous case

σ_{wlmax} Maximum shear stress at the weak layer

σ diff Maximum shear stress for a non-homogeneous slab minus the stress for a homogeneous slab

σ_g Stress induced by the gravity of the slab

σ_{tot} Total stress reaching the weak layer (external load plus slab gravity)

kh Ratio between the results for a non-homogeneous and a homogeneous slab

S Stability index

Laura Josephine Swinkels

Tromsø, 2017